Faculty of Science and Engineering
Department of Chemical Engineering

Floatability of the Water Droplet with Oil Decomposing Reagents on Paraffin Oil

Lily Ng Cen

This thesis is presented for the Degree of
Master of Philosophy
of
Curtin University

November 2014

"To the best of my knowledge and belief this thesis contains no material previously published by any other person except where due acknowledgment has been made. This thesis contains no material which has been accepted for the award of any other degree or diploma in any university."

ACKNOWLEDGMENT

I would take this opportunity to express my deep appreciation and gratitude to my supervisors, Dr. Chi M. Phan and Prof. Moses O. Tade for their guidance, deep insights and support throughout the course of this work. Their enthusiasm for research and abundance of knowledge has always been a constant source of motivation for the entire work of this project.

I am also highly indebted to my parents, Mr. Kwok Tim Ng and Mrs. Yanshen Cen and to my siblings, Gilberto, Raiza and Sandra; but for their support, encouragement and love, this work would have never been possible. I would also like to extend my gratitude to all my friends and relatives for all their well wishes and encouragement. A special thanks to my grandmother Mrs. Zhang Aiyue for always being my life's mentor and for being my guardian angel. God blessed you all and brighten your way always.

PUBLICATIONS

The following publications were produced in conjunction with the material used in this thesis.

Journal Article

Ng, L., Phan, C. M. and Tade, M. O. Influence of salinity on the floatability of water droplet on paraffin oil. Environmental Science & Technology under review.

Conference poster

Ng, L., Phan, C.M. and Tade, M.O., 2013. Floatation of water droplets on complex oil surface. *9TH World Congress of Chemical Engineering, Coex, Seoul, Korea, 18-23 August*.

ABSTRACT

Oil spillage is one of the most serious problems for the oil industry. The oil spillages can have catastrophic impact on the environment as seen in the Horizon accident in the Gulf of Mexico (2010). Although the hydrocarbons can decompose via various methods, the in-situ decomposition of oil spillage remains a challenging problem. Recently, it has been found that water droplets can float on oil under special conditions. This phenomenon opens up a new possibility to decomposing oil spillage. In particular, inside the water droplets, a solution with decomposing reagents can be placed. However, the oil decomposing reagents behaviour of such droplets during the decomposition remains unpredictable.

This study investigates the floatability of water droplets on a paraffin oil. This oil has similar properties to crude oils. Different decomposing reagents were also included in the droplets for photo-catalysts, chemical and biological decomposition. The photo-catalytic process was obtained by using TiO_2 particles under a solar simulator. The employed chemical oxidation process was Fenton reaction. Finally, the bio-reagent process was obtained by providing nutrients to the naturally-occurring micro-organisms.

Sodium chloride was also included to simulate seawater, which is more realistic than fresh water in oil-spill scenarios. The main stabilising agent is a common anionic surfactant, Sodium Dodecyl Sulphate (SDS) and hydrochloric acid for pH control. The stability of water droplets was evaluated by the contact angle between the interfaces and shape of each drop, following Young-Laplace equation and previous models.

The decomposing processes can significantly affect the droplet shape. The overall findings, however, show that droplet size can go up to 9 µL and remain stable on a paraffin oil surface for most cases. The influences of the composition processes are visually observable in some systems. Most interestingly, the bio-reagent grew in a one-dimensional direction and formed thin filaments from the oil/water interface. In terms of the reaction, the Fenton

process was the fastest process. However, the reaction time depended mostly on the type of organic pollutants to be eliminated and the amount of catalyst that was used.

The results indicate a possibility for complex surfactant systems to support seawater in a crude oil layer. Such feasibility can lead to the successful treatment of oil spillages without employing toxic solvents. The practicality and accuracy of such chemical mixtures utilised in this investigation, should be tested further under different conditions.

NOMENCLATURE

B_O	Bond number	Dimensionless
D	Dimensionless density	Dimensionless
D*	Maximum dimensionless density of a sphere	Dimensionless
g	Acceleration due to gravity	m s^{-2}
H	Shape factor, as defined by Boucher (1980)	
h_3	Height of the “helm” on the water droplet	m
h*	Height of the contact line above the undeformed interface	mm
J	Surface curvature	Dimensionless
k_m	Curvature of the interface	Dimensionless
l_{ca}	Capillary length	mm
ΔP	Local hydrostatic pressure in the bulk phase	kPa
R	Radius	mm
$R_{max,a}$	Maximum sphere radius	mm
r_o	Radius of a cylinder	μm
S	Arc length of meridian	Dimensionless
V	Volume of water droplet	mm^3

V_b	Volume of bubble	μL
V_1	Volume of air/water section	μL
V_2	Volume of water/oil section	μL
Δz	System characteristic length	m

Greek letters

ϕ	Angle of inclination of the interface to the horizontal	o
γ	Surface tension	mN m^{-1}
γ_{oa}	Interfacial tension between oil/air interface	mN m^{-1}
γ_{ow}	Interfacial tension between oil/water interface	mN m^{-1}
γ_{wa}	Interfacial tension between water/air interface	mN m^{-1}
λ	Factor from the generic form of the Young-Laplace equation, used to modify the shape factor	Dimensionless
θ	Tangent angle	o
θ_1	Contact angle between water/air interface	o
θ_2	Contact angle between oil/water interface	o
θ_3	Contact angle between oil/air interface	o
$\Delta\rho$	Density difference across an interface	Kg m^{-3}

ρ	Density	Kg m^{-3}
ρ_a	Density of air	Kg m^{-3}
ρ_o	Density of oil	Kg m^{-3}
ρ_w	Density of water	Kg m^{-3}
ρ^*	Critical density of sodium chloride solution	g cm^{-3}
ρ_s	Density of a sphere	Kg m^{-3}
ρ_M	Density of marble	g cm^{-3}
ψ	Angular position of the contact line	o

Table of Contents

Acknowledgement i

Publications ii

Abstract iii

Nomenclature v

Chapter 1 Introduction

1.1 Background to the study 1

1.2 New phenomena 3

1.3 Objectives 4

1.4 Format of the thesis 4

Chapter 2 Literature review

2.1 Interfacial phenomena 6

2.1.1 Capillary phenomena 6

2.1.2 Interfacial tension 8

2.1.3 Axisymmetric fluid bodies 9

2.1.4 Contact angles 11

2.2 Changes in interfacial tension 13

2.2.1 Interfacial activity of surfactants 13

2.2.2 Influence of electrolytes in interfacial tension 15

2.2.3 Influence of pH in interfacial tension 17

2.3 Previous modelling of a floating object on a liquid surface 18

2.3.1 Floatation of a solid object on liquid 19

2.3.2 Floatation of liquid lenses in a heavier liquid 23

2.3.3 Floatation of heavier liquid droplets in a lighter liquid 25

2.4 Oil decomposition 27

2.4.1 Chemicals reagents 29

2.4.1.1 Effect of Iron concentration 31

2.4.1.2 Effect of Iron type (Ferrous or Ferric) 31

2.4.1.3 Effect of H_2O_2 concentration 32

2.4.1.4 Effect of temperature 32

2.4.1.5 Effect of pH 32

2.4.1.6 Effect of reaction time 34

2.4.1.7 The effect of ratio peroxide to sample on the reduction of oil 34

2.4.2 Photo-catalysts reagents 35

2.4.2.1 Catalysts/UV light process 35

2.4.2.2 Hydrogen peroxide/UV light process ……..…. 36

2.4.3 Biological reagents ……..…. 38

2.4.3.1 Micro-organisms and bacteria ……..……..…. 38

2.4.3.2 Enzymes ……..…….…. 40

2.4.4 Combination of different processes …..……..…. 42

2.4.4.1 Combination of Fenton process under UV light ……..…. 42

2.6.4.2 Combination of biological process with Fenton reagents …. 43

2.5 Summary ……..…. 43

Chapter 3 Experimental

3.1 Materials ……..……..…. 45

3.1.1 Chemicals ……..…. 45

3.1.2 Preparation of aqueous solutions ……..…. 46

3.2 Measurements methods ……..……..……..... 46

3.2.1 Physical properties ……..…. 46

3.2.1.1 Surface tension …..……..……..…. 46

3.2.1.2 Density ……..……..…. 48

3.2.2 Droplet shape analysis …..……..…. 49

3.2.2.1 Experimental setup ……..…….. 49

3.2.2.2 Image Analysis of droplet shape ……..…….. 50

3.2.3 Oil decomposition processes ……..…….... 53

Chapter 4 Influences of volume and physical properties on the floating droplets

4.1 Experimental results and image processing ……. 54

4.2 Results ……. 54

4.2.1 Sodium dodecyl sulphate ……..……...…… 59

4.2.2 SDS with NaCl ……..……...…….. 61

4.2.3 SDS with NaCl at low pH ……..…….. 64

4.3 Summary ……..…….. 66

Chapter 5 The influences of Oil Decomposition processes on the Floating Droplet

5.1 Using catalysts and combination with UV irradiation ……. 70

5.2 Using enzyme and micro-organisms ……. 72

5.3 Summary ……. 74

Chapter 6 Conclusions and recommendations

6.1 Conclusions ……..…. 77

6.1.1 Floatability of water droplets ……..…….. 77

6.1.2 Oil decomposition process ……...…….. 78

6.2 Recommendations for future work ……..…. 79

References ……..…. 81

Appendix A Modelling of water droplets

A.1 SDS droplet images ……..…. 88

A.2 (SDS and NaCl) droplet images ……..…….. 97

A.3 (SDS and NaCl) at low pH droplet images ……... 107

Appendix B MATLAB – Edge detection code …… 118

List of Figures

Figure 2.1. Interfacial configurations for axisymmetric fluid bodies in a gravitational field: (a) pendant drop, (b) sessile drop, (c) submerged holm meridians ……... 10

Figure 2.2. Three phases α, β, γ, in a three-dimensional scheme of angles positions between locally planar interfaces, which meet the three-phase line …….. 11

Figure 2.3. Neumann's Triangle that satisfy the equilibrium configuration in a three phases system ……..……. 12

Figure 2.4. Surfactant structure and interfacial activity ……..…. 14

Figure 2.5. Schematic diagram showing hydrogen bonding in water and the formation of a cage-like structure is surrounding an inorganic ion such as Na^+ ……..…. 16

Figure 2.6. Illustration of a floating sphere describing the various parameters and angles ……... 20

Figure 2.7. Single cylinder floating at the interface between two fluids ….. 21

Figure 2.8. Illustration of parameters involved in the floating of the marble 22

Figure 2.9. Graphic of a generic liquid lens (A) floating on a sub fluid phase (B) surrounded by vapour (C). The contact angles θ_1, θ_2, and θ_3 are defined from the horizontal …… 24

Figure 2.10. Diagram of a water droplet on oil surface. The three contact angles are arranged according to Neumann's triangle …….. 26

Figure 2.11. Water droplets at different volumes on vegetable oil surface 27

Figure 2.12. Reaction efficiency on Fenton's Reagent under pH influence 33

Figure 2.13. pH profile of Fenton reactions …… 33

Figure 3.1. (a) Example of Pendant drop method utilised to estimate the interface tension between phases. (b) Pendant bubble …….. 47

Figure 3.2. ADSA software to measure surface tension ……..…….... 47

Figure 3.3. Measurement of solutions' densities using an Anton Paar Densimeter ……..….. 48

Figure 3.4. Deposition process of the water droplet ……..……..…. 50

Figure 3.5. Edge detection to estimate a fit droplet shape ……. 51
Figure 3.6. Edge profile of water droplet by applying polynomial function 52
Figure 4.1. Modelling procedure to obtain contact angle between water droplet and liquid interfaces; and droplet size ……... 55
Figure 4.2. Image cropped with the droplet in contact with the oil surface 56
Figure 4.3. Program code and image inputted for fitting-edge detecting using MATLAB ……..…. 56
Figure 4.4. Edge of droplet detected by MATLAB ……... 57
Figure 4.5. Excel profile data of droplet obtained from MATLAB ……. 57
Figure 4.6. Fitted-edge of a droplet by applying a polynomial function model …….. 58
Figure 4.7. Water droplets containing SDS at different volumes (in μL) ….. 60
Figure 4.8. Variation of contact angle at different size of water droplets containing SDS ……..…. 61
Figure 4.9. Water droplets containing a mixture of SDS and Sodium Chloride at different volumes ……..…. 62
Figure 4.10. Variation of contact angle at different size of water droplets containing a mixture of SDS and electrolyte ……. 63
Figure 4.11. Water droplet shapes containing with SDS and 3.5% NaCl at low pH at different volume ……... 65
Figure 4.12. Variation of contact angles at different sizes of water droplets containing a mixture of SDS and electrolyte with low pH ……... 66
Figure 4.13. Variation of contact angle at different size of water droplets containing a mixture of SDS and electrolyte. The maximum volume of a stable droplet is less than 9 μL ……..…. 67
Figure 5.1. No reaction occurs inside the droplet in presence of peroxide with SDS, TiO_2 and $Fe_2(SO_4)_3$ solution at low pH ……..... 70
Figure 5.2. (a) Water droplet in presence of SDS, peroxide, NaCl, HCl, TiO_2 and $FeSO_4$. **(b)** Water droplet in presence of SDS, peroxide, NaCl, HCl, TiO_2 and $FeSO_4$. Reaction occurred from the bottom of water droplet. **(c)** Water droplet contents mixture of SDS, TiO_2, H_2O_2 and $FeCl_3$. **(d)** Water droplet in presence of SDS, peroxide and TiO_2 ……..……..... 71
Figure 5.3. (a) Enzyme and soil droplets sunk at the bottom of the glass

container. **(b)** Water droplet with enzymes only, after three days of reaction 72

Figure 5.4. (a) Droplet of enzyme solution with SDS and soil, first time deposited. (b) Droplet of enzyme solution with SDS and soil, after 5 days of reaction. (c) Droplet of enzyme solution with SDS and soil, after 6 months of reaction ..…….. 74

Chapter 1

Introduction

1.1 Background to the study

Ecological impacts as a result of oil derivatives exposure in the environment have arisen during this century. Oil derivatives compounds are classified as hazardous; once it has stayed in contact with the environment (Grzechulska, Hamerski et al. 2000) (Rubio, Souza et al. 2002). In particular the most significant groups of contaminants in the marine environment are oil and grease. These groups contain many compounds, which can be present in varying proportions depending on the nature of the material (Tong, Goh et al. 1999).

Derived from diverse sources, components of oil and grease range from crude petroleum and industrial derivatives to edible oils and fats and their oleo-chemical derivatives (Rubio, Souza et al. 2002). Due to lower biodegradability, the main contaminants of concern are oil and grease originating from petroleum (i.e., derived from fossil fuels) and their derivatives which have found wide industrial uses. Being composed predominantly of aliphatic and aromatic hydrocarbons or derivatives of long chain hydrocarbons, the densities of crude oil and petroleum products are less than that of water.

One of the most difficult and dangerous situations with hydrocarbon contamination is oil spillages. In this case, hydrocarbon can spread quickly on water surface and seriously compromise the marine environment. For instance, the Alaskan oil-spill accident in 1989 severely damaged the environment for more than two decades. This was caused by the spillage of 200,000 barrels of crude oil from the oil tanker *Exxon Valdez* in Prince William Sound, Alaska (Wolfe, Hameedi et al. 1994) (Leahy and Colwell 1990). A similar situation occurred in the Gulf of Mexico in 2010, where the

Deepwater Horizon drilling rig released oil into the ocean. It was considered the largest man-made disaster, which costs BP around 60 billion dollar in damages (Kostka, Prakash et al. 2011).

The oil-spills can remain floating on the water surface and drift along with surface currents and wind. Volatile components evaporate at rates depending on vapour pressure and mass-transport conditions. As oil spreads, physical and chemical properties are modified or altered depending on chemical reactions with oxygen, sunlight and water as well as with micro-organisms. The composition of oil from oil-spills not only reflects the oil's origin but also the duration of exposure and the environmental conditions (Tong, Goh et al. 1999).

In this thesis, floatability is defined as the ability of a fluid droplet or solid object to stay on the surface of another liquid (Snir 1991). Hence, oil bodies can naturally float on water surface due to lower density (Langmuir 1933). On contrast, water droplets do not float on oil in normal conditions. In most cases, a water droplet will sink in oil due to higher density. Recently, researchers at Curtin University have discovered that water droplets, in a very narrow condition, can float on an oil surface. Different oils including both mineral and vegetable oils were assessed. The outcomes have shown that vegetable oil, with density of 90% water density, could support a water droplet up to 170 µL (Phan, Allen et al. 2012). On the other hand, pure mineral oils (hexane, octane and decane) were less successful because of the lower densities (Wang, Hollebone et al. 2003).

In this case, the floating water droplet can be used as a new method to treat oil spillages. The droplets can contain oil decomposing reagents and then be applied to oil-spills. The systems are particularly important for applications in the oil industry, and will be part of this project alongside testing for oil decomposition methods. Nevertheless, the behaviour of the droplets during oil decomposing process remains unknown. In addition, the "floatability" of a heavier liquid droplet on the surface of hydrocarbons surface and the action of chemicals reactions in the degradation of oil, has not been explored. This

study addresses the problems by investigating the floating droplet with different decomposing reagents.

1.2 New phenomena

The present study is significant for new advancement towards environmental and industrial problems. First, it will potentially provide new information that could be widely used for industrial processes where it could use natural forces to support a heavier liquid on top of a lighter liquid. Additionally, it could provide new developments in chemical and petroleum engineering studies as well.

This project intends to investigate experimentally the floatability of a water droplet on an oil surface such as paraffin oil. Subsequently, the oil decomposition is investigated by using a combination of innovative methods. The result will lead to new knowledge and a wide contribution in solving environmental problems such as oil spillages and biodegrading process.

Previously, the floatability of water droplets was tested on vegetable oil, where the large size of droplets floating on the oil surface was reported (Phan, Allen et al. 2012). However, little information can be found related to floatability on a hydrocarbon interface. Therefore, this study will evaluate the floatability of water droplets by performing it with a density of the heavier liquid similar to the seawater (density of 1022 kg/m^3) on a commercial paraffin oil (density of 830 kg/m^3), which has a density and chemical compounds similar to hydrocarbons (Phan 2014).

One potential application of the phenomena is employing small water floating droplets on immiscible oil (such as fatty waste, oil sands tailings, or oil spillages floating in the ocean) to facilitate biodegradation in open sea. The efficiency of oil biodegradation depends on the level of dissolved oxygen, water/oil interfacial area, and bacterial/nutrient availability.

Moreover, it could be relevant as an alternative method for the usage of dispersants to disperse oil spillages in the ocean to increase the oil/water contact area as well as concentrated/selected bacterial population.

1.3 Objectives

The aim of this study is to determine the floatability of water on paraffin oil, which has similar properties to hydrocarbon oils. This research pursues the following objectives:

1. Determination of the influence of physical properties on the floatability of water droplets on paraffin oil surface at:

    - Variation of the water droplet volume for stability on oil surface
    - Variation of the contact angle to determine the stability of water droplets on oil surface
    - Variation of the surfactants and mixtures with electrolytes and changes in pH, to modify the interfacial tensions

2. Determination of the influence of different techniques such as photo-catalytic, chemical and biological processes, which can interfere with the floatability of the water droplet.

1.4 Format of thesis

Chapter 2 presents a literature review of the influence of the contact angles and interfacial tension in the stability of water droplets on liquid-liquid interfaces. A review of different techniques approachable for oil decomposing applications is included. Also, the available theoretical analyses and limitation of these theories are included.

The methodology and materials used for experimental works are presented in Chapter 3.

In Chapter 4, the theoretical analysis is developed for contact angles of water droplets using surfactants at oil/water interfaces. The experimental data of contact angles at different concentrations of surfactant and with other chemical combinations is determined fitting procedure, which is also used to obtain the volume of water droplets and contact angles measurement between the interfaces and parameters of the systems.

Evaluation of chemical and biological reagents techniques, especially on paraffin oil which can influence in the reduction of the oil by changes in droplet shape, is presented in Chapter 5. Verification of oil reduction through the approach of combined chemicals compounds is also included. Chapter 6 concludes the study with recommendations for further work.

Chapter 2

Literature Review

This literature review explores the dominant concepts of the research study. The scope of this literature review is expanded to include previous studies that examine the understanding of capillary phenomena, interfacial tension and other parameters that are involved in the floatability of water droplet on oil surface. The current models on the floatability of droplets on a liquid surface are also included. In addition, the oil decomposition processes are reviewed as a method that promotes a further biodegradation of organic contaminants into less complex and less harmful intermediate products.

2.1 Interfacial phenomena

The interface between liquid/liquid or liquid/air is governed by different phenomena. While the interface can be described by mathematical equations, the boundary conditions of these equations are constrained by the contact angles.

2.1.1 Capillary phenomena

Several kinds of phenomena have arisen from the basic fundamentals of capillary. Throughout time, application of the fundamentals of capillary have come from (a) the need to exploit secondary and tertiary methods for enhanced oil recovery (EOR) (b) space laboratories' experiments where near-zero gravity conditions is possible with long periods of time involved, and (c) numerical model which have enabled the prediction of systems in a gravitational field, especially those with an axis of symmetry (Boucher 1980).

A relevant characteristic in capillary systems is represented by those in which the curvature of a liquid/fluid interface is important. Often a constraining solid is also present, which together with the interfacial tension

and the hydrostatic pressure drop across the interface, determines the interfacial configuration. There is a number of important applications of capillary phenomena. For instance, they form the basis of fundamental measurements, e.g. interfacial tensions. Moreover, due to its scientific and engineering relevance to mineral floatation, to the flow and drainage of fluids and to adsorbent/absorbate interactions in porous media continuous solids or compacts. And finally, their prevalence plays a significant role in natural systems, such as biological or otherwise (Boucher and Evans 1975, Boucher and Kent 1978, Boucher and Jones 1982).

The condition for mechanical equilibrium of an interface separating two immiscible phases given by the Laplace equation:

$$\Delta P = \gamma J \qquad (2.1)$$

where, ΔP is the differential of local hydrostatic pressure in the bulk phases, and $\gamma$is the interfacial tension; whilst the mean curvature *J* of an interface, which has principal radii R_1 and R_2, is given (Boucher and Evans 1975, Boucher and Kent 1978, Boucher and Jones 1982):

$$J = R_1^{-1} + R_2^{-1} \qquad (2.2)$$

Generally, laws of capillarity are constituted by certain expressions that link interfacial tensions with other physical quantities (Brochard-Wyard, de Gennes et al. 2003).

From diverse approaches, Young and Laplace recognised that a liquid/fluid interface behaves mechanically as though in tension, with what is now called the interfacial tension acting in the surface of tension (Brochard-Wyard, de Gennes et al. 2003) (Boucher 1980). Simple treatments of capillarity require only three intrinsic properties for a system of two fluid phases, the densities of each fluid and the interfacial tension, which is the intensive quantity associated with interfacial areas. By combining these two properties it leads

to the third property, a one-dimensional capillary constant (a scaling factor). So, the surface contribution to the free energy of the system is then involved in the interfacial tension and the area in contact for each interface (Boucher 1980).

2.1.2 Interfacial tension

The main effect of interfacial tension (IFT) in a system is to minimise its interfacial area, from energy or tensile forces. This tendency for interfacial contraction is the reason that a small drop of one fluid in another will (gravitational effects presence are small) be spherical, which minimises the drop area for a given drop volume. However, it has been highlighted that the energy and force arguments lead not only to qualitatively features, but also influence the quantitative value of interfacial tension (Miller and Neogi 2007).

The molecular basis of surface and interfacial tension are explained by the short range attractive forces existing between the neighbouring molecules. Consider an oil-water system with a distinct interface separating the bulk oil and water phases (Miller and Neogi 2007) (Venkataraman 2007). The molecules in the bulk have equal and balanced attractive Vander Waals forces in all directions, while the molecules at the interface have unbalanced forces of attraction as they are exposed to both phases. This inequality in the Vander Waals forces pulls the interfacial molecules toward the interior of the liquid. As many molecules leave the interface to the bulk liquid, the interface tends to contract spontaneously. For this reason, the droplets of liquid and bubbles of gas tend to adopt a spherical shape, because this shape reduces the surface free energy. Surface free energies are generally described in terms of tensile forces that contribute to stress by acting parallel to the surface or interface. Surface or interfacial tension is generally defined as the force per unit length acting in a surface, or the free energy required creating a new surface area. There is no fundamental distinction between surface and interface although it is traditional to describe the boundary between two phases; one of which is gaseous as surface and

the boundary between two non-gaseous phases as an interface (Hartland 2004).

The magnitude of surface or interfacial tension decreases significantly when a surface active molecule is accumulated at the interface. The adsorption of surface active agent (surfactant) at the interface results in an enlarge force acting against the normal interfacial tension. This feature is the surface or interfacial pressure which tends to expand the interface (Venkataraman 2007) (Miller and Neogi 2007).

2.1.3 Axisymmetric fluid bodies

In most realistic cases, fluid bodies are bounded by the axisymmetric interfaces, in which the axis of symmetry is axis of body forces, such as gravity. The axisymmetric capillary systems where surface curvature changes with vertical position due to gravitational effects, can be replicated under laboratory conditions. This study will be limited to the axisymmetric fluid bodies in a gravitational field, especially pendant drops.

Several kinds of standard interfaces have been classified by Boucher (1980). In all cases, the general Young-Laplace equation, equation 2.2, is reduced to two-dimensional systems. Moreover, the equilibrium and stability – instability characteristics of capillary systems can be realised by the application of these methods (Boucher 1980). Bond number (Equation 2.3) establishes the relative effects of gravitational and surface effects, where γ is the interfacial tension and Δz is a characteristic length of the system. ρ and g retain their usual meanings of density and acceleration due to gravity, correspondingly (Boucher 1980).

$$B_O = \Delta\rho g(\Delta z)^2 / \gamma \qquad (2.3)$$

Several kinds of meridians of a curvature can be defined by a series of three ordinary differential equations (2.4, 2.5 and 2.6) from the Young-Laplace equation, which describe the shape of a range of classical capillary systems.

$$\frac{d\theta}{dS} + \sin\left(\frac{\theta}{X}\right) = 2(\lambda H - Z) \qquad (2.4)$$

$$\frac{dX}{dS} = \cos\theta \qquad (2.5)$$

$$\frac{dZ}{dS} = \sin\theta \qquad (2.6)$$

X and *Z* are coordinates at distance *S* along the surface of the drop with a contact angle of θ. The meridian angle θ at (*X, Z*) is defined as $\tan^{-1}(dZ/dX)$. The parameter λ takes values $\pm$ 1 depending on the meridian shape required, and $H = \Delta P^0/2$, i.e. the shape factor H for most shapes takes the value equal to one-half of the pressure difference across the liquid/fluid interface at the starting position (Boucher 1980) (Morita, Carastan et al. 2002).

Overall, from the existing different types of interfacial configurations, the pendant drop method (Figure 2.1) is chosen to evaluate the interfacial tension between the systems in this study.

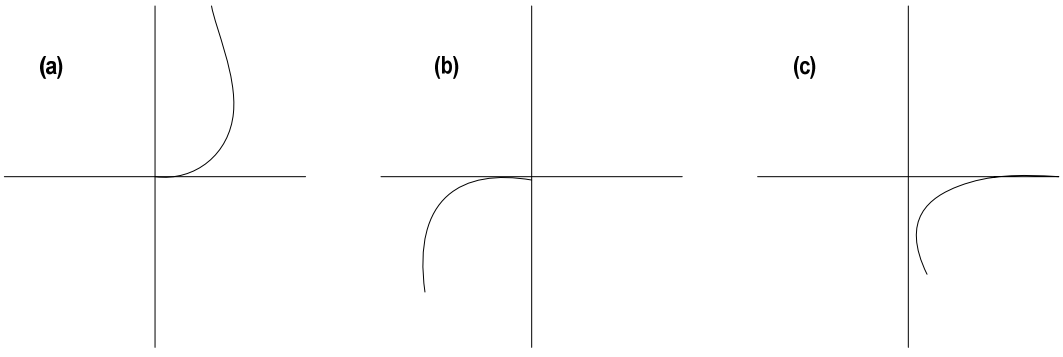

Figure 2.1. Interfacial configurations for axisymmetric fluid bodies in a gravitational field: (a) pendant drop, (b) sessile drop, (c) submerged holm meridians. Adapted from (Boucher 1980).

2.1.4 Contact angles

By considering the simultaneous equilibrium of three phases α, β, γ (considered as a phase only for this instance), one can see that there are circumstances in which the phases meet in a line of three-phase contact. Macroscopically, this set of points in which they meet is one-dimensional and locally linear, where there is an excess free energy per unit length, or line tension, associated with the three-phase line. As a result, on this line of three-phase contact, the three-dimensional structure at the molecular level can be noticeable with its structure and tension related (Rowlinson and Widom 1982).

Many studies have been configured extensively to determine the contact angle between fluid/fluid interfaces on a solid surface, from developing models to demonstration through experimental data (De Gennes 1985) (Brochard-Wyard, de Gennes et al. 2003). On the other hand, for fluid/fluid/fluid systems, theoretical and experimental reports are quite limited (Burton, Huisman et al. 2010) (Phan, Allen et al. 2012).

In this instance, this investigation will focus on a three fluids configuration system. Thus, the contact angle where that these three-phases should meet a macroscopic condition for the existence of such a line contact, as it shown in Figure 2.2. Also, the final contact angle between the interfaces may predict the final shape and spreading area of the water droplet on oil surface in air medium.

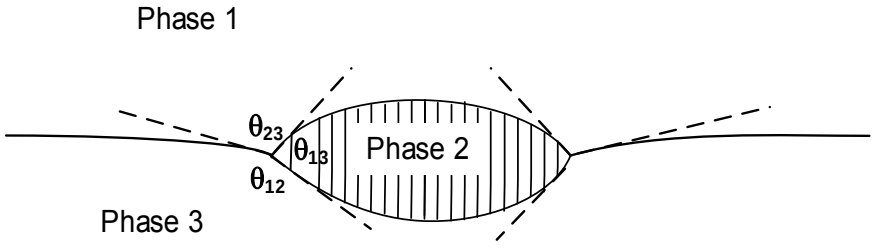

Figure 2.2. Three phases 1, 2, 3 in a three-dimensional scheme of angles positions between locally planar interfaces, which meet the three-phase line (Rowlinson and Widom 1982).

It has been recognised that the three interfacial tension magnitudes form the sides of a triangle, they satisfy the triangle inequalities.

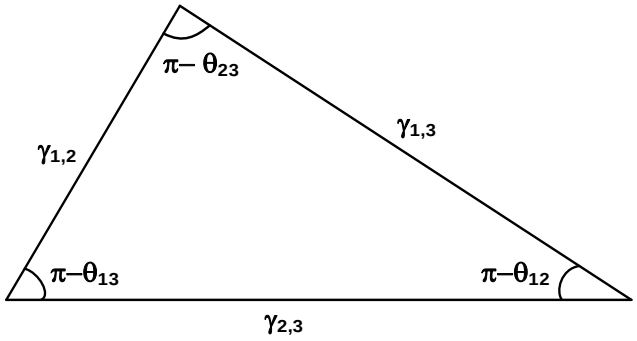

Figure 2.3. Neumann's Triangle that satisfy the equilibrium configuration in a three phases system (Rowlinson and Widom 1982).

Finally, these are the conditions for the equilibrium of three phases at a line of mutual contact. The three inequalities in Figure 2.3 may be replaced by the single condition that the largest of the three tensions be less than the sum of the two smaller. When this condition is met, the equilibrium configuration of the three phases is formed (Rowlinson and Widom 1982) (Luangpirom, Dechabumphen et al. 2001).

It should be noted that when the largest of the three two-phase tensions is greater than the sum of the two smaller, there is no longer a line of three-phase contact. Instead, the equilibrium configuration of the three phases is that in which one of them (the one whose interfaces with the other two are those of lowest tension) spreads at and completely covers the high-tension interface. The relation of the three tensions in this case of spreading (complete wetting), vice versa that the largest is the sum of the two smaller, is called Antonow's rule (Rowlinson and Widom 1982).

With changing thermodynamic state the system may undergo a transition from the condition in which one phase wets the interface between the other two and in which the three tensions satisfy Antonow's rule, to the condition in which the three phases meet at a line of three-phase contact with

measurable contact angles and in which the three tensions satisfy the relations of the Neumann triangle (Figure 2.3). This scenario is called the Cahn transition (Rowlinson and Widom 1982).

2.2 Changes in interfacial tension

The action of different chemicals concentration in water can change interfacial tensions (with oil or air) and consequently affect the capillary action and contact angles. Surfactants, or surface active agents, can dramatically reduce the interfacial tensions. In addition, the electrolytes, pH and colloids can also affect the interfacial tension.

2.2.1 Interfacial activity of surfactants

Surfactants are widely used in a large number of applications because of their ability to change the surface or interface properties. These molecules (Figure 2.4) have a polar (hydrophilic), water-soluble group attached to a nonpolar group. The hydrophobic or nonpolar group is usually a hydrocarbon chain with neutral charge. On the other hand, the hydrophilic group can be any polar groups. They are more often used as emulsifiers/ de-emulsifiers affecting the emulsion stability. These materials get adsorbed at the interface and can effectively change the interfacial properties, including the interfacial tension and viscoelastic behaviour (Schramm 2000) (Hartland 2004). Surfactants can significantly decrease the interfacial tension between crude oil and water. Hence they are employed to lower the capillary forces, facilitates oil mobilisation and enhances oil recovery (West and Harwell 1992).

Surfactant solutions exhibit dynamic interfacial tensions where the interfacial tension is dependent on the rate of interface formation and by the diffusion rate of surfactants from the bulk to the interface. Static or equilibrium interfacial tension is approached at long contact times when the interface reaches saturation by adsorption of sufficient surfactant molecules (Hartland 2004). In addition to synthetic surfactants, many

natural-occurring chemicals can be very strong surfactants. For instance, it is well-known that asphaltenes in crude oils can be extremely resilient surfactants (Mullins 2008).

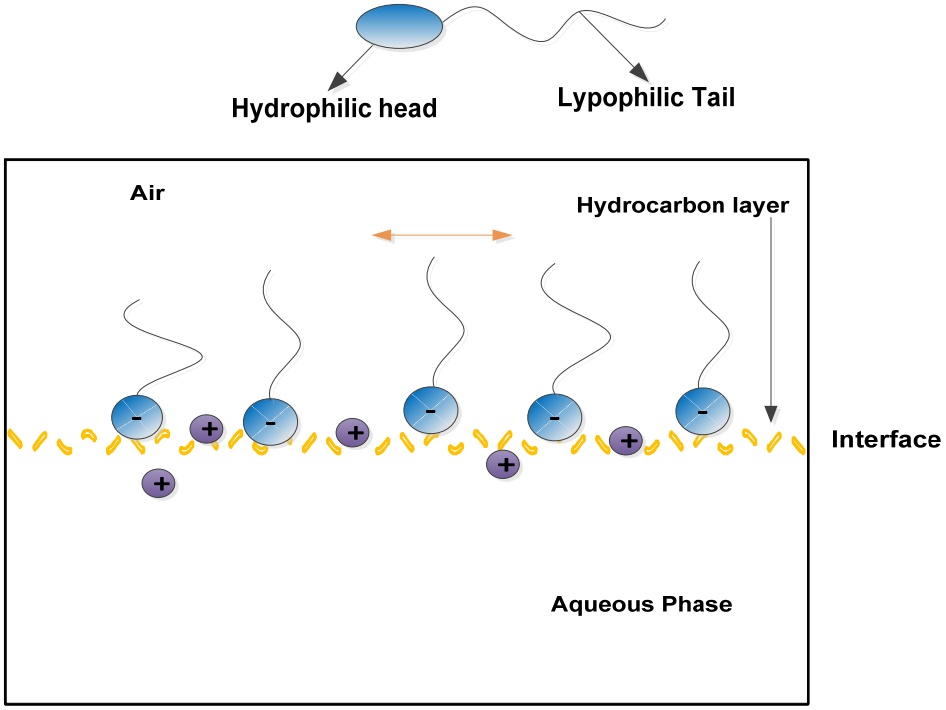

Figure 2.4. Surfactant structure and interfacial activity.

In a system of two immiscible phases, a surface-active agent can strongly adsorb into the oil/water and air/water interfaces, which is the main focus of this study. Certain surfactants such as sodium dodecyl sulphate expectedly orient by itself, with the hydrophilic group pointing toward the water and the hydrophobic group toward the oil phase (see Figure 2.4). When the surfactant molecules enter in contact with water and/or paraffin oil molecules, the interaction across the interface is now between the hydrophilic group of the surfactant and water molecules on one side of the interface; and between the hydrophobic group of the surfactant and paraffin oil on the other side of the interface (Venkataraman 2007) (Aveyard, Binks et al. 1985) (Aveyard, Binks et al. 1987). Since these interactions are now much stronger than the original interaction between the highly distinct paraffin oil and water molecules, the tension across the interface is considerably reduced by the presence there of the surfactant.

Since air consists of molecules that are mainly nonpolar, surface tension reduction by surfactants at the air-aqueous solution interface is similar in many respects to tension reduction at the oil-water interface (Rosen and Kunjappu 2012) (Miller and Neogi 2007).

2.2.2 Influence of electrolytes in interfacial tension

Electrolyte solutions are characterised by the long-range nature of charge-charge Coulombic interactions, and to the fact that many common solvents are highly polar and, as in the case of water, may present strong hydrogen-bonding interactions between solvent and solute molecules in dissociation (Patel, Paricaud et al. 2003) (Garvey and Robb 1979).

Solubility is inversely proportional to the activity coefficient (a thermodynamic factor for deviations from ideal behaviour in a mixture of chemicals), which can affect the final decomposition of organic compounds, especially petroleum hydrocarbons, in the marine environment by processes such as adsorption, evaporation and bioaccumulation. Differences in the behaviour of oil-spills are thus expected in fresh, brackish and marine waters. The effect is also used to facilitate the separation of organic compounds from aqueous solutions (Xie, Shiu et al. 1997).

When inorganic salts are present in the aqueous phase, the water molecules form a cage-like hydrogen bonded structure around the salt ions, Figure 2.5. At the interface, water molecules are in contact with another phase and the hydrogen bonding is disrupted, creating a higher energy around the ions. As a result, the salts are depleted near the interface and the surface excess concentration of salts is negative (Zylyftari, Lee et al. 2013).

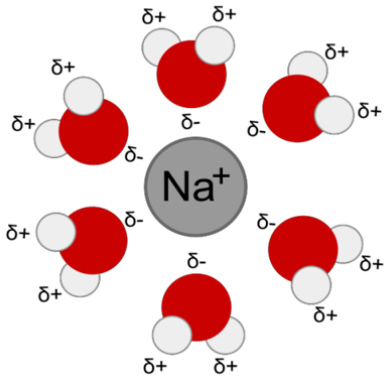

Figure 2.5. Schematic diagram showing hydrogen bonding in water and the formation of a cage-like structure is surrounding an inorganic ion such as Na^+.

The influence of ions on surface tension is relatively small in comparison with surfactants. The influence of ions on adsorption layer of surfactants is more profound and has been investigated extensively in the literature. Electrolytes, such as Sodium Chloride (NaCl), can enhance the surface tension reduction due to synergistic adsorption between ions and surfactant (Aveyard, Binks et al. 1985). The synergistic effect is applicable to all the involved interfaces, both air/water and oil/water (Lucassen-Reynders 1981). It has been well accepted that the addition of salt reduces the electrical repulsion between surfactant head groups within an adsorbed monolayer, thus reducing the effective value of the cross-sectional area of the polar head group and increasing the packing ratio (Aveyard, Binks et al. 1985) (Lima, Melo et al. 2013).

In the presence of NaCl salt, the critical micelle concentration and the surface tension of the surfactant solution decrease, and also the salt lowers the solubility limit of the surfactant. The solubility of surfactant decreases with the addition of salt and therefore makes it less ionised. Hence, the surfactant molecules adsorb strongly at the oil-water interface which reduces IFT. Such effects have been employed for enhanced oil recovery (Bera, Mandal et al. 2013).

Another important aspect, related with the influence of electrolytes on oil/water interface, is the salting out effect. Organic compounds can be less miscible in aqueous salt solutions, such as seawater, than in pure water (Xie, Shiu et al. 1997) (Mackay and Shiu 1975). Therefore, solubility of alkanes in water is of interest in environmental control, so prediction of all hydrocarbon contents in the water phase is relevant (Patel, Paricaud et al. 2003). Studies of the salting-out effects in partially miscible liquids are, however, scarcer.

Dissolve salts dramatically affect the phase equilibrium of aqueous solutions. This can become an advantage in processes such as salting out, where the removing of an organic solvent from an aqueous solution is carried out by adding salt. Thus, this will depend on the nature of the ionic and organic compounds (Patel, Paricaud et al. 2003).

Finally, by increasing concentration of salt, an increment of water density can be observed, which is an important factor in determining the droplet floatability.

2.2.3 Influence of pH in interfacial tension

The pH of the aqueous phase affects the dissociation of acidic and basic components present in a crude oil. It may also change when separating the surface active components between the two phases (Zylyftari, Lee et al. 2013). The dissociation of acidic and basic components present in crude oil can be represented as:

$$HA \leftrightarrow H^+ + A^- \qquad (2.7)$$

$$BOH \leftrightarrow B^+ + OH^- \qquad (2.8)$$

Where *HA* and *BOH* represent acid and basic components present in crude oil, $\boldsymbol{A^-}$ is the surface active ion, and $\boldsymbol{H^+}$ is the hydroxyl ion (Equation 2.7). When the pH of the aqueous phase is high, the concentration of hydroxyl ion is low and according to Le Chatelier's principle, the above reaction proceeds

in the forward direction. This favours an increase in the surface active ions and a consequent decrease in interfacial tension of the system. Similarly, the basic components present in crude oil ($\boldsymbol{B}^{+}$) causes the IFT to drop at lower pH values (Equation 2.8) (Zylyftari, Lee et al. 2013).

A reduction in IFT values between oil solutions of water-insoluble fatty acids and aqueous solutions was observed with increasing pH due to dissociation. Similarly, the dissociation of water-insoluble bases results in lower IFT values at low pH (Berry and Mueller 1994). The reorganisation of the interfacial film at the crude oil/water interface is fast when the pH is less than 5 because of less partitioning of surfactants ions into the aqueous phase and less dissociation at the interface (Zylyftari, Lee et al. 2013).

On the other hand, the addition of sodium dodecyl sulphate solutions of sufficient hydrochloric acid to reduce the pH to 4.2 caused a decrease in interfacial tension of 5 to 4 dynes/cm in the concentration range 5×10^{-3} to 8×10^{-4} M sodium dodecyl sulphate. Some researchers have concluded therefore that at pH 4.2 some hydrogen ions are adsorbed at the interface (Cockbain 1954).

The influence of pH in the experimental samples can create changes in the droplet shape. Some of the chemical reactions need to be in an acid or a basic medium that could influence the drop and optimise its shape. This can lead to a major spreading area and stability for the droplet to float on the oil surface.

2.3 Previous modelling of a floating object on liquid surface

The above phenomena can be combined to describe the floatability of a single object, either solid or liquid, on a fluid/fluid interface. All of these models mathematically connect the contact angles and interfacial tensions (Phan, Allen et al. 2012). Currently three models for floating objects on liquid surface are available, namely: (1) solid object on liquid, (2) lighter liquid droplet on a heavier liquid and (3) heavier liquid droplet on a lighter liquid. It

should be noted that in the first and third models, the combination tension forces and deformation is used to balance against gravity.

2.3.1 Floatation of a solid object on liquid

The surface tension, in capillary rise, can work against gravity and support a solid body floating in a water surface, which has been noticed centuries ago (Finn 1999). Experimentally, spherical particles (Extrand and Moon 2009), cylinder (Vella, Lee et al. 2006) and liquid marbles (Bormashenko, Bormashenko et al. 2009) have been floated on water surface.

The buoyancy of small polymer spheres in a variety of lighter liquids was studied (Extrand and Moon 2009). A sphere composed of poly (tetrafluoroethylene) (PTFE) or polycarbonate (PC) was placed in a clear container, and liquid (water, formamide, or ethylene glycol) was slowly added. As capillary forces aided buoyancy, it allows some of the sphere to float. A combination of greater disperse phase or lyophobicity, and surface tension enabled water to suspend larger spheres than the other two liquids. As compared to PTFE, a smaller density difference between water and PC permitted much larger PC spheres to be buoyed. The largest PTFE that floated was approximately 5 mm in diameter versus 10 mm for PC. The smallest sphere floated the highest and had the smallest meniscus. Furthermore information and details of this study can be found in Extrand and Moon (2009) paper.

The following represents a simple analytical expression that allowed the estimation of the approximate values of maximum sphere diameter ($2R_{max,a}$) that can be suspended in this case (Extrand and Moon 2009),

$$2R_{max,a} = \left[\frac{24\gamma}{(\rho_S-\rho_l)g}\frac{sin^2\frac{\theta_a}{2}}{2+3cos\frac{\theta_a}{2}-cos^3\frac{\theta_a}{2}}\right]^{1/2} \qquad (2.9)$$

Where, ρ_S and ρ_l are the density of the sphere and the liquid, and γ is the surface tension of the liquids, respectively (see Figure 2.6).

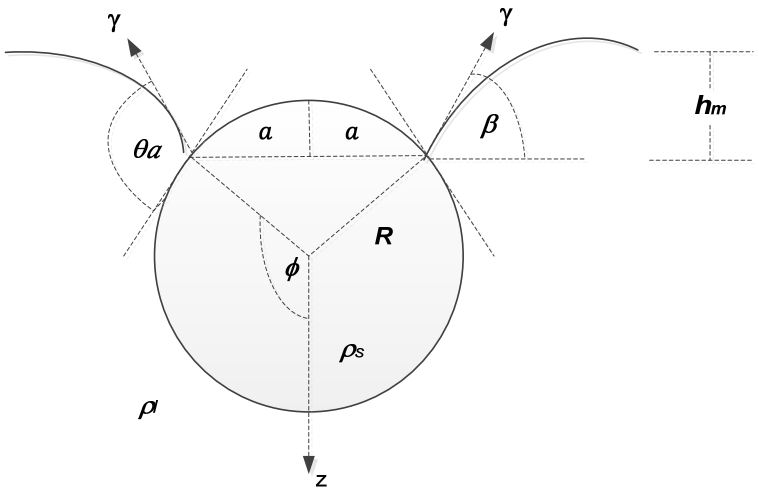

Figure 2.6. Illustration of a floating sphere describing the various parameters and angles.

Another study (Vella et al., 2006) demonstrated the equilibrium flotation of a two-dimensional cylinder at an interface between two fluids. It has been showed that the surface properties of an object can significantly affect its load-supporting properties. Conditions on the density and radius of these objects for them to be able to float at the interface were quantified. In particular, the role played by the contact angle in determining these conditions was analysed in details. For cylinders with a small radius range of between 1.5 and 3.6 mm, it has been found that the maximum density is independent of the contact angle. This is fundamental different to floating spheres, where the contact angle plays a dominant role in determining the particle radius.

Considering the equilibrium of a cylinder of density ρ_s, radius r_o, and contact angle θ at the interface between two fluids of density ρ_A and ρ_B, with $\rho_A < \rho_B$, as shown in Figure 2.7. The interface has a tension, γ_{AB}, associated with it. Balancing the weight per unit length of the cylinder with the restoring forces arising from surface tension and the Archimedes up thrust of fluid B on the object, the equilibrium requires (Vella, Lee et al. 2006):

$$\pi(\rho_S - \rho_A)r_0^2 g = 2\gamma_{AB} sin\phi + (\rho_S - \rho_A)r_0^2 g \left(-2\frac{h_*}{r_0} sin\,\psi + \psi - sin\,\psi\, cos\,\psi\right)$$

(2.10)

Here, the angular position of the contact line, ψ, the inclination of the interface to the horizontal, ϕ, and the height of the contact line above the under-formed interface, h_*, determine the position of the cylinder at the interface. The first term on the right-hand side of equation 2.10, is the vertical component of the surface tension acting on the cylinder. The second term is the vertical force provided by the Archimedean upthrust on the cylinder, which is equal to the weight of fluid B displaced by the hatched region (Vella, Lee et al. 2006). The reader is referred to the Vella et al. (2006) paper for more details of this study.

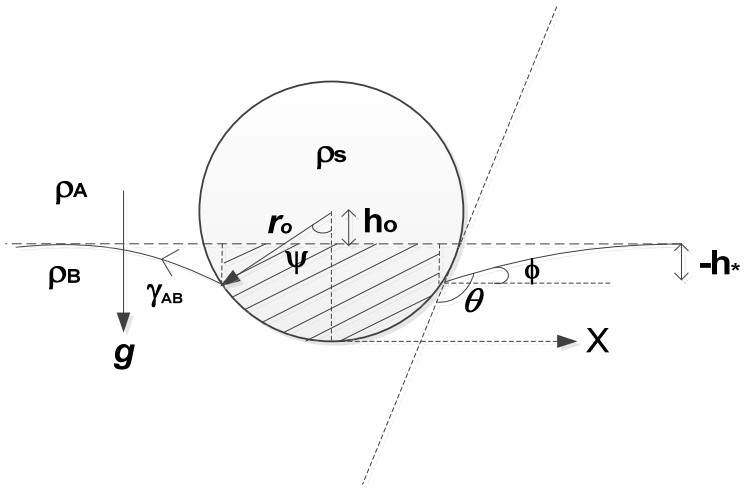

Figure 2.7. Single cylinder floating at the interface between two fluids.

Another relevant case of study was based on the flotation of liquid marbles containing NaCl solution. Comparison between experimental and theoretical values was estimated and reported for both critical density and marble sizes (Bormashenko, Bormashenko et al. 2009).

The liquid marbles containing NaCl solutions float until a certain critical concentration of the salt. The critical density of a NaCl solution ρ_{exp} allowing marbles of a certain volume to float has been estimated experimentally. On

the other hand, it could be calculated in the framework in which, floating of a marble of a radius R is governed by the interplay between surface tension and gravity (see Figure 2.8). Establishing that the maximum dimensionless density of a sphere that still floats on the water surface is given by

$$D^* \approx \frac{3}{4R_0^2}(1 - cos\theta) \qquad (2.11)$$

Where $R_0 = \frac{R}{l_{ca}}$, l_{ca} is the capillary length, $l_{ca} = \sqrt{\frac{\gamma}{(\rho_B - \rho_A)g}}$, γ is the surface tension at the A-B interface, ρ_A, ρ_B are the densities of phases A and B correspondingly; D* is the dimensionless density given by $D = \frac{\rho_M - \rho_A}{\rho_B - \rho_A}$, where ρ_M is the density of the marble. In this case, phase A is air, thus $\rho_B >> \rho_A$, θ is the contact angle. Thus, equation 2.11 implies:

$$\rho^* = \rho_w \frac{3}{2R_0^2} \qquad (2.12)$$

Where, ρ^* is the critical density of a NaCl solution allowing floating of the marble, and ρ_w is the density of water.

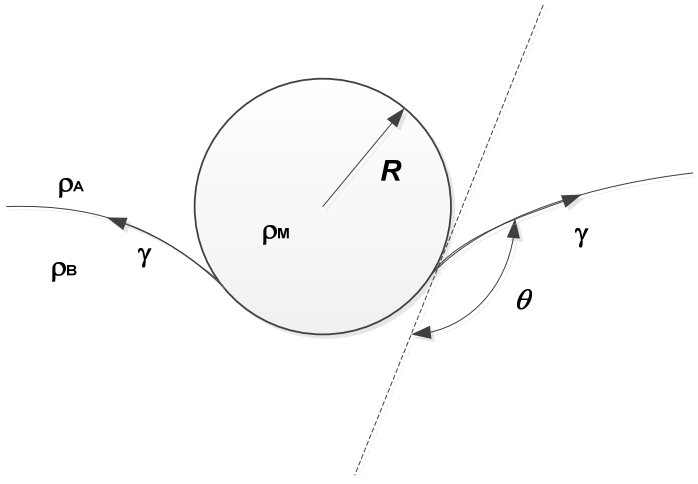

Figure 2.8. Illustration of parameters involved in the floating of the marble.

The relevant results found from experiments show that the maximum density corresponding to the maximum solubility of NaCl in water ρ = 1.23 g/cm^3. Therefore, drops with V < 105 μL will float under any achievable density of the NaCl solution. The reader is referred to Bormashenko et al. (2009) paper for further details and experimental pictures of the model.

2.3.2 Floatation of liquid lenses in a heavier liquid

In opposite of rigid bodies, a fluid droplet at the surface of another fluid has three deformable interfaces (those formed between the two fluids and when each of them are in contact with air) and variable contact angles. The equilibrium of three interface tensions at the contact line, if it exists, results in a unique combination of three contact angles, which form a Neumann's triangle (Buff and Saltsburg 1957). The interfacial interaction between three fluids has been investigated for an oil droplet spreading on water surface by (Langmuir 1933) and for a fluid droplet at the interface between two fluids by Princen (1963); and Princen and Mason (1965). Subsequently, numerical methods were applied to the liquid to identify the shape of such droplets (Burton, Huisman et al. 2010). In these instances, the liquid droplet is less dense than the supporting liquid, and gravity always plays a stabilising role in the system.

The main characteristic of this system is the formation of a floating liquid lens, where the lens resides between an upper and lower phase. By using the axisymmetric profiles of the three interfaces, they have been computed by solving the nonlinear Young–Laplace differential equation for each interface with coupled boundary conditions at the contact line. The nonlinear differential equation is because the curvature term contains products of derivatives of the surface profile, as follow (Burton, Huisman et al. 2010):

$$\Delta P = 2k_m\sigma - \Delta\rho g z \qquad (2.13)$$

where, $\Delta P = P_{in} - P_{out}$ is the pressure difference between the interior and exterior fluid, k_m is the mean curvature of the interface, σ is the surface tension at the relevant interface, $\Delta\rho = \rho_{in} - \rho_{out}$ is the density difference between the fluids, *g* is the gravitational acceleration, and *z* is the axial position of the interface, as it shown in Figure 2.9.

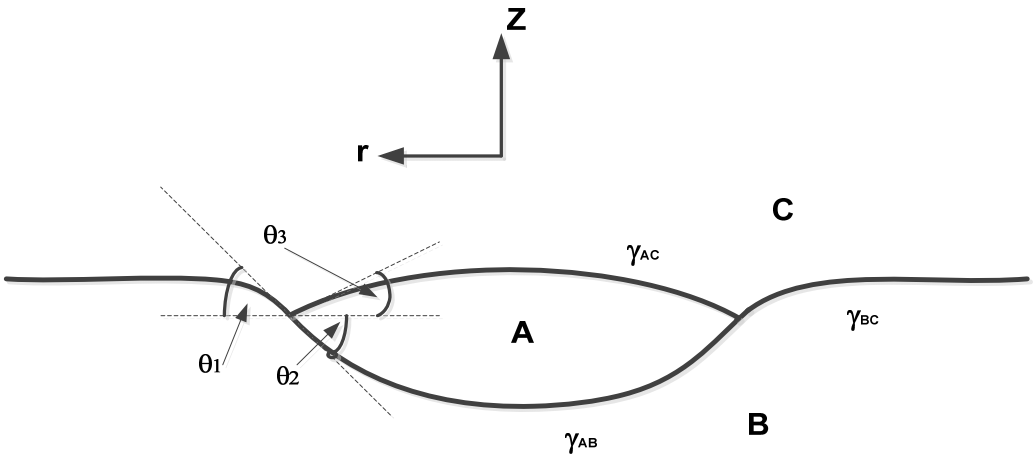

Figure 2.9. Scheme of a generic liquid lens (A) floating on a sub fluid phase (B) surrounded by vapour (C). The contact angles θ_1, θ_2, and θ_3 are defined from the horizontal.

Description of a numerical method was made and it was applicable to different kind of lens profiles. Results of the calculations were compared and analysed with optical photographs of various liquid lens systems. If surfactants are present, the sub phase surface tension must also be self-consistently determined. Additional information was provided for extracting characteristics features in the optical images to uniquely determine both parameters (Burton, Huisman et al. 2010).

The method gave good agreement with literature values for pure fluids such as alkanes on water and also for systems with a cationic surfactant (dodecyltrimethylammonium bromide), which showed a transition from partial wetting to the pseudo partial wetting regime. This technique is the analogy of axisymmetric drop shape analysis, applied to a three fluid system. The

effectiveness of this procedure has been verified for both pure fluids and systems containing surfactants (Burton, Huisman et al. 2010).

In summary, this model is focused on the equilibrium geometry of heavy alkane's liquid lenses on water under the influence of surface tension and gravity. Also, it shows the static geometry of such a system and the surrounding gas as well as three surface tensions associated with three separate interfaces. Moreover, this study compared experimental measurements of the geometry of liquid lens systems to the equilibrium shapes computed from the Young-Laplace equation.

2.3.3 Floatation of heavier liquid droplets in a lighter liquid

Another model was developed for a water droplet, with an up to certain volume V_b, depositing on vegetable oil surface. Floatation of the water droplets can be seen in Figure 2.11. The physical properties involved in the system were three densities (ρ_a, ρ_w and ρ_o) and three interfacial tensions (γ_{wa}, γ_{ow} and γ_{oa}), as fixed parameters. Numerical model focus on predicting the vertical force on water droplets as a function of droplet shape, as it shown in Figure 2.10 (Phan, Allen et al. 2012):

$$F = g[V_b\rho_w + (\pi r^2 h_3 - V_1)\rho_a - (\pi r^2 h_3 - V_2)\rho_o] \qquad (2.14)$$

Where r is the contact line radius; h_3 is the height of the "holm", V_1 and V_2 are the volumes of air/water and water/oil sections, respectively ($V_1 + V_2 = V_b$). These quantities are depicted in Figure 2.10. In equation 2.14, the first two terms account for gravity; while the last term accounts for the upward force that allow the floatability of the droplet on the oil surface.

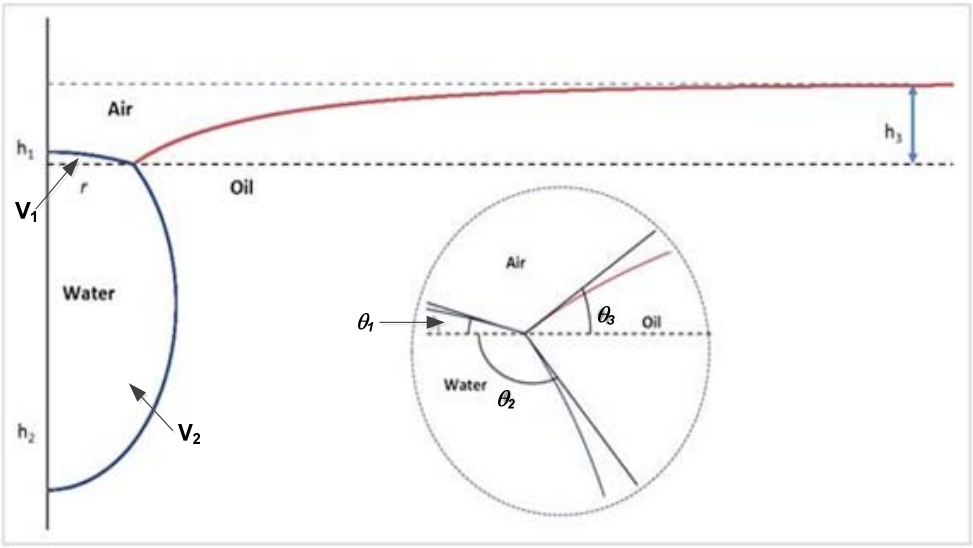

Figure 2.10. Diagram of a water droplet on oil surface. The three contact angles are arranged according to Neumann's triangle (Phan, Allen et al. 2012).

The numerical model first finds V_1, V_2, r and h_3 from the contact angles equations (see below).

$$\theta_1 + \theta_2 = \pi - \arccos\left[\frac{\gamma_{wa}^2 + \gamma_{ow}^2 - \gamma_{oa}^2}{2\,\gamma_{wa}\gamma_{ow}}\right] \qquad (2.15)$$

$$\theta_1 + \theta_3 = \arccos\left[\frac{\gamma_{oa}^2 + \gamma_{wa}^2 - \gamma_{ow}^2}{2\,\gamma_{oa}\gamma_{wa}}\right] \qquad (2.16)$$

The above two equations were derived directly from Neumann's triangle. As it can be seen, this model integrates the Young-Laplace equation along the three interfaces, from the initial points to the contact line, and matches three contact angles. The evaluated system was axis-symmetric; the air/water, oil/water, and oil/air interfaces are part of sessile drop, pendant drop, and "submerged helm", respectively.

Summarily, the model was verified with experimental data. The model also showed that the stability of the floating droplet depends on the combination of three interface tensions, oil density and droplet volume (Phan, Allen et al. 2012).

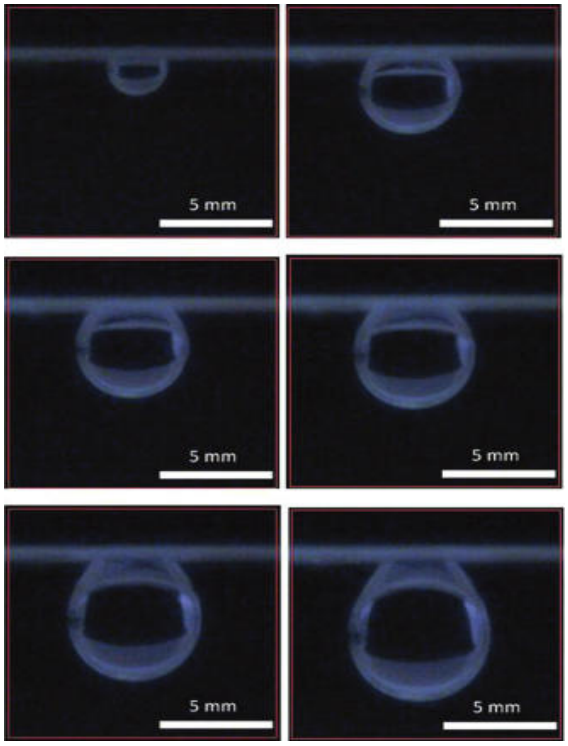

Figure 2.11. Water droplets at different volumes on vegetable oil surface (Phan, Allen et al. 2012).

The model has been extended for floating water droplet with acute contact angle (Phan 2014). The third model has a potential application in oil-spills treatment, and lays the foundation for this study.

2.4 Oil decomposition

A wide range of organic compounds is detected in oil industrial wastewater. Different fractions of alkanes, alkenes, aromatic hydrocarbons and asphalts are containing in petroleum hydrocarbons (Lazar, Petrisor et al. 2007). Most of these compounds are resistant to biodegradation and stay in the environment for a long period of time. Disposal of oily sludge or residual, i.e. oil spillages, into the environment is harmful for people, animals as well as the environment. The removal of oil pollutants are often performed by physical or chemical processes. These methods are commonly expensive with the potential of producing by-product pollutants (Farzadkia, Dehghani et al. 2014).

As a result, the use of alternative treatment technologies aiming to mineralise or decompose molecules into others, which could be further biodegraded, especially in oil spillages into seawater scenario, is a matter of great concern. Advanced oxidation processes are often used for removing organic hydrocarbons.

Advanced oxidation processes (AOPs) are characterised by a variety of free radical chain reactions consisting in combinations of chemical agents. AOPs are processes involving in situ generation of highly reactive species such as the hydroxyl radical ($HO^{\bullet}$), which is the primary oxidant in AOPs, while the other free radicals and active oxygen species are superoxide radical anions ($O_2^{\bullet-}$), hydroperoxyl radicals ($HO_2^{\bullet-}$), triplet oxygen ($3O_2$), and organic peroxyl radicals (ROO^{-}). A relevant property of $HO^{\bullet}$ radicals is its non-selective character and thus readily attacks a large group of organic chemicals to convert them to less complex and less harmful intermediate products. Depending on the AOPs, $HO^{\bullet}$ can be generated by any of one or combination of the following methods: (i) chemical oxidation using H_2O_2, O_3, O_3/H_2O_2, Fenton's reagent; (ii) radiation methods including UV radiation, gamma-radiation, electron-beam, and ultrasonic waves; (iii) combination of any one of (i) with any of (ii), in particular UV radiation or ultra-sonication; and (iv) photo-catalysis using UV and titanium dioxide (TiO_2) (Olmez-Hanci 2012). Among these chemical processes, Fenton's method is the most popular one since it is economically feasible, has fast reaction time and low energy consumption, ease to control (Brillas, Sirés et al. 2009). The basis of Fenton method is the decomposition of hydrogen peroxide (H_2O_2) and the production of hydroxyl radicals in the presence of ferrous iron (Fe^{3+}) ions as a catalyst. The produced hydroxyl radicals can decompose a wide range of organic contaminants including petroleum hydrocarbons (Farzadkia, Dehghani et al. 2014).

Modern and optimum technologies in water treatment have been rapidly developed. Practical and applicable alternatives for new procedures of AOPs have been compared with techniques such as adsorption, reverse osmosis or air stripping as non-destructive treatments. In most cases, chemical

treatment of wastewater by Fenton's reaction, or by UV-irradiation, oxidants (H_2O_2, O_3) and/or catalysts (Fe-salts, TiO_2) have shown effectiveness, for example in a complete mineralisation of the pollutants to CO_2. Decomposition of non-biodegradable organic contaminants in main water sources, such as halogenated aromatics and/or alkanes, by these so-called advanced oxidation processes (AOPs) is feasible. Furthermore, combinations of an advanced oxidation process as a preliminary treatment, followed by an inexpensive biological process (using micro-organism and/or enzymes) seem very promising (Bauer 1994).

For the floating droplet, the chemical processes are the most convenient method. Hence, these processes are reviewed in details.

2.4.1 Chemical reagents

The conventional dark Fenton process involves the use of one or more oxidising agents (usually H_2O_2 and/or oxygen) and a catalyst (a metal salt or oxide, usually iron) at acidic pHs, while the photo-Fenton (or photo-assisted Fenton) process also involves irradiation with sunlight or an artificial light source, which increases the rate of organic pollutant degradation by stimulating the reduction of Fe^{3+} to Fe^{2+} (Olmez-Hanci 2012).

This method has the advantage that H_2O_2, used as oxidant, is cheaper than other oxidants, and it uses iron as catalyst which is highly abundant and nontoxic. The Fenton process is efficient in the pH range 2 to 6 and is usually most efficient at around pH 2.8 (Olmez-Hanci 2012). Hydrogen peroxide is the fourth most reactive chemical species known, with a relative oxidation power of 1.31. And in combination with Iron, together can form the so-called Fenton's reagents (Bishop, Stern et al. 1968) (Walling 1975).

The active species responsible for the destruction of the contaminants is in many cases the hydroxyl radical (OH^-) with its very high oxidation potential (+2.8 V). It decomposes almost all organics, but specially favours unsaturated compounds in aqueous solution.

The general chemistry of Fenton's reagent is as follows:

$$Fe^{2+} + H_2O_2 \rightarrow Fe^{3+} + OH^- + {}^{\cdot}OH \qquad (2.17)$$

$$Fe^{3+} + H_2O_2 \rightarrow Fe^{2+} + {}^{\cdot}OOH + H^+ \qquad (2.18)$$

The procedure requires the following considerations:

- pH of the solution must be adjusted to values between 2 and 6.
- Addition of the Iron catalyst (such as a solution of $Fe_2(SO_4)_3$) are needed.
- For the peroxide, this must be slowly added. Because a hazardous situation can be created if the pH is too high, the iron can precipitate as iron (III) hydroxide $Fe(OH)_3$ and catalytically decomposes the H_2O_2 to oxygen.

Limitations in reaction rates with Fenton's reagent can be observed by the rate of OH^- generation (i.e., concentration of iron catalyst), as shown in equations below (2.19 and 2.20), and less so by the specific wastewater being treated. Typical Fe:H_2O_2 ratios are 1:5 to 10 wt/wt. In addition, iron levels less < 25-50 mg/L can require excessive reaction times (10-24 hours). This is particularly true where the oxidation products (organic acids) isolate the iron and remove it from the catalytic cycle. Fenton's Reagent is most effective as a pre-treatment tool, where COD's are > 500 mg/L (Bishop, Stern et al. 1968) (Walling 1975). This is due to the loss in selectivity as pollutant levels decrease:

$${}^{\cdot}OH + H_2O_2 \rightarrow {}^{\cdot}O_2H + H_2O \qquad (2.19)$$

$${}^{\cdot}OH + Fe^{3+} \rightarrow Fe^{2+} + OH^- \qquad (2.20)$$

Several physical and chemical conditions should be considered when using Fenton's process, in order to obtain a high performance of the method. These factors may be altered during the decomposition process and are described in the following sections.

2.4.1.1 Effect of Iron concentration

Presence of iron must be controlling, so it can lead to hydroxyl radical formation. As a Fenton's reagent, an optimal dose range of iron can affect the reaction efficiency. However, the definition of the range varies between wastewaters. Three factors typically influence its definition (Bishop, Stern et al. 1968) (Walling 1975):

- A minimal threshold concentration of 3-15 mg/L Fe which allows the reaction to proceed within a reasonable period of time regardless of the concentration of organic material;

- A constant ratio of Fe: substrate above the minimal threshold, typically 1 part Fe per 10-50 parts substrate, which produces the desired end products. Note that the ratio of Fe substrate may affect the distribution of reaction products

2.4.1.2 Effect of Iron type (Ferrous or Ferric)

For most applications, it does not matter whether Fe^{2+} or Fe^{3+} salts are used to catalyse the reaction. The catalytic cycle begins quickly if H_2O_2 and organic material are in abundance. However, if low doses of reagent are being used (e.g., < 10-25 mg/L H_2O_2), some research suggests ferrous iron may be preferred. The anions, either chloride or sulphate, are not very influential for application (Bishop, Stern et al. 1968) (Walling 1975).

2.4.1.3 Effect of H_2O_2 concentration

As the H_2O_2 dose is increased, a steady reduction in COD may occur with little or no change in toxicity until a threshold is reached, whereupon further addition of H_2O_2 results in a rapid decrease in wastewater toxicity (Bishop, Stern et al. 1968).

2.4.1.4 Effect of temperature

Temperature can directly influence in the rate of reaction with Fenton's Reagent, especially at < 20 ^oC. However, as temperatures increase above 40-50 ^oC, the efficiency of H_2O_2 utilisation declines. This is due to the accelerated decomposition of H_2O_2 into oxygen and water. As a practical matter, most commercial applications of Fenton's Reagent occur at temperatures between 20-40 ^oC. Applications of Fenton's Reagent for pre-treating high strength wastes may require controlled or sequential addition of H_2O_2 to moderate the rise in temperature which occurs as the reaction proceeds. This should be expected when H_2O_2 doses exceed 10-20 g/L. Moderating the temperature is important not only for economic reasons, but for safety reasons as well (Bishop, Stern et al. 1968) (Walling 1975).

2.4.1.5 Effect of pH

The optimal pH occurs between pH = 3 and pH = 6 (see Figure 2.12). The drop in efficiency on the basic side is referred to the transition of iron from a hydrated ferrous ion to a colloidal ferric species. In the final form, iron catalytically decomposes the H_2O_2 into oxygen and water, without forming hydroxyl radicals. The drop in efficiency on the acid side is less dramatic given the logarithmic function of pH, and is generally a concern only with high application rates (Bishop, Stern et al. 1968) (Walling 1975).

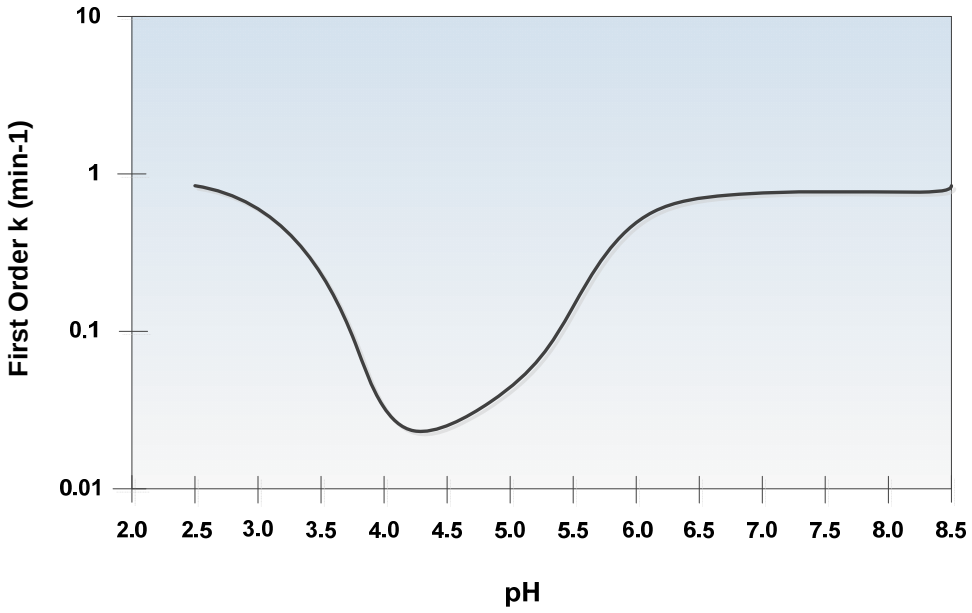

Figure 2.12. Reaction efficiency on Fenton's Reagent under pH influence (Peroxide 2009).

A second aspect of pH deals with its oscillation as the reaction progresses. Provide an initial wastewater pH of 6, as it shown in Figure 2.13.

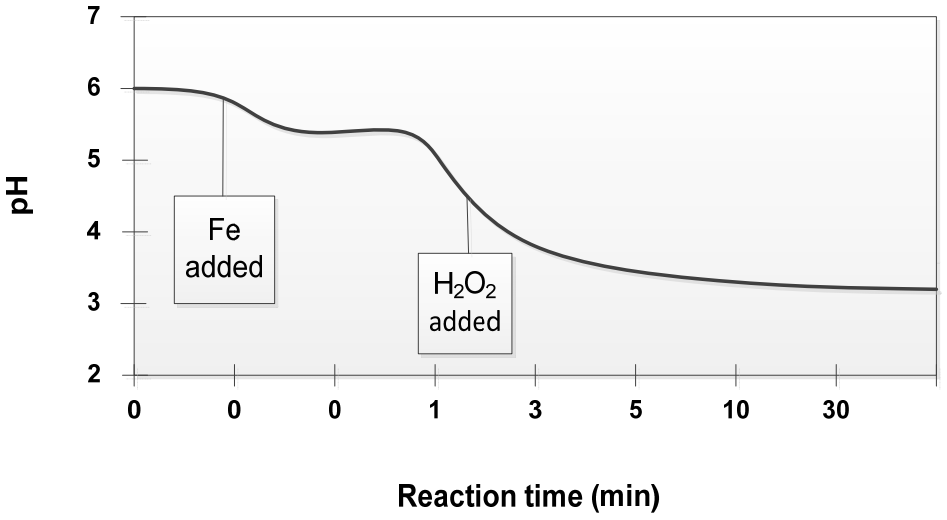

Figure 2.13. pH profile of Fenton reactions (Peroxide 2009).

The first inflection is caused by the addition of $Fe_2(SO_4)_3$ catalyst which typically contains residual H_2SO_4. A second, more pronounced drop in pH

occurs as the H_2O_2 is added, and continues gradually at a rate which is largely dependent on catalyst concentration. This drop in pH is attributed to the fragmenting of organic material into organic acids. This pH change is often monitored to ensure that the reaction is progressing as planned; the absence of such a pH decrease may mean that the reaction is inhibited and that a potentially hazardous build-up of H_2O_2 is occurring within the reaction mixture (Bishop, Stern et al. 1968) (Walling 1975).

In highly concentrated waste streams (>10 g/L COD), it may be necessary to perform the oxidation in steps, readjusting the pH upwards to pH 4-5 after each step so as to prevent low pH from restraining the reaction (Bishop, Stern et al. 1968) (Walling 1975).

2.4.1.6 Effect of reaction time

Fenton reaction will depend on all the variables mentioned above in particular, the catalyst dose and wastewater strength are the most relevant parameters to estimate the time needed to complete the reaction. For example, for simple phenol oxidation (less than 250 mg/L), typical reaction times are 30 - 60 minutes. For more complex or more concentrated wastes, the reaction may take several hours and/or days. In such cases, performing the reaction in steps (adding both iron and H_2O_2) may be more effective (and safer) than increasing the initial charges (Bishop, Stern et al. 1968) (Walling 1975).

Completion of the reaction may prove troublesome on its determination; this is due to the presence of residual H_2O_2 that will interfere with many wastewater analyses (Bishop, Stern et al. 1968) (Walling 1975).

2.4.1.7 The effect of ratio peroxide to sample on the reduction of oil

Fenton process can be affected by certain compounds such as heavy metals, salt, water, and also many other unidentified compounds that are contained in oily sludge. Due to these compounds consuming hydrogen peroxide,

setting the exact amount of hydrogen peroxide H_2O_2 is crucial. At higher concentrations of H_2O_2, which is more than the required for the optimum condition, an increase of the COD can occur in the effluent. Furthermore, several micro-organisms can be affected by the excess of hydrogen peroxide, since this excess amount acts as hydroxyl radical's scavenger (HO^o) and reduces the reaction as well as the biodegradation rate. Using low concentrations of H_2O_2 makes the Fenton process economically acceptable. The required concentration of H_2O_2 for the reaction depends on the concentration and type of the pollutant (Farzadkia, Dehghani et al. 2014).

In summary, successful Fenton decomposition process will depends on the criteria above mentioned (Iron and H_2O_2 concentrations, pH, reaction time, temperature). On the other hand, how these components affect the floatability of water droplet on oil surface is remaining unclear.

2.4.2 Photo-catalysts reagents

Originally, organic waste compounds are decomposed by the help of several reactions existing in nature, as part of a natural cycle. As one of the most abundant elements on earth, Iron is always involved in this "natural process" acting as a photo-catalyst and is helped by the sun as excitation light source (Bauer 1994).

More recently, the combination of UV-irradiation and oxidants (O_3, H_2O_2) and/or catalysts (Fe^{2+}, TiO_2) has become a realistic alternative to conventional large scale water treatment plants based on adsorption or reverse osmosis principles (Ruppert, Bauer et al. 1994).

2.4.2.1 Catalysts/UV light process

Recently much attention has been drawn to TiO_2 for the degradation of dissolved organic pollutants as a relevant alternative wastewater treatment. The mechanistic details of how TiO_2 photo-catalyses the degradation of organics are well studied and it is believed to oxidise water with dissolved

oxygen to hydrogen peroxide, which will subsequently oxidise the organics. The rate of reaction is dependent upon the intensity of light and the amount of oxygen available in the system (Berry and Mueller 1994).

The major factors affecting TiO_2/UV light process are: the initial organic load, amount of catalyst, reactor's design, UV irradiation time, temperature, solution's pH, light intensity and presence of ionic species. The use of excessive amounts of catalyst may reduce the amount of energy being transferred into the medium due to the opacity offered by the catalyst particles. For temperature values between 20 and 80^{o}C, a minor effect of temperature has been noticed. However, at temperature higher than 80^{o}C, a reduction of the reaction rate has been reported. A solution's pH has a complex effect on photo-catalytic oxidation rates. For weakly acidic pollutants, reaction rates increase at lower pH. On the other hand, pollutants which are hydrolysed under alkaline conditions may show an increase of reaction rate with increase of pH. Finally, the presence of ionic species could increase the degradation process via adsorption of the pollutants, adsorption of UV light and reaction with hydroxyl radicals (Stasinakis 2008).

The most interesting features of TiO_2 are high stability, good treatment performance and low cost. It has the disadvantage of catalyst separation from solution, as well as fouling of the catalyst by organic matter. Photo-catalysis over a semiconductor oxide such as TiO_2 is initiated by the absorption of a photon with energy equal to or greater than the band gap of the semiconductor (Olmez-Hanci 2012).

2.4.2.2 Hydrogen peroxide/UV light process

Hydrogen peroxide (H_2O_2) reacts with organic pollutants present in water through direct and indirect pathways. In the direct mechanism, H_2O_2 participates in redox reactions where it behaves as an oxidant or as a reductant. Indirect reactions are due to the oxidising action of free radicals that are formed from the decomposition of H_2O_2 when it reacts with other inorganic compounds such as O_3 or Fe^{2+}, or when it is photolysed. H_2O_2 has

been used to oxidise aldehydes, alcohols, amines, azo compounds, phenols, cyanides, sulphur compounds, and metal ions (Olmez-Hanci 2012).

Ozone-based and H_2O_2-based AOPs such as O_3/H_2O_2, H_2O_2/UV, O_3/UV, and O_3/H_2O_2/UV are attractive alternative for the degradation of organic pollutants and have been used with an increasing interest due to their high potential of $HO^{\bullet}$ generation.

UV-based AOPs also transform pollutants in two ways. Some organic chemicals absorb UV light directly, and absorption of this high-energy radiation can cause destruction of chemical bonds and subsequent breakdown of the contaminant. However, some organic species do not degrade very quickly or efficiently by direct UV photolysis. Therefore, addition of O_3 or/and H_2O_2 to the UV process creates AOP conditions, often increasing the rate of contaminant degradation significantly (Olmez-Hanci 2012).

UV/H_2O_2 process is efficient in mineralising organic pollutants. A disadvantage of this process is that it cannot utilise solar light as the source of UV light due to the fact that the required UV energy for the photolysis of the oxidiser is not available in the solar spectrum (Stasinakis 2008).

The major factors affecting this process are the initial concentration of the target compound, the amount of H_2O_2 used, wastewater pH, presence of bicarbonate and reaction time. Specifically, the kinetic rate constant for the degradation process is inversely proportional to the initial concentration of the pollutant. As a result, wastewater dilution should be done at an optimum level (Stasinakis 2008).

Overall, the action of UV light on catalyst and H_2O_2 can accelerate the reaction time in the decomposition of organic pollutants and its oxidation process. However, the influence of these processes in organic compounds decomposition, such as in paraffin oil, has not been studied yet.

2.4.3 Biological Reagents

It is well-accepted biological reagents can decompose hydrocarbons. These include the diversity of micro-organism and bacteria cultures, as well as the action of enzymes on oil compounds.

2.4.3.1 Micro-organism and bacteria

In natural biodegradation, the main mechanisms used to eliminate petroleum and other kind of oil pollutants is by the action of several natural communities of micro-organisms in the environment. Many previews research have been done based on influences of environmental parameters, metabolic and genetic adaptation bases for hydrocarbon decomposing by micro-organisms (Leahy and Colwell 1990). In some cases, such as in the decomposition of aromatic compounds from high molecular hydrocarbons, bacteria action occurs via oxidation on the oil fractions with the help of a multicomponent enzyme system (Kanaly and Harayama 2000) (Juhasz and Naidu 2000). Most of studies were related with degradation of oil in the marine environment (Juhasz and Naidu 2000) (Kanaly and Harayama 2000) (Leahy and Colwell 1990).

Most relevant hydrocarbon-degrading bacteria in marine and soil environments are *Achromobacter, Acinetobacter, Alcaligenes, Arthrobacter, Bacillus, Flavobacterium, Nocardia,* and *Pseudomonas spp*. and the *coryneforms* (Leahy and Colwell 1990). Different rates percentage of oil degradation has been shown by using diverse cultures and combination of bacteria from different sources. However, overall rate of decomposition varied on composition of both hydrocarbons and its components fractions (Juhasz and Naidu 2000) (Kanaly and Harayama 2000) (Leahy and Colwell 1990).

Due to the difference in their susceptibility to microbial attack, hydrocarbons have generally been ranked in the following order of decreasing susceptibility: n-alkanes > branched alkanes > low-molecular-weight

aromatics > cyclic alkanes. Biodegradation rates have been shown to be highest for the saturates, followed by the light aromatics, with high-molecular-weight aromatics and polar compounds exhibiting extremely low rates of degradation (Leahy and Colwell 1990).

However, depending on the environmental conditions, the main differences between petroleum biodegradation in soil and aquatic ecosystems following an oil-spill are related to the movement and distribution of the oil and the presence of its fractioned compounds. Each of these conditions will affect the physical and chemical nature of the oil and hence its susceptibility to microbial degradation (Juhasz and Naidu 2000) (Kanaly and Harayama 2000) (Leahy and Colwell 1990).

Several aspects are considered in the biodegradation of petroleum and other hydrocarbons in the environment. Due to its complex process, the nature and amount of the oil present, the ambient and seasonal environmental conditions, and the composition of the autochthonous microbial community are factors that can influence the rate of decomposition (Juhasz and Naidu 2000) (Kanaly and Harayama 2000) (Leahy and Colwell 1990). Therefore, the microbial degradation of petroleum in aquatic environments is limited primarily by nutrients such as nitrogen and phosphorus; salinity and pressure. Oxygen, nutrient concentrations, moisture, and pH are predominant factors in determining biodegradation rates in soil (Leahy and Colwell 1990).

Microorganisms live in biofilms, as their predominant mode of life in nature, to multiply and protect themselves from environmental stresses such as UV radiation, pH shifts, desiccation and osmotic shock. Bacterial biofilms undergo several stages of development, from the initial attachment of bacteria to detachment and colonisation of new interfaces. The viscoelastic matrix can be composed of extracellular DNA, polysaccharides, and proteins. Biofilm formation is often triggered by changes in the environment and involves several stages often referred to as the biofilm lifecycle (Rühs,

Böcker et al. 2014). These steps include attachment of the floating cell(s) to a surface, maturation, maintenance and dissolution (Rühs, Böni et al. 2013).

2.4.3.2 Enzymes

Hundreds of amino-acids are contented in enzymes. Therefore, they are produced by living organisms. As proteins, enzymes are responsible for a number of reactions and biological activities in plants, animals, human beings and micro-organisms. They can be found in the human digestive system to break down carbohydrates (sugars), fats or proteins present in food. Thus, even minimal pieces can be absorbed into the blood stream. Each enzyme is made of a sequence of amino acids, folded into a unique three-dimensional structure that determines the function of the enzyme. Even the slightest change in the sequence of the amino acids can alter the shape and function of the enzyme. Only a small part of the enzyme participates in the catalysis of biochemical reactions represented by the active site (Rosenthal, Pyle et al. 1996) (Man, Asbi et al. 1996) (Sharma, Khare et al. 2002) (Dominguez, Nunez et al. 1994) (Sharma, Khare et al. 2001) (Hanmoungjai, Pyle et al. 2001) (Najafian, Ghodsvali et al. 2009) (McGlone, Canales et al. 1986).

Enzymes are therefore very specific (e.g. cellulose can only degrade cellulose). Enzymes are essential for all metabolic processes, but are not themselves living materials. They are distinguishable from other proteins because they are known as biological catalysts (substances which speed up reactions but which do not get used up themselves) (Rosenthal, Pyle et al. 1996) (Man, Asbi et al. 1996) (Sharma, Khare et al. 2002) (Dominguez, Nunez et al. 1994) (Sharma, Khare et al. 2001) (Hanmoungjai, Pyle et al. 2001) (Najafian, Ghodsvali et al. 2009) (McGlone, Canales et al. 1986).

Enzymes are classified in five categories. Each of them has features and characteristics distinctively, described as follows:

1. **Proteases:** Act on soils and stains containing proteins. Examples are collar & cuff soil-lines, grass and blood. Proteases are enzymes that

break down a long protein into smaller chains called peptides (a peptide is simply a short amino acid chain).

2. **Amylases:** Remove starch-based soils and stains, e.g. sauces, ice-creams, gravy. Amylases break down starch chains into smaller sugar molecules.

3. **Lipases:** Are effective in removing oil / greasy body and food stains.

4. **Cellulases:** Provide general cleaning benefits, especially on dust and mud, and also work on garments made from cellulosic fibres, minimising pilling to restore colour and softness.

Recent new technologies combine all four different types of enzymes in one formulation, under normal conditions, using a stabilisation process to achieve this. The technology behind this formulation is in its ability to allow each one of the enzymes to co-exist together without destroying each other. The yield resulting from this combination can act as a catalyst to accelerate the degradation of organic material.

Some of the advantages on applying this technique are as follow (Rosenthal, Pyle et al. 1996) (Man, Asbi et al. 1996) (Sharma, Khare et al. 2002) (Dominguez, Nunez et al. 1994) (Sharma, Khare et al. 2001) (Hanmoungjai, Pyle et al. 2001) (Najafian, Ghodsvali et al. 2009) (McGlone, Canales et al. 1986):

- Enzymes are plant based. Therefore, it will not upset the natural bacteria
- Enzymes accelerate the destruction of organic material
- As its pH is neutral, this will not cause damage on surfaces
- Biodegradable, powerful action and positive effects
- Chemical agents and phosphates are not contented

Overall, biological reagents have been proved its effectiveness as natural mechanism in biodegrading organic material. However, its influence in the decomposition process by acting directly on the surface of hydrocarbons is unclear.

2.4.4 Combination of different processes

In theory, all the chemical, physical and biological methods can be combined within the floating droplet. In the literature, Fenton process is typically combined with irradiation of solar light to enhance its efficiency. On the other hand, a new approach of Fenton process in combination with biological process can reduce environmental risks by using natural reagents in decomposing organic material.

2.4.4.1 Combination of Fenton process under UV light

The combination of Fenton reaction with UV light (180-400 nm), the so-called photo-Fenton reaction, had been shown to enhance the efficiency of the Fenton process.

The reason for the positive effect of irradiation on the degradation rate includes the photo-reduction of Fe^{3+} to Fe^{2+} ions, which produces new $HO^{\bullet}$ with H_2O_2 as it shows as follows:

$$Fe^{3+} + H_2O \xrightarrow{uv} Fe^{2+} + HO^{\bullet} + H^{+} \qquad (2.21)$$

$$H_2O_2 \xrightarrow{uv} 2HO^{\bullet} \quad (\lambda < 400 \text{ nm}) \qquad (2.22)$$

The main compounds absorbing UV light in the Fenton system are ferric ion complexes, e.g., $[Fe^{3+}\ (OH)^{-}]^{2+}$ and $[Fe^{3+}\ (RCO_2)^{-}]^{2+}$, which produce additional Fe^{2+} by following reactions I and II photo-induced, ligand-to-metal charge-transfer (LMCT) reactions:

$$[Fe^{3+}(OH)^{-}]^{2+} \text{ ----} \rightarrow Fe^{2+} + HO^{\bullet} \quad \text{(approx. < 450 nm)} \qquad (2.23)$$

$$[Fe^{3+}(RCO_2)^{-}]^{2+} \text{ ----} \rightarrow Fe^{2+} + CO_2 + R^{\bullet} \quad \text{(approx. < 500 nm)} \qquad (2.24)$$

Additionally, equation 2.23 generates $HO^{\bullet}$ while equation 2.24 results in a reduction of the total organic carbon (TOC) content of the system due to the decarboxylation of organic acid intermediates.

The overall degradation rate of organic compounds is considerably increased in the photo-Fenton process, even at a lower concentration of iron salts present in the system. In the combined photo-Fenton process, the energy requirement is reduced and the effectiveness in the treatment of organic pollutants is increased (Olmez-Hanci 2012).

2.4.4.2 Combination of biological process with chemical reagents

Simultaneously, combination of Fenton process with photo-catalyst or bioprocess has not been well studied. However, in the biological process, during the interaction with organic material, a form of biofilm can be developed. The interaction of bio-film and bio-excreted materials on the chemical/ physical processes could be critical for successful decomposition.

In addition, microorganisms, forming water-oil biofilms, have a very diverse metabolism which allows them to use crude oil as a carbon source and form a biofilm around the oil droplets to enhance carbon uptake (Rühs, Böni et al. 2013).

2.5. Summary

The floating droplet is the newly discovered phenomenon, which can be used to decompose oil spillages. From the literature, there are three different processes (photo-catalytically, chemical oxidation and biological), which can be employed within the floating droplets. The survey of the literature indicates that during these processes, a range of compounds can be removed and

formed. This includes but not limited to: organics, ions, biofilm, etc. These compounds can affect the surface tension in one way or the other, and consequently influence of the stability of the floating droplet. Hence, the surface tensions can vary significantly with chemical reagents/ by-product during the decomposing process. However, the net impact of these parameters is difficult to predict theoretically. Consequently, this study focuses on experimental verification of the floatability under different conditions.

This study will address two of the most important aspects for the floating droplets:

- Influence of physical factors (electrolyte, pH) on the shape,
- Influence of the decomposing processes on the stability of droplet by the action of diverse reagents compounds.

By successfully addressing these two questions, the project will verify the applicability of the floating droplet in treating oil-spills. Consequently, the method could open a new and environmentally method to deal with oils spillages.

Chapter 3

Experimental

The experimental program utilised in this study, is described by the following materials and procedures:

3.1 Materials

3.1.1 Chemicals

The main surfactant for this study is Sodium dodecyl sulphate (SDS), which is a strong anionic surfactant. The SDS was purchased from Sigma-Aldrich, which was listed as 99% pure. Sodium chloride (NaCl) was used to prepare electrolyte solutions. The oil throughout this study is a paraffin oil obtained from (Digger^{TM}, Australia). As paraffin oil is chemically similar to crude oils, its physical properties have the required performance for this study. Moreover, its transparency facilitates the optical verification of the floating droplet.

Hydrogen peroxide at 20% concentration (H_2O_2), Ferrous Chloride ($FeCl_2$), Ferric Sulphate [$Fe_2(SO_4)_3$], Titanium Oxide (TiO_2), acted as catalysts and intermediates in the experimental systems. These chemicals were purchased from Chem-Supply PTY LTD, Australia.

An enzyme, specifically a heavy duty surface cleaner, was tested as its specifications provide a high performance on reducing a grease surface. This enzyme was purchased from Enzyme Wizard PTY LTD, Australia. To control the pH in all systems studied, Hydrochloric Acid (HCl) and Sodium hydroxide (NaOH) were used. HCl was supplied by Scharlab S.L. and by MERCK KGAA Germany, respectively. Deionized water and paraffin oil were used as the heavier and lighter liquid phases, respectively. Natural soil was used to assure the presence of micro-organisms, when is required, as a natural catalyst.

3.1.2 Preparation of aqueous solutions

Deionized water was used to prepare all aqueous solutions. Most solutions of 8mM SDS were prepared with deionized water (Millipore, 18 MΩ), which was above the critical micelle concentration. A 3.5% NaCl was dissolved in deionized water to prepare synthetic seawater.

The reproducibility of all tests and measurements was evaluated, ensuing the reliability of the experimental data.

3.2 Measurements methods

The following techniques were used to obtain the main parameters in this study, such as surface tension, density of solutions alongside with the procedure to estimate the shape of the water droplet. The experimental consists of three parts:

- Section 3.2.1. Measurements of the physical properties: surface tension and density
- Section 3.2.2. Droplet shape analysis
- Section 3.2.3. Evaluation of the oil decomposition

3.2.1 Physical properties

3.2.1.1 Surface tension

The surface tension between the air/water was measured by using the pendant drop method (Adamson and Gast 1997). A liquid droplet (few microliters) was formed at the end of an inverted u-shape needle by the use of a micro syringe and a syringe pump (Figure 3.1). The images were recorded by a camera and stored in a computer for further off-line analysis.

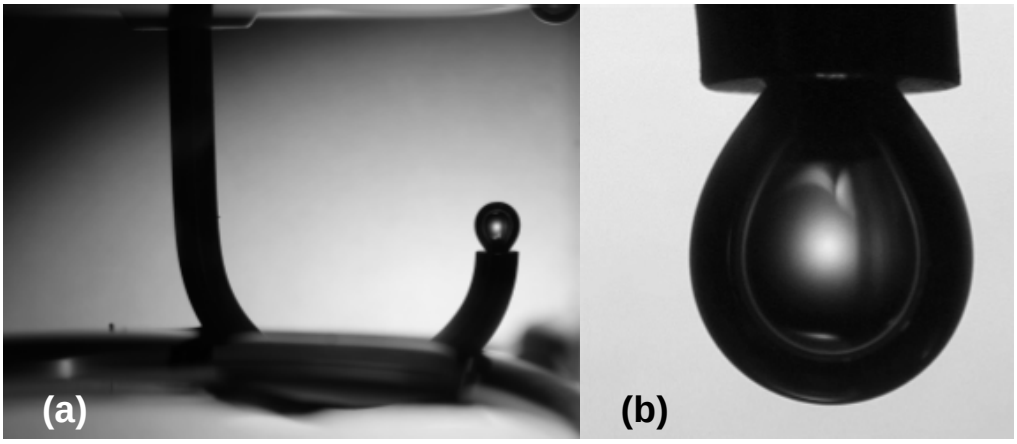

Figure 3.1. (a) Example of Pendant drop method utilised to estimate the interface tension between phases. (b) Pendant bubble (after being flipped vertically).

To obtain the surface tension between the air/water interfaces, the ADSA method was used as is shown in Figure 3.2 by considering the physical properties and scale factor of the image in the involved system. Images were analysed by fitting the drop profile with the Young-Laplace expression (equation 2.4) to estimate the value of the surface tension (see Table 1).

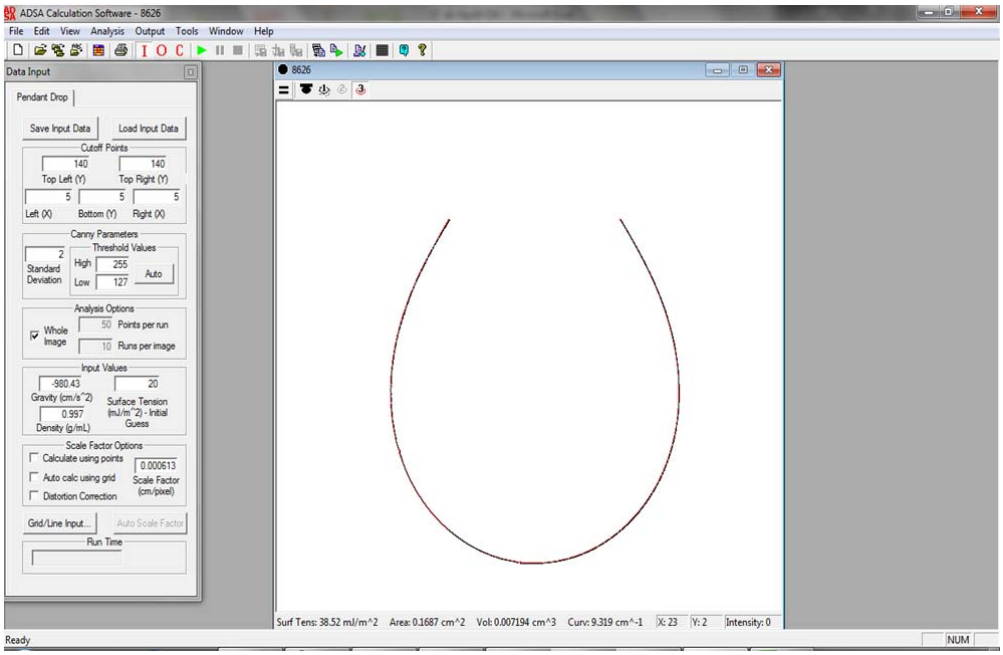

Figure 3.2. ADSA software to measure surface tension.

Table 1. Surface tension.

Solutions (in air medium)	Surface Tension (mN/m)
SDS	38.58 ± 0.06
SDS + 3.5% NaCl	33.10 ± 0.20
Paraffin oil	31.60 ± 0.03

3.2.1.2 Density

Densities of oil and surfactant solutions were measured by using a DMA 4500 instrument (Anton Paar), see Figure 3.3. All measurements were repeated three times and reproducible at room temperature (25°C); standard deviation values were calculated as an average of data collected, as it is shown in Table 2.

Figure 3.3. Measurement of solutions' densities using an Anton Paar Densimeter (Anton Paar GmbH, Graz, Austria).

Table 2. Physical properties of the solutions.

Solution	Density (g/cm^3)
SDS	0.9999 ± 0.0001
SDS + 3.5% NaCl	1.0220 ± 0.0001
SDS + 3.5% NaCl + HCl	1.0172 ± 0.0006
Paraffin Oil	0.8303 ± 0.0001

3.2.2 Droplet shape analysis

3.2.2.1 Experimental setup

In a glass cuvette an amount of deionized water and an oil layer were placed, where half of the container's capacity was filled with both liquids.

A micro syringe of 10 µL of capacity (SGE Analytical Science Syringe) was used to help deposit a small droplet (< 10 µL) on the oil/air surface, as shown in Figure 3.4.

From the moment when the droplet fell from the dispositive and come into contact with the oil interface, all scenarios were recorded and captured by using a digital camera with 2x magnification. The equilibrating time estimated was approximately 15 minutes.

Therefore, the same procedure was applied by replacing the solution of SDS the water droplet with the addition of NaCl and HCl into the surfactant. All measurements were repeated twice and were conducted at room temperature (25 ^{O}C).

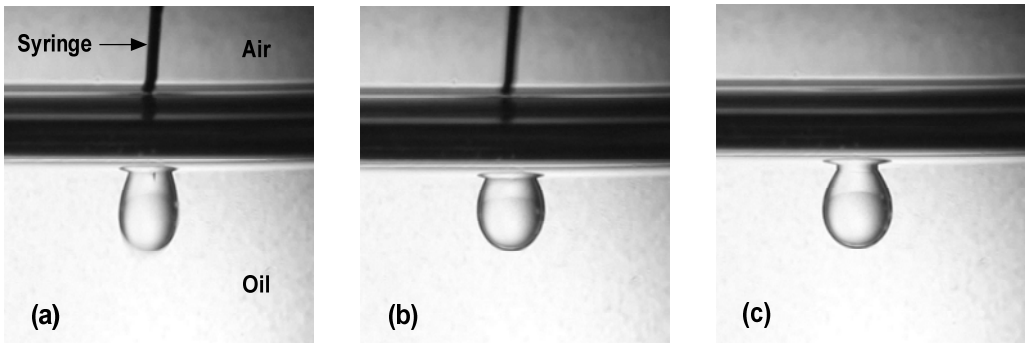

Figure 3.4. Deposition process of the water droplet.

Consequently, all the images recorded were analysed to obtain the contact radius and contact angle (i.e. r and θ_2) for model verification.

3.2.2.2 Image Analysis of Droplet Shape

To analyse the images, the following models were used to determine shape of the droplet and contact angles.

MATLAB – edge detection

For detection and measurement of the shape of the droplet, Matlab™ software was used. The program required that images of the droplet should be cropped to contain only the pendant drop floating on the oil surface on a uniform background to aid edge detection.

The raw image was converted to a greyscale image (*rgb2gray*) and a default threshold value was manually inputted into Matlab™'s *edge* function along with canny edge detection from the Image Analysis Toolbox. Figure 3.5 shows an example of the accuracy of these functions in detecting the fitting edge profile of the droplet. In some cases of the water droplet, some points have been cut manually before its analysis, in order to determine the x_{max} and x_{min} values that will represent the contact angles for each extreme of the water droplet and obtain an accurate shape of the droplet profile, correspondingly.

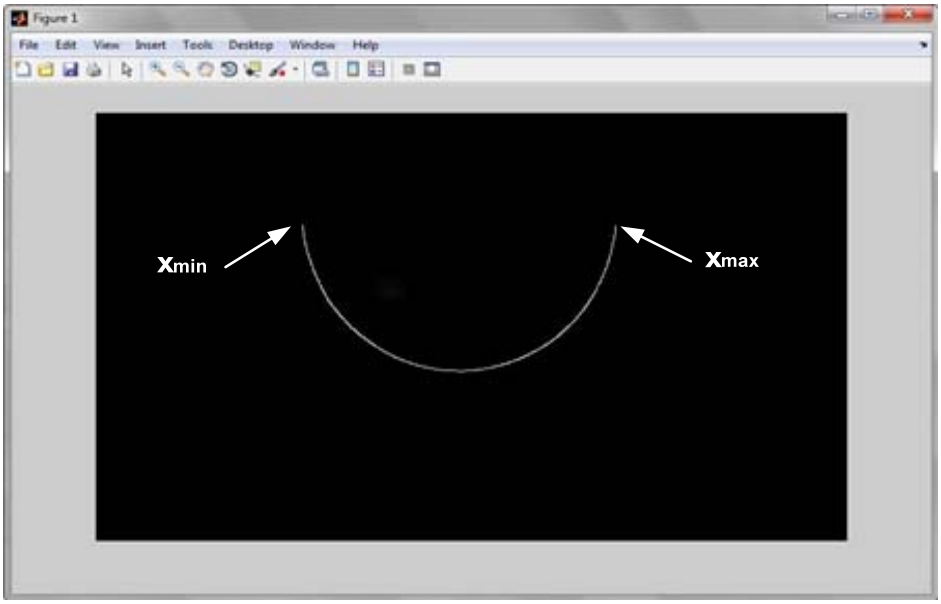

Figure 3.5. Edge detection to estimate a fit droplet shape.

Then, the profile of the drop was exported to an Excel file format, to obtain the best edge fitting by using a polynomial function.

Polynomials function

With the data collected from the previous step and the pixels of drop image, which was measured using a scale factor, the shape of the droplet can be described by the following equation:

$$y_{poly} = a_0 + a_2(x-b)^2 + a_4(x-b)^4 + a_6(x-b)^6 + a_8(x-b)^8 \qquad (3.1)$$

where a_i and b are mathematical constants parameters; *y* and *x* are the vertical and horizontal coordinates of the droplet shape, respectively.

The values of a_i and *b* for each droplet were obtained by fitting the edge to equation (3.1). Consequently, the contact angle between the droplet and oil layer (*rad*) can be determined by the following differential equation:

$$\tan\theta_{2(right)} = \frac{dy}{dx}_{x=x_{max}} = 2a_2(x-b) + 4a_4(x-b)^3 + 6a_6(x-b)^5 + 8a_8(x-b)^7 \quad (3.2)$$

$$\tan\theta_{2(left)} = \frac{dy}{dx}_{x=x_{min}} = 2a_2(x-b) + 4a_4(x-b)^3 + 6a_6(x-b)^5 + 8a_8(x-b)^7 \quad (3.3)$$

Where $\theta_{2(right)}$ and $\theta_{2(left)}$ represent the right and left contact angles, respectively. x_{max} and x_{min} are the horizontal limits of the contact line (in Figure 3.5).

Moreover, the volume of the droplet (in mm^3) can be estimated by numerical integration of Equation 3.4.:

$$V = \int_{ymin}^{ymax} \pi x^2\, dy = \int_{a0}^{ybaseline} \pi x^2\, dy \quad (3.4)$$

By applying this polynomial function, the values of contact angles and droplet volume can be obtained throughout an accurate edge profile of the droplet, as it shown in Figure 3.6).

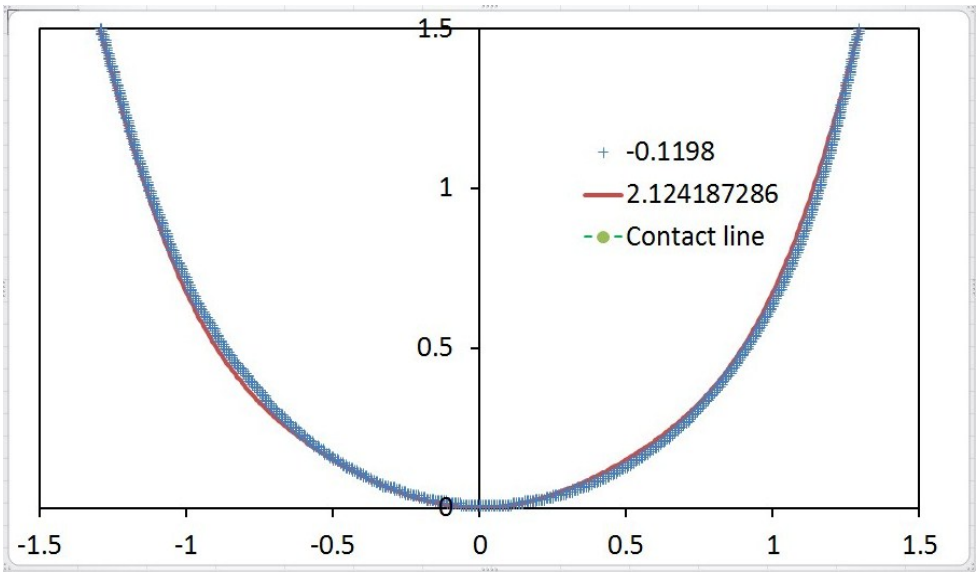

Figure 3.6. Edge profile of water droplet by applying polynomial function.

3.2.3. Oil decomposition process

The experimental set up as described in section 3.2.2.1 was also applied for oil decomposition process, by replacing solutions with Fenton reagents and addition of microorganism and enzyme. The combinations of chemical reactants used were as follows:

1. SDS, TiO_2
2. SDS, TiO_2, $Fe_2(SO_4)_3$. In acid medium
3. SDS, 3.5% NaCl, $Fe_2(SO_4)_3$. In acid medium
4. SDS, naturally-occurring micro-organisms, enzyme
5. SDS, $FeCl_2$, TiO_2.

Each solution was used to study its influence on different oil decomposition process reaction that can occur inside the droplet. Solar simulator equipment was used in some cases, where the action of UV light is required to accelerate the reaction time.

Chapter 4

Influences of Volume and Physical Properties on the Floating Droplet

This chapter will discuss the influence of volume and contact angle parameters on the shape of water droplet by its interactions with different chemicals solutions. Also, implications of the floatability of the droplet present are discussed.

4.1 Experimental results and image processing

Physical parameters of the experimental systems, such as surface tensions and densities were measured and tabulated in Tables 1 and 2 of Chapter 3, respectively. In the literature, the reported density of crude oils varied from 840 to 980 kg/m^3, depending on the oilfields and weathering condition (Wang, Hollebone et al. 2003).

The oil properties in Table 2 (see Chapter 3) show a good representative for crude oils in model verification. Water density was expectedly similar to seawater density, when corresponding. The water droplet was able to float easily on an oil surface in all systems. More interestingly, the droplet shape changed dramatically with time in some cases.

4.2 Results

The scheme in detail of the procedure (Figure 4.1) used to determine the contact angles and volume of water droplets is described below. Consequently, the average droplet volume was determined for each case in mm^3 and then converted in μL.

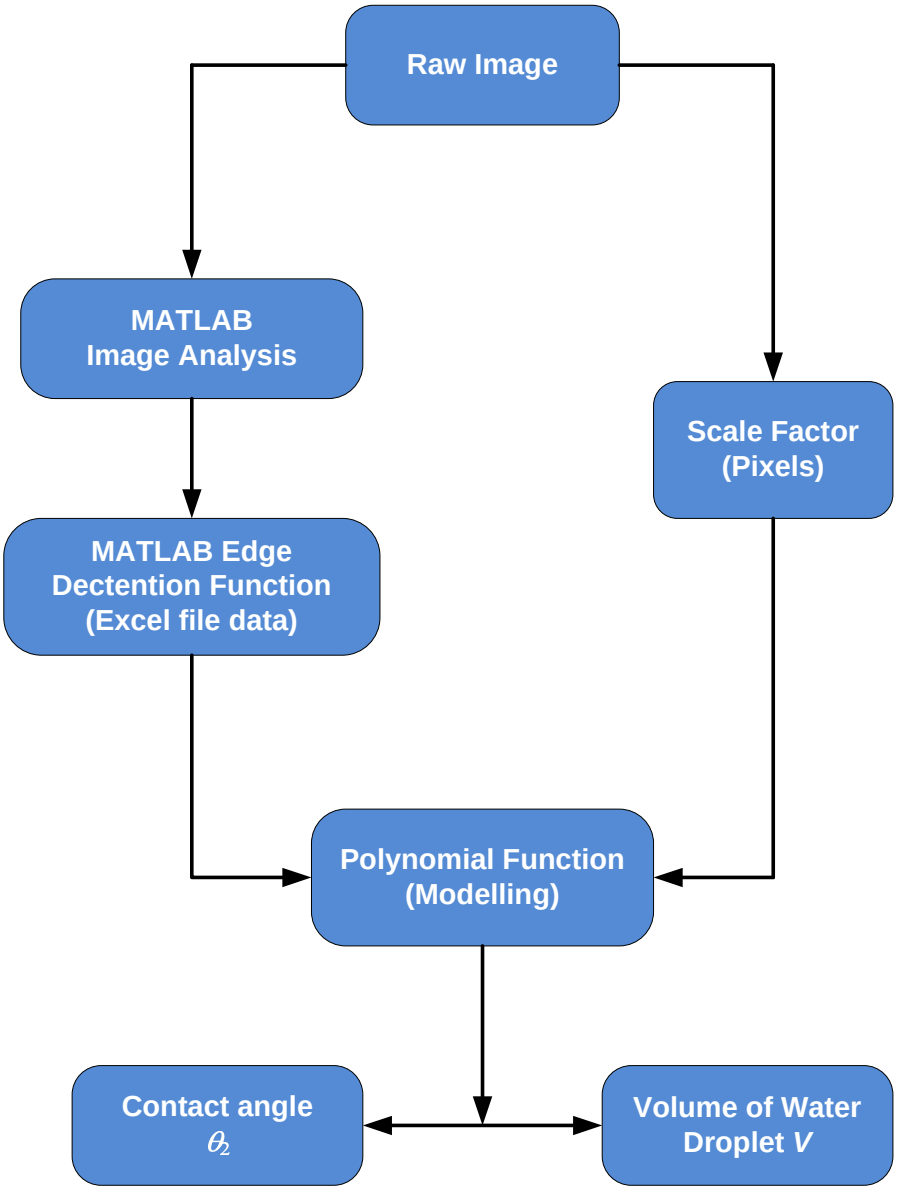

Figure 4.1. Modelling procedure to obtain contact angle between water droplet and liquid interfaces; and droplet size.

The following are the steps in detail, utilised to determine the contact angle and volume of the water droplet by using the procedure mentioned above.

a. Raw image cropped

Raw images taken with the digital camera were cropped by using image software. The section selected from the image, should be clear and shows the floating droplet on the oil layer area, as seen in Figure 4.2.

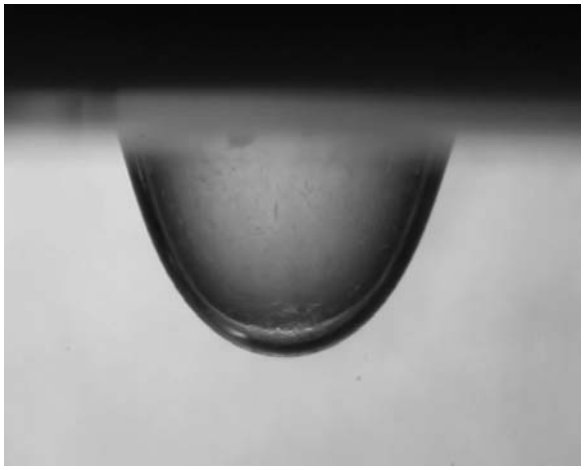

Figure 4.2. Image cropped with the droplet in contact with the oil surface.

b. Matlab image (Image and program code)

In figure 4.3, the image cropped was uploaded into MATLAB. Program code was inputted with all the parameters needed, such as threshold value, which will provide the best fitted-edge image as a result.

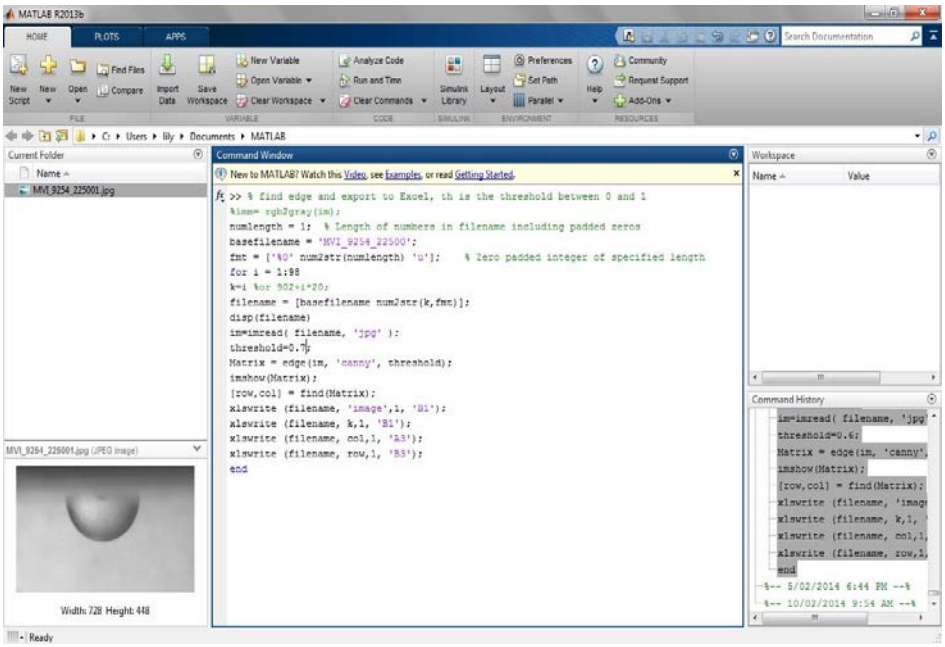

Figure 4.3. Program code and image inputted for fitting-edge detecting using MATLAB.

c. Matlab edge figure image

By running the program, an image with the best fitting edge can be obtained, as it is shown in Figure 4.4. Quality of the edge image is affected by the threshold's value inputted in the code.

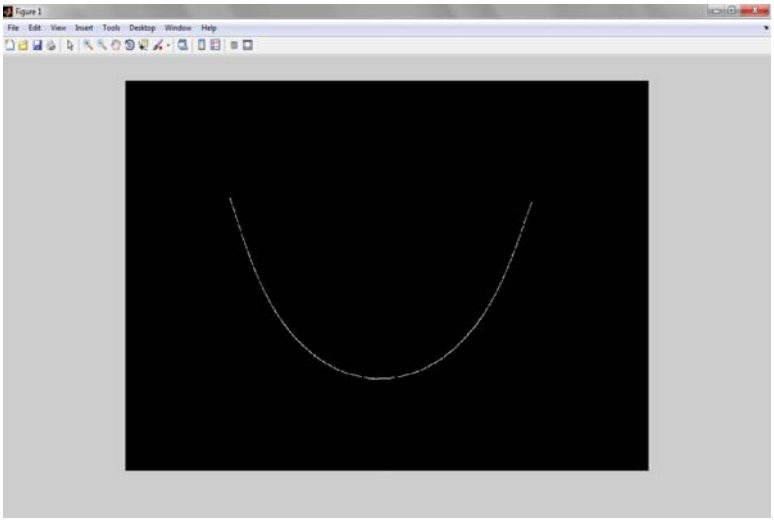

Figure 4.4. Edge of droplet detected by MATLAB.

d. Excel profile data image

An Excel profile data of the image was obtained (see Figure 4.5). This data will be transferred to the modelling program using a polynomial function.

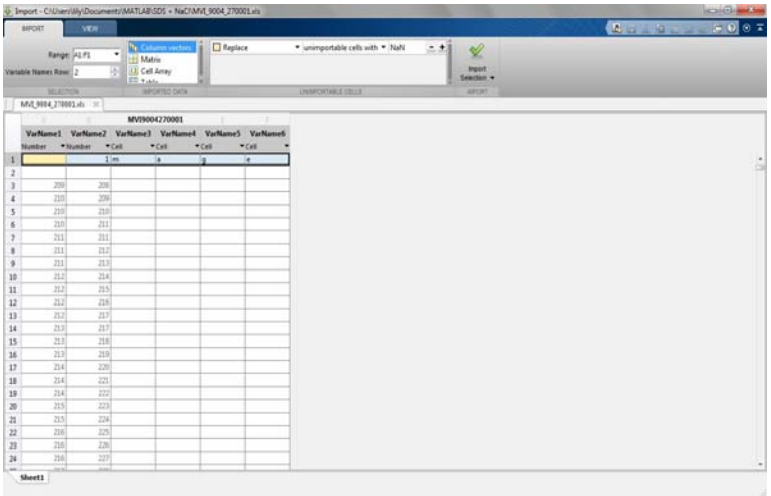

Figure 4.5. Excel profile data of droplet obtained from MATLAB.

e. Polynomial function

With the Excel profile data from the step mentioned above, the model can predict a more accurate fitted-edge (as can be seen in Figure 4.6) for a droplet by applying the equations mentioned in section 3.3.2. Therefore, this leads to obtain realistic values of contact angles and the volume of a water droplet, correspondingly.

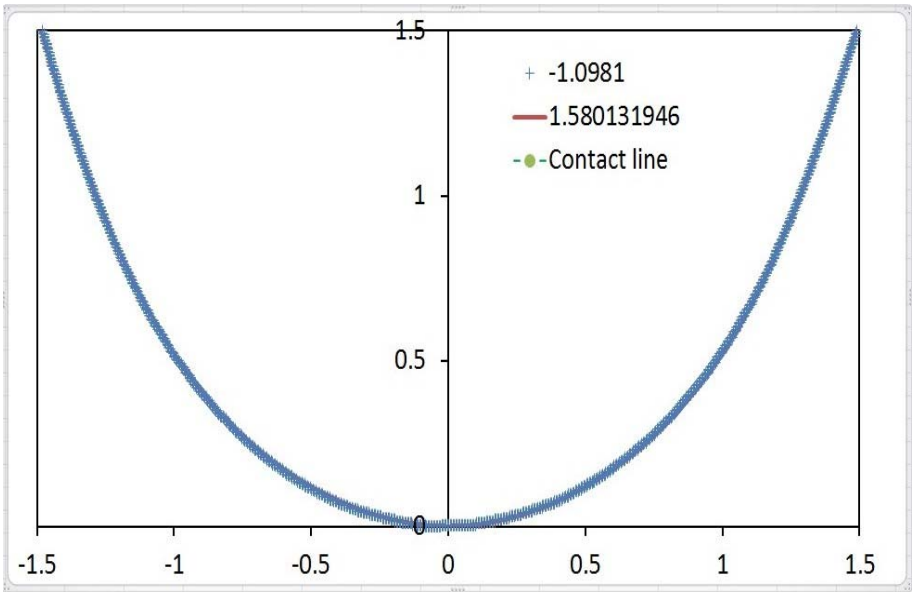

Figure 4.6. Fitted-edge of a droplet by applying a polynomial function model.

All the water droplets profile in this study can be observed in Appendix A; as well as the subroutine used to detect the edge of the droplets in MatLab in Appendix B.

4.2.1 Sodium dodecyl sulphate

The nature of immiscibility of oil/water system had been recognised in preview studies. However, in the presence of a suitable surfactant, this property can be stabilised and optimised the interactions between the interfaces (De Gennes and Taupin 1982).

Water is a highly polar element and resists incorporation into its structure of nonpolar entities such as hydrocarbon chains, because of this particular property. One familiar consequence is that pure hydrocarbons are rather insoluble in water. Polar materials, in contrast, have considerable solubility in water (Miller and Neogi 2007).

Sodium dodecyl sulphate (SDS) is the surfactant of choice in this study, which has a separate nonpolar and polar region. This feature helps the molecules adsorb at the interface between the water and an adjacent fluid as a monomolecular layer or monolayer (Miller and Neogi 2007). Moreover, it had been classified as very hydrophilic in character. The characteristic of Dodecyl sulphate is an ion consisting of a normal dodecane tail and a covalently bound sulphate anionic head group. The use of SDS here as it can be obtained in a very pure form commercially; it has been well studied; and it is quite similar chemically to the petroleum sulphonates being studied for use in enhanced oil recovery processes (Natoli 1980).

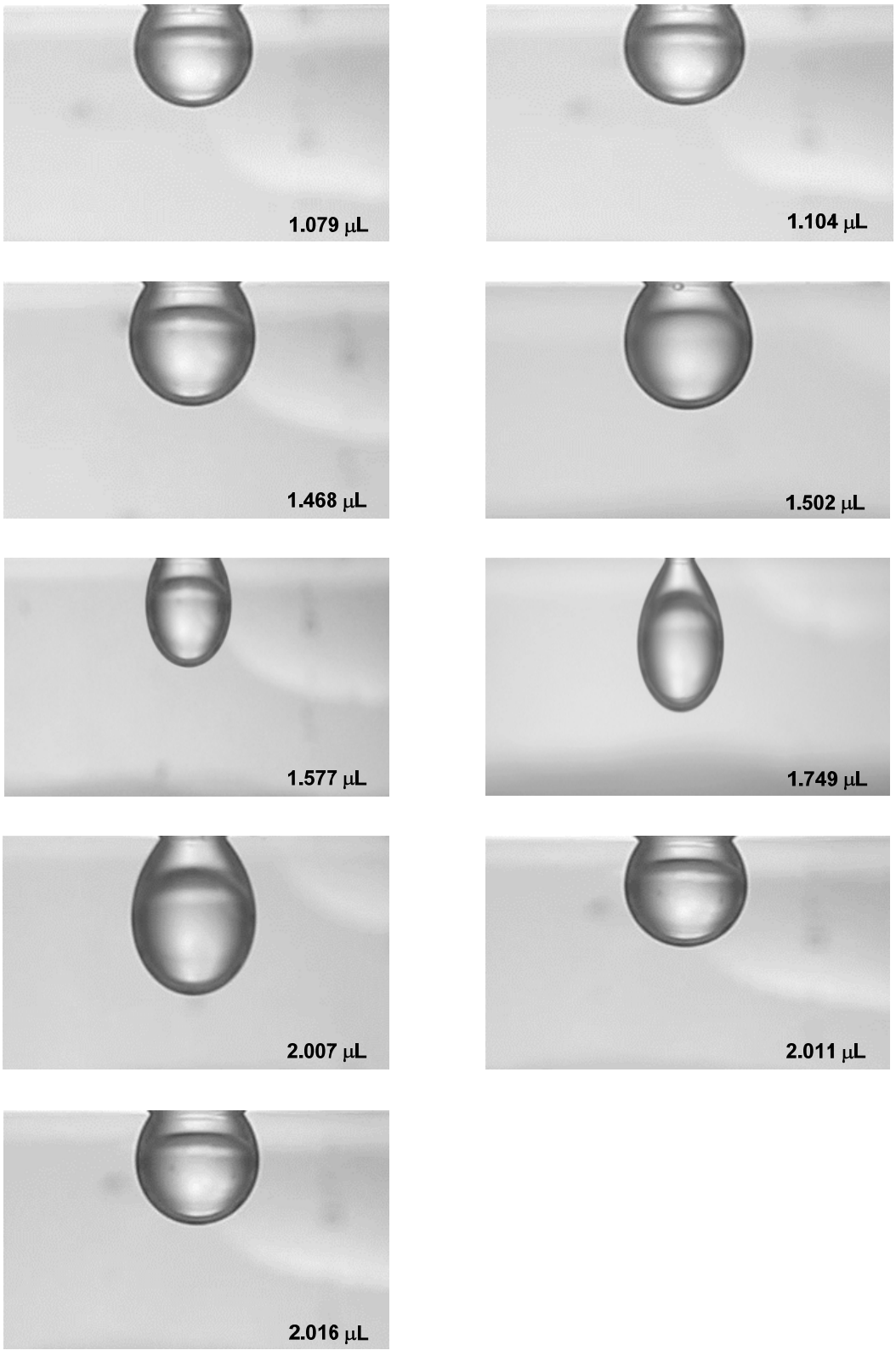

Figure 4.7. Water droplets containing SDS at different volumes (in μL).

From Figure 4.7, one can observed that the main highlight from using pure SDS is that it produces a constant and stable spherical capsule shape at a different size. The droplet's shape remains almost invariable through the time until it has reached equilibrium. The water droplet was able to float easily on a paraffin oil surface once is deposited on it.

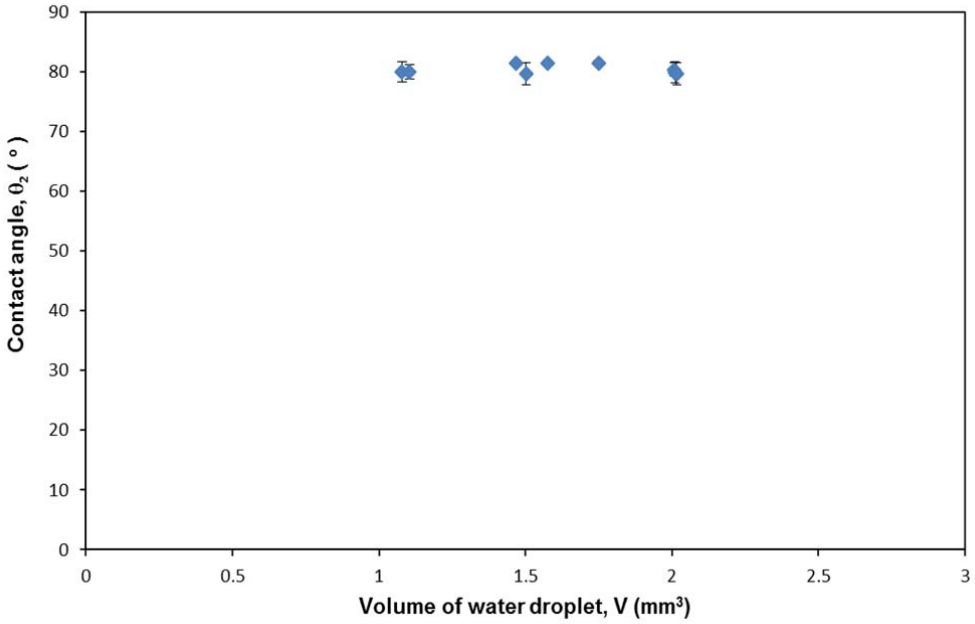

Figure 4.8. Variation of contact angle at different size of water droplets containing SDS (error bars represent standard deviation).

The contact angles as a function of the droplet volume are plotted in Figure 4.8, which describes an insignificant change with increasing volume.

4.2.2 SDS with NaCl

When a solution of sodium chloride was added, the droplet shape changed dramatically in time until equilibrium had been reached and eventually the final shape remained constant, as shown in Figure 4.9.

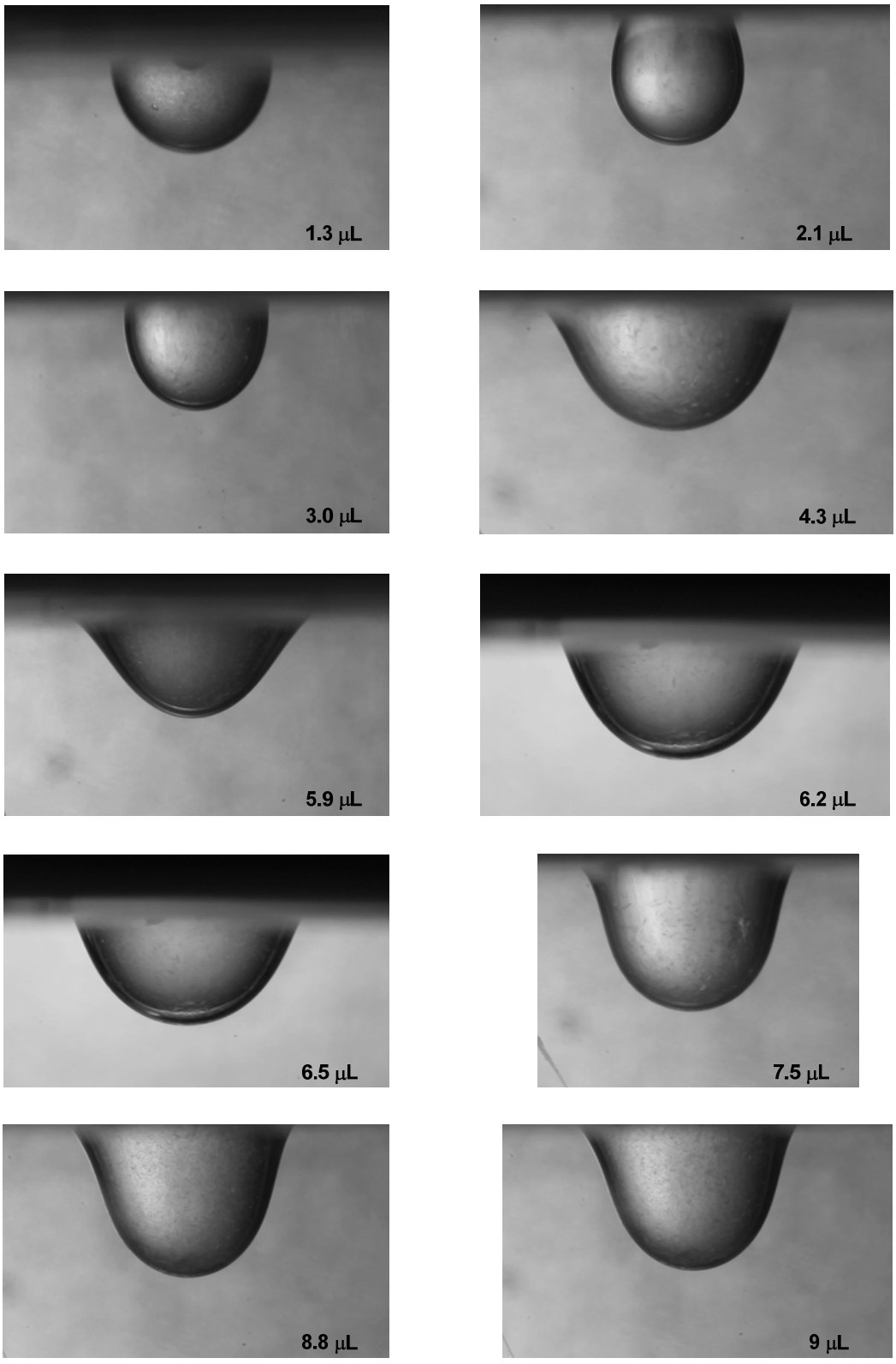

Figure 4.9. Water droplets containing a mixture of SDS and Sodium Chloride at different volumes.

As it shown in equations 2.15 and 2.16, mentioned in Chapter 2, the contact angle depends on the interfacial tension between the three phases in contact oil/water, water/air and oil/air and consequently the stability of the water droplet.

Variation on droplet volume, showed that higher contact angle, i.e. θ_2 is close to 90^o (Figure 4.10). Subsequently, θ_2 decreased while volume increased. An increment of the contact area between droplet and oil surface can also be observed correspondingly in the images above.

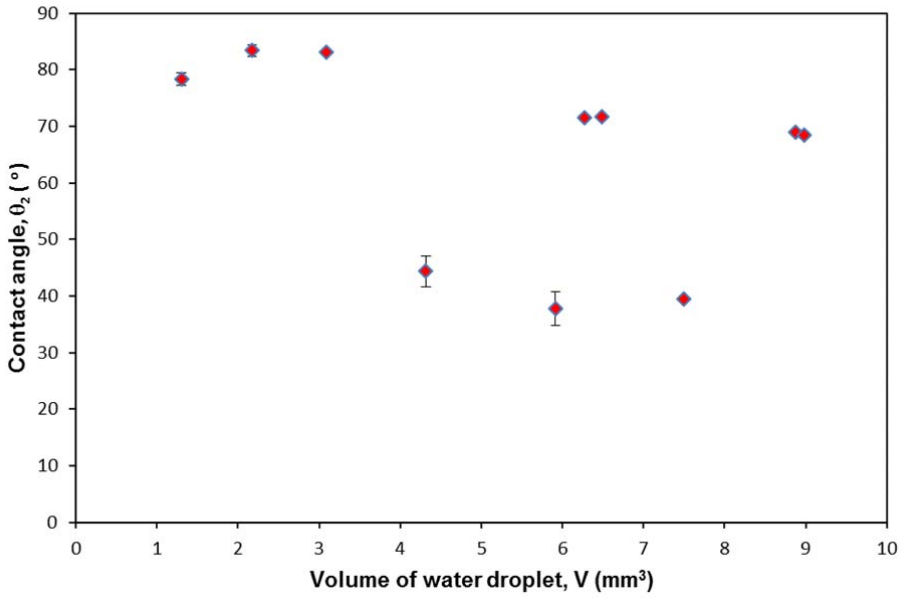

Figure 4.10. Variation of contact angle at different size of water droplets containing a mixture of SDS and electrolyte (error bars represent standard deviation).

It was discovered centuries ago that the addition of salt to concentrated soap solutions caused the separation of a surfactant-rich phase (Lucassen-Reynders 1981). The presence of electrolytes can reduce the surface tension and the critical micelle concentration (CMC) of SDS, which is approximately 0.008 mol/L (Rosenthal, Pyle et al. 1996). In Table 1 of Chapter 3, it can be seen that the inclusion of NaCl can reduce surface tension of SDS solution.

Surface active impurities tend to accumulate in the interface region rather than in the bulk aqueous phase due to the salting out phenomena, resulting in a decrease in interfacial tension. Unsaturated alkanes react with water resulting in acidic components which may behave as surfactants (Zylyftari, Lee et al. 2013). From the obtained images, it is clear that the salting out effects was evident on oil/water interface. However, the crystals on the interface did not modify the shape of the water droplet and its floatability. On the other hand, the solidated oil/water interface may prevent materials transfers across the interface and hence prevent the oil bio- or chemo-degradation.

4.2.3 SDS with NaCl at low pH

As the natural pH of SDS and NaCl solution is relatively high between 9 and 10, the low pH was obtained by adding HCl solution. In Figure 4.11, the presence of a low pH (approximately 4) in the water droplet shapes have shown a wider spread area on oil surface.

Visible small crystals can be observed on the oil/water interface. This could be due to salting out effects. In cases of the water and alkanes, no hydrogen-bonding interactions occur between the two components (experimentally or theoretically) and so it is difficult to present arguments for this behaviour (Patel, Paricaud et al. 2003). In order to accurately assess the fate and effects of organic solutes in marine waters, it is essential to allow for a factor which increases the apparent hydrophobicity of the substance or its tendency to partition out of the aqueous phase (Xie, Shiu et al. 1997).

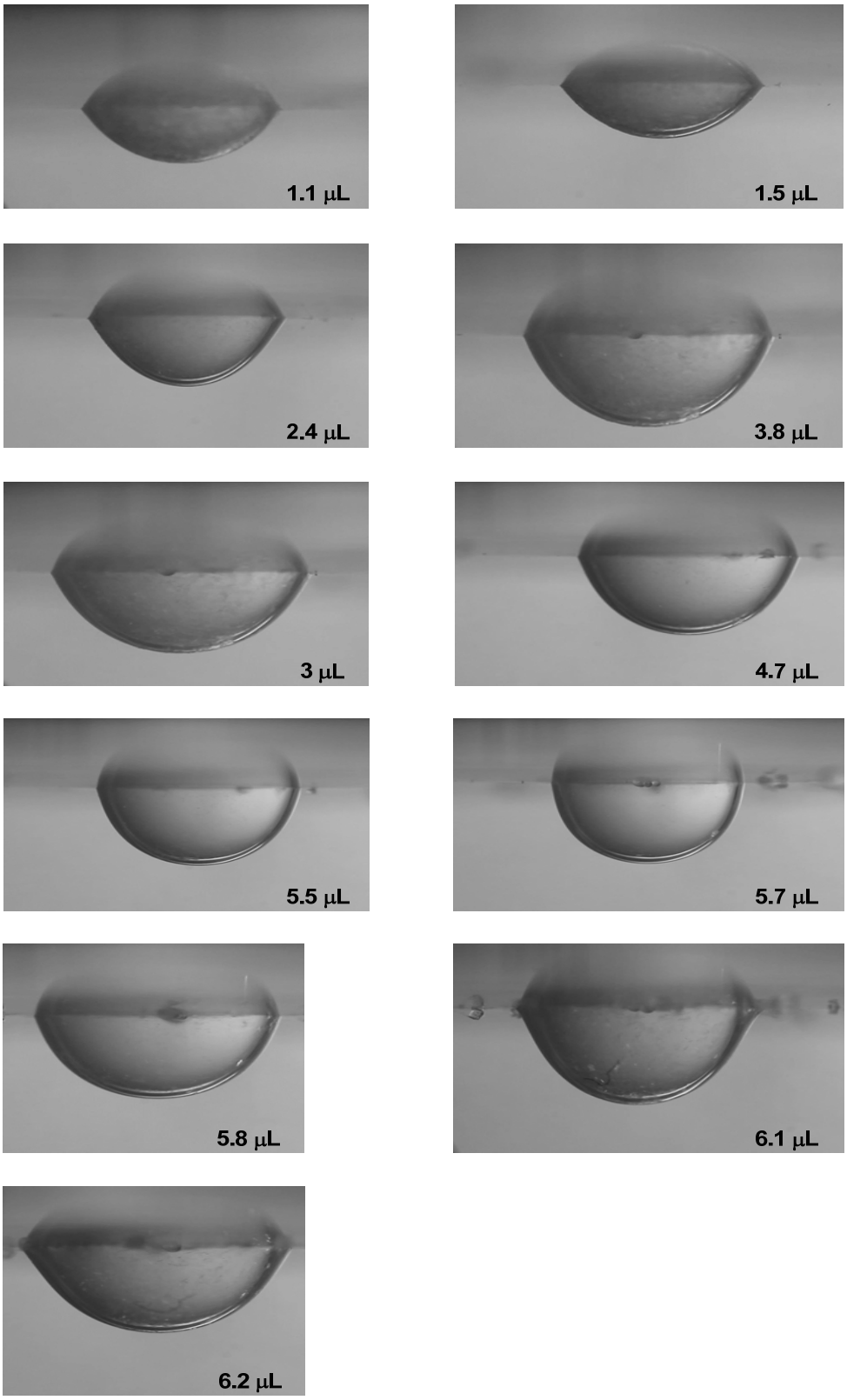

Figure 4.11. Water droplet shapes containing with SDS and 3.5% NaCl at low pH at different volume.

This occurs due to the addition of inorganic acid to water slightly decreases the interfacial tension between the phases, as a function of acid concentration. The relationship between surface tension and acid concentration is not linear (Vecino Bello, Devesa-Rey et al. 2012). However, the addition of surfactants to a strong acid reduces its surface tension until the critical micelle concentration, CMC, after which increasing surfactant concentration does not affect surface tension (Schramm 2000).

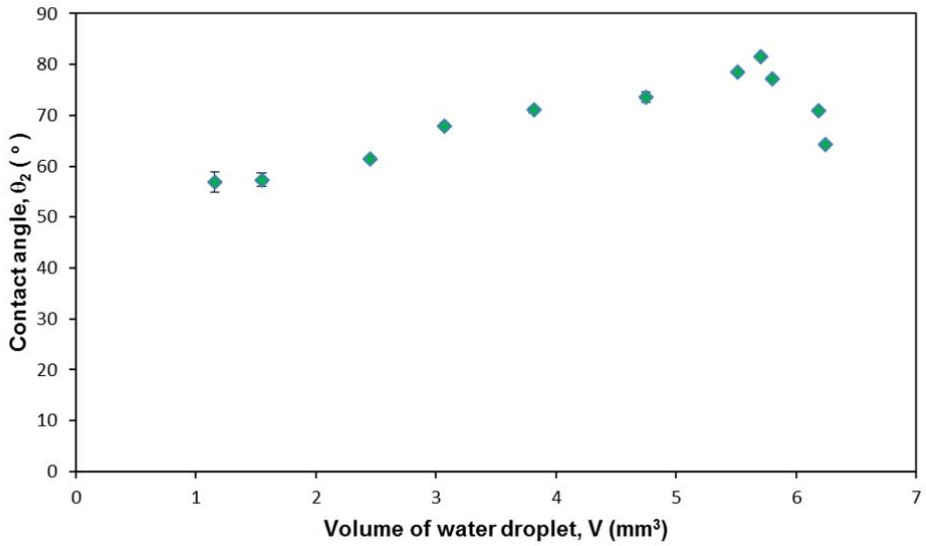

Figure 4.12. Variation of contact angles at different sizes of water droplets containing a mixture of SDS and electrolyte with low pH (error bars represent standard deviation).

Consequently, as shown in Figure 4.12, the contact angle increased proportionally as the volume increase, when volumes of the water droplet are less than 6 µL.

4.3 Summary

The experimental contact angles $\theta_{2,}$ where θ_2 represents the angle of contact between the water droplet and the oil/water interfaces, was obtained for each system at different sizes of water droplets. These values were estimated by using a polynomial function alongside the MatLab edge detection function. In

Figure 4.13, it can be seen that values of θ_2 are less than 90^O for all cases. The droplet's shape is also distinctive, due to the nature of the system's composition.

Water droplets sizes vary up to a volume approx. not greater than 9 µL, as it can be observed in Figure 4.13. However, at higher volume, greater than 9 µL, water droplets can be detached from the oil layer during the deposition process.

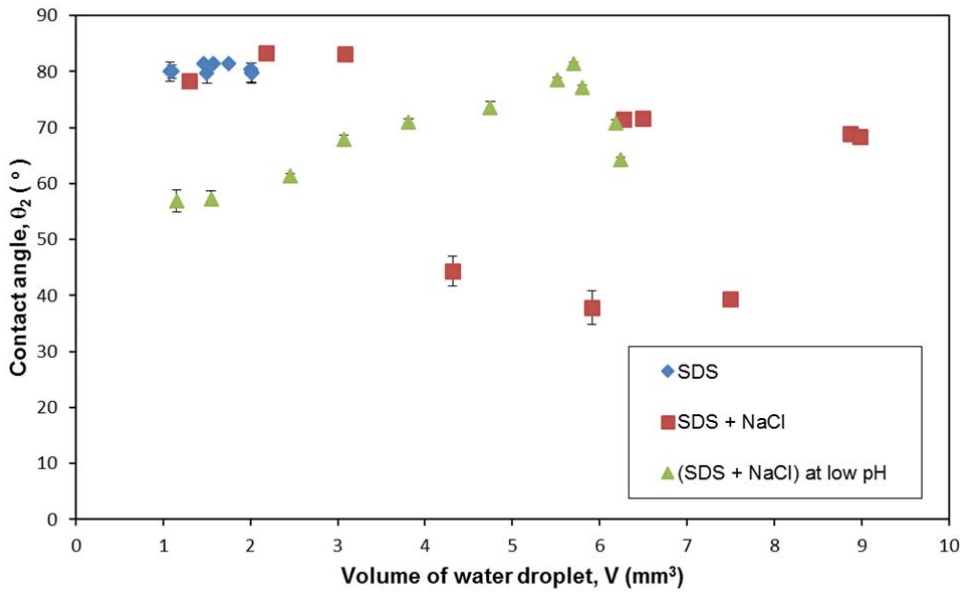

Figure 4.13. Variation of contact angle at different size of water droplets containing a mixture of SDS and electrolyte.

As shown in Figure 4.13, in presence of SDS only, it is evident that the contact angle presents slight changes and constantly invariable whilst increment of the volume. On the other hand, the addition of NaCl made a significant variation on the system, with maximum floating volume increased about 3 times. This is surprised given that the seawater is 10% heavier than freshwater. In practice, the results indicate the usage of seawater is more favourable than freshwater for floating droplet.

It is noteworthy that the data for SDS with NaCl did not follow any clear correlations. This can be explained by considering the salting effects on the contact line. As the interface was solidated with salt crystals, the contact line may not move and prevent the droplet from attaining the theoretical shape, as prescribed by the three interfacial tensions. Such effects were greatly diminished by pH adjustment. In the presence of acid, the contact angle correlated with the increasing volume.

In summary, the results show that aqueous droplet of SDS and NaCl can float stably on the oil surface. The system is applied with decomposing reagent in the next Chapter.

Chapter 5

The Influences of Oil Decomposition Processes on the Floating Droplet

This chapter determines how decomposition of the oil can interfere in the droplet shape and interfacial tension, by being exposed to multiple chemical reactions. The variation in droplet shape during the reaction was also monitored.

The combination of chemical reagents solutions with or without UV irradiation by using Fenton's reactions to decompose paraffin oil can be seen in Table 3. For all cases, each droplet was able to float on the oil surface.

Table 3. Combinations of chemicals reagents for decomposition of paraffin oil.

Solutions	Chemicals reagents solutions	UV irradiation (Solar simulator)
1	SDS, TiO_2	Yes
2	SDS, TiO_2	No
3	SDS, TiO_2, $Fe_2(SO_4)_3$ with low pH	Yes
4	SDS, TiO_2, $Fe_2(SO_4)_3$ with low pH	No
5	SDS, Soil, Enzyme	No
6	SDS, NaCl, $Fe_2(SO_4)_3$. with low pH	No
7	SDS, $FeCl_2$, TiO_2	No

5.1 Using catalyst and combination with UV irradiation

At a laboratory scale, the effectiveness of the method performed by the combination of SDS, TiO_2, $Fe_2(SO_4)_3$ solution at pH= 3 in presence of peroxide, showed a reduction of 4.44 g/m^2 in a short period of reaction time. This reaction was carried on under a solar simulator, which presents an irradiation level up to 550 W UV-lamp.

However, visible reactions have not been observed inside the droplet. The droplet remained stable for approximately 30 minutes on the oil surface until it sunk (see Figure 5.1).

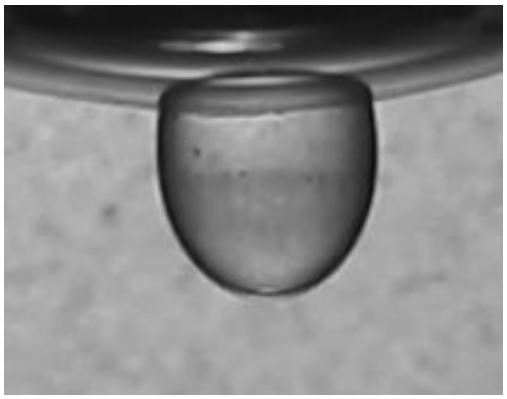

Figure 5.1. No reaction occurs inside the droplet in presence of peroxide with SDS, TiO_2 and $Fe_2(SO_4)_3$ solution at low pH.

Measurements have shown that light irradiation improves the effectiveness of the Fe^{2+}-H_2O_2 system significantly. The main advantage is the regeneration of the consumed Fe^{2+} ions by illumination. Every Fe^{2+} ion can produce many OH radicals. This means that the amount of ferrous salt added may be small, which is important for industrial use to avoid or minimise further separation of the iron ions (Ruppert, Bauer et al. 1993) (Chamarro, Marco et al. 2001).

On the other hand, without employing the solar simulator, the mixture of SDS, TiO_2, NaCl (3.5%) and $Fe_2(SO_4)_3$ solution at pH= 4.1 presented the highest rate of paraffin oil reduced by 4.44 g/m^2.

In most cases, the reaction occurred for about 5 minutes. This was mostly due to the presence of oxygen liberated from the peroxide. In Figure 5.2.a, the water droplet maintains stable its shape and size for about 30 minutes before it sunk.

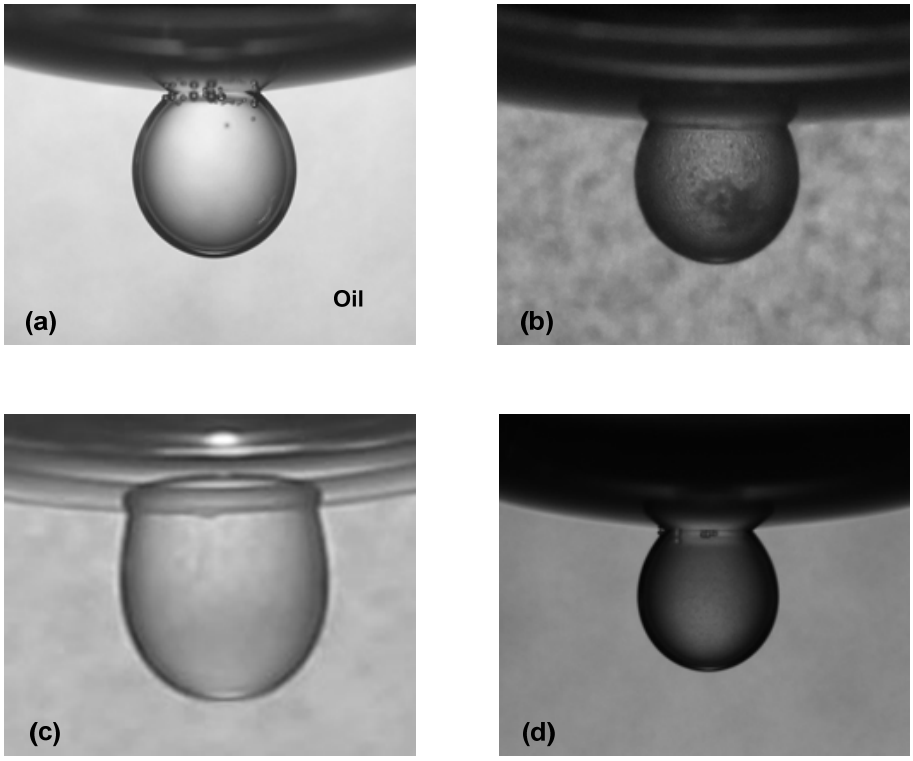

Figure 5.2. (a) Water droplet in presence of SDS, peroxide, NaCl, HCl, TiO_2 and $FeSO_4$. **(b)** Water droplet in presence of SDS, peroxide, NaCl, HCl, TiO_2 and $FeSO_4$. Reaction occurred from the bottom of water droplet. **(c)** Water droplet contents mixture of SDS, TiO_2, H_2O_2 and $FeCl_3$. **(d)** Water droplet in presence of SDS, peroxide and TiO_2.

In some cases, significant observations have been found where the reaction occurs at the bottom of the water droplet, as it shown in Figure 5.2.b. The formation of a thin film as a result of the chemical reactions inside the droplet was also visible.

One disadvantage of the Fenton's reaction is its sensitivity to pH. At pH > 4 Fe-OH species start to precipitate (Bauer 1994). Figure 5.2.c, shows the combination of SDS, TiO_2, H_2O_2 and $FeCl_3$ without UV exposition. Besides,

reagents mixture reacted in a shortest time compared with other chemical combinations; reduction rates of the organic compounds were irrelevant as oil level remained invariable.

In cases such as the mixture of SDS and TiO_2 solution, in the presence of peroxide, the amount of paraffin oil reduced were similar approximately 0.002 with or without contact of UV irradiation on the solution. Chemical reaction between compounds is fast and short. However, the droplet remained steady on the oil surface for about an hour (see Figure 5.2.d).

5.2 Using Enzyme and Micro-organisms

Without SDS, the mixture of enzyme and soil drops went down to the bottom of the container and only one droplet floated on top of the oil surface. However, reduction of the oil did not occur (Figure 5.3.a).

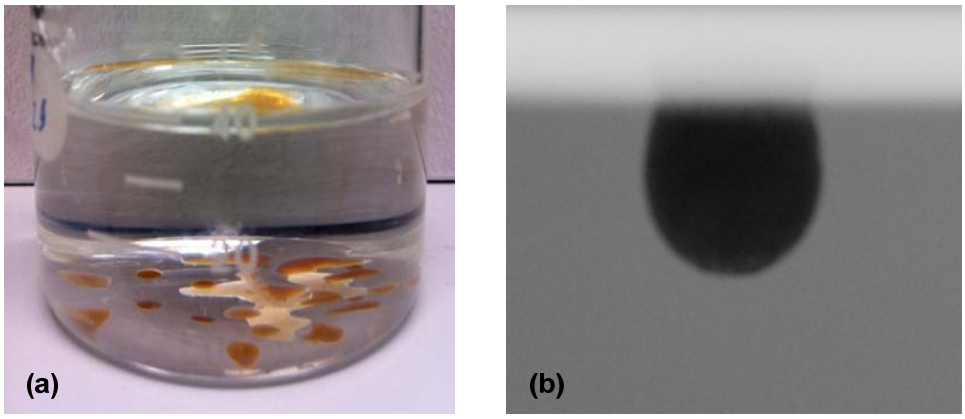

Figure 5.3. (a) Enzyme and soil droplets sunk at the bottom of the glass container. **(b)** Water droplet with enzymes only, after three days of reaction.

When using enzymes only, several droplets were deposited on top of the oil layer, at which only one drop was stable on the surface for a long period of time. However, oil reduction did not occur (see Figure 5.3.b).

Then SDS had to be included to the mixture above to help the droplet remain on the oil surface (Figure 5.4.a) and accelerate the reaction of the enzyme

and soil over the oil. Reduction of the paraffin oil was approximately 0.05 mL. The droplet stayed stable for a period of 5 days on the oil surface. Special attention was taken, when a particular appearance of long filaments were observed around the droplet, as it can be seen in Figure 5.4.b. The grown filaments can form a thickness around 20 to 30 micrometres, after a long period of reaction time, undertaken by a microscopic lens with 66X magnification (Figure 5.4.c).

Bacteria in the ground can be used to consume the oil on the surface and decompose it. Assuming that both oil and bacteria are exposed in the right environment; bacteria can act effectively. This can lead to the appearance of a one-dimensional growth of bio-filaments from the bacterial action (Figure 5.4.b and c).

Moreover, the bacterial action alongside with enzyme can dramatically change the shape of the droplet. The effectiveness of biofilm formation is dependent on the cell surface hydrophobicity, as the hydrophobicity is important in the initial attachment process of bacteria to hydrophobic surfaces (Rühs, Böcker et al. 2014).

During biofilm formation, the different stages of biofilm development are hard to monitor (Rühs, Böni et al. 2013). Although the genetics, biochemistry, and biology of biofilms have been reported, there are relatively few studies examining the physical and mechanical properties of bio-films. Furthermore, the variation of these properties during the course of bio-film development remains unknown. To our knowledge, the formation of bio-film filament has not been reported in the literature.

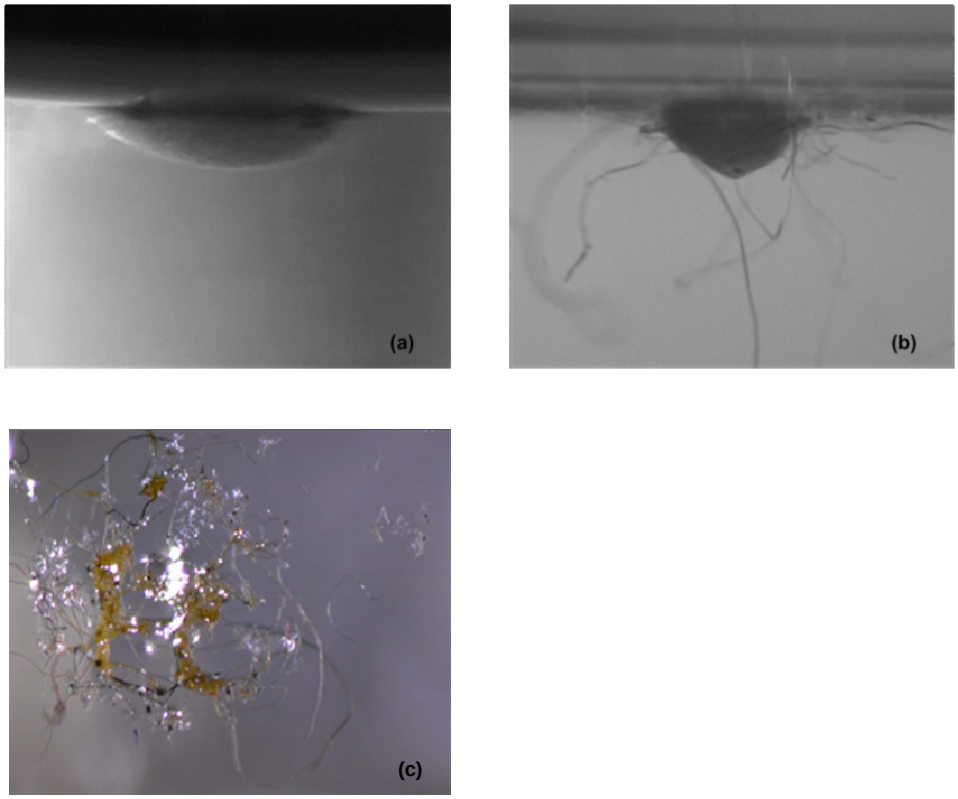

Figure 5.4. (a) Droplet of enzyme solution with SDS and soil, first time deposited. (b) Droplet of enzyme solution with SDS and soil, after 5 days of reaction. (c) Remaining of the bio-filaments (after 3 months of reaction).

One of the most important advantages of the Fenton process is that the reaction is very fast compared with other oxidation methods (Walling 1975). However, the reaction time depends mostly on the type of organic pollutants and the amount of catalysts used (Ruppert, Bauer et al. 1993) (Ruppert, Bauer et al. 1994). The results show that the biological decomposition within the floating droplet is expectedly slow, but can be effective.

5.3 Summary

The experimental results showed that chemical and biological decomposition can affect the oil/water interface; thus the shape of droplet. Relevant results can be resumed in Table 4.

Table 4. Results obtained under different conditions of chemicals reagents for paraffin oil decomposed.

Solutions	Chemicals reagents solutions	UV irradiation (Solar simulator)	Time of reaction	Oil decomposed (g/m^2)
1	SDS, TiO_2	Yes	60 min.	1.66
2	SDS, TiO_2	No	60 min.	2.22
3	SDS, TiO_2, $Fe_2(SO_4)_3$ with low pH	Yes	20 min.	4.44
4	SDS, TiO_2, $Fe_2(SO_4)_3$ with low pH	No	35 min.	0.91
5	SDS, Soil, Enzyme	No	5 days	3.33
6	SDS, 3.5% NaCl, $Fe_2(SO_4)_3$ with low pH	No	5 min.	3.33
7	SDS, $FeCl_2$, TiO_2	No	15 min.	0.22

Without employing the solar simulator, the mixture of SDS, TiO_2, NaCl (3.5%) and $Fe_2(SO_4)_3$ solution at pH= 4.1 presented the highest rate of paraffin oil reduced of 3.33 g/m^2. Reaction occurred for about 5 minutes. This was mostly due to presence of oxygen liberated from the peroxide inside the drop.

Bacterial activity in the ground can be used to consume the oil on the surface and decompose it. Assuming that both oil and bacteria are exposed in the right environment bacteria can act effectively.

However, in most cases the droplet can remain on the surface. An exception is when some of them sink after 30 minutes or when a one-dimensional growth of bio-filament appears from the bacterial action. This bio-filament can form a thickness up to 30 micrometres after a long period of reaction.

Although the biological method is slow, the decomposing action results with a reduction of the oil of about 0.05 mL.

One of the best advantages of the Fenton process is that the reaction is very fast compared with other oxidation techniques. However, the reaction time depends mostly on the type of organic pollutants and the amount of catalyst used. The practicality and accuracy of chemicals mixtures methods utilised in this investigation should be tested further in future work under different conditions.

Chapter 6

Conclusions and Recommendations

6.1 Conclusions

6.1.1 Floatability of water droplets

The first objective of this study was the floatability of water droplets with reagents on a paraffin oil surface. For this study, SDS was employed as a surfactant to support the floating droplet.

The main highlight from using pure SDS was a constant and stable water droplet shape at different sizes. The contact angles as a function of the water droplet volume described an insignificant change with increasing volume. The water droplet was able to float easily on a paraffin oil surface once it was deposited on it. The maximum volume value observed, in presence of SDS, was ~ 2 μL with a contact angle θ_2= 81.87^O.

With the addition of NaCl, the droplet remained floating with a minor deviation. The droplet's shape changed dramatically with time until equilibrium had been reached and the final shape remained constant on a paraffin oil surface. The variation on droplet volume showed that a higher contact angle, i.e. θ_2 is close to 90^o. Subsequently, θ_2 decreased while the volume increased.

The natural pH of SDS and NaCl is relatively high between 9 and 10. Consequently, low pH was also tested. At pH ≈ 4, the water droplet shapes showed a wider spread area on a paraffin oil surface. Values of contact angles θ_2 increased proportionately as the volume increased.

Moreover, the addition of decomposing reagents (biological, chemical and photo-catalysts) has a minor impact on the floatability of the water droplet.

Overall, water droplet sizes vary up to a volume of approximately not greater than 9 µL and stable on a paraffin oil surface. θ_2 values are less than 90^O for all cases.

6.1.2 Oil decomposition process

The second objective of this study was the determination of the influence of the oil decomposing process on the droplet. The experimental results showed that the decomposing processes can significantly affect the droplet shape. However, in most cases the droplet can remain on the surface. Occasionally, some of the droplets sank after 30 minutes. The influences of the composition processes are visually observable in some systems.

The processes have a visible impact on the interface. For instance, the Fenton systems produce bubbles from the oil/water interface. More interestingly, the biological process formed a one-dimensional growth of bio-filament from the oil/water interface.

The rate of oil decomposition was very small due to the experimental setup (i.e. using a single droplet). However, the decomposition based on a single droplet was measured in order of **4 g/ m^2**.

Without employing the solar simulator, the mixture of SDS, TiO_2, NaCl and $Fe_2(SO_4)_3$ solution at pH= 4.1 presented the highest rate of reduction. The chemical reaction occurred for about 5 minutes. This was mostly due to the presence of oxygen liberated from the peroxide inside the drop.

Bacterial activity in the ground can be used to consume the oil on the surface and decompose it. Assuming that both oil and bacteria are exposed in the right environment bacteria can act effectively. Although the biological method is slow, the decomposing action results were very effective.

Fenton process is faster than other oxidation techniques. However, the reaction time depends mostly on the type of organic pollutants and the amount of catalyst used.

The results indicate a possibility for complex surfactant systems to support seawater in a crude oil layer. Such feasibility can lead to the successful treatment of oil spillages without employing toxic solvents. The practicality and accuracy of such chemical mixture methods, utilised in this investigation, should be tested further under different conditions.

6.2 Recommendations for future work

This research determined the floatability of water droplets on oil surfaces, especially on paraffin oil, in the presence of various combinations of surface active agent and chemicals solutions. A fitting-edge model was developed to estimate the bulk of water droplets and contact angles between this and the interfaces involved. Another aspect has also been studied, such as oil decomposition, using paraffin oil as well. In this case, several chemical combinations were tested alongside UV irradiation to help the reaction's speed. Some recommendations for future work are provided below.

All the experiments in this thesis were measured at ambient pressure and temperature. Some of these experiments can be repeated at the higher pressures and temperatures encountered at reservoir conditions to assess any changes in behaviour. Extending this investigation to other kinds of crude oil with properties similar to the one extracted from reservoirs, can achieve results that are closer to reality.

As for instruments and equipment, the size of the micro-syringe can be changed in order to fit the needs of the smaller tip that could yields a higher control of the droplets. Regarding oil decomposition, promising techniques such as biological reagents, need further investigation in this area under different conditions and methodologies. For example, by varying the

concentrations of chemical combinations or changing to a different catalyst such as ozone; or by varying the reaction time.

It is recommended that for future investigations based on current results a sensitivity analysis to be done through an experimental design to determine new combination of chemicals and methods to be performed.

References

Adamson, A. W. and A. P. Gast (1997). Physical chemistry of surfaces. New York, Wiley.

Aveyard, R., et al. (1985). "Interfacial tension minima in oil-water-surfactant systems. Effects of salt, temperature and alkane in systems containing ionic surfactants." J. Chem. Soc., Faraday Trans. 1 **81**(9): 2169-2177.

Aveyard, R., et al. (1987). "Interfacial tension minima in oil–water–surfactant systems. Effects of cosurfactant in systems containing sodium dodecyl sulphate." J. Chem. Soc., Faraday Trans. 1 **83**(8): 2347-2357.

Bauer, R. (1994). "Applicability of solar irradiation for photochemical wastewater treatment." Chemosphere **29**(6): 1225-1233.

Bera, A., et al. (2013). "Synergistic Effect of Surfactant and Salt Mixture on Interfacial Tension Reduction between Crude Oil and Water in Enhanced Oil Recovery." Journal of Chemical & Engineering Data **59**(1): 89-96.

Berry, R. J. and M. R. Mueller (1994). "Photocatalytic Decomposition of Crude Oil Slicks Using TiO2 on a Floating Substrate." Microchemical journal **50**(1): 28-32.

Bishop, D., et al. (1968). "Hydrogen peroxide catalytic oxidation of refractory organics in municipal waste waters." Industrial & Engineering Chemistry Process Design and Development **7**(1): 110-117.

Bormashenko, E., et al. (2009). "Water rolling and floating upon water: marbles supported by a water/marble interface." Journal of Colloid and Interface Science **333**(1): 419-421.

Boucher, E. (1980). "Capillary phenomena: properties of systems with fluid/fluid interfaces." Reports on Progress in Physics **43**(4): 497.

Boucher, E. and M. Evans (1975). "Pendent drop profiles and related capillary phenomena." Proceedings of the Royal Society of London. A. Mathematical and Physical Sciences **346**(1646): 349-374.

Boucher, E. and H. Kent (1978). "Capillary phenomena VII. Equilibrium and stability of pendent drops." Journal of Colloid and Interface Science **67**(1): 10-15.

Boucher, E. A. and T. G. Jones (1982). "Capillary phenomena. Part 18.—Conditions for the flotation of solid spheres at liquid/liquid and liquid/vapour interfaces in a gravitational field." Journal of the Chemical Society, Faraday Transactions 1: Physical Chemistry in Condensed Phases **78**(5): 1499-1506.

Brillas, E., et al. (2009). "Electro-Fenton process and related electrochemical technologies based on Fenton's reaction chemistry." Chemical Reviews **109**(12): 6570-6631.

Brochard-Wyard, F., et al. (2003). Capillarity and wetting phenomena : Drops, bubbles, pearls, waves. New York, Springer.

Buff, F. P. and H. Saltsburg (1957). Curved fluid interfaces. I. The generalized Neumann formula. The Journal of Chemical Physics. **26:** 23-31.

Burton, J., et al. (2010). "Experimental and numerical investigation of the equilibrium geometry of liquid lenses." Langmuir **26**(19): 15316-15324.

Chamarro, E., et al. (2001). "Use of Fenton reagent to improve organic chemical biodegradability." Water research **35**(4): 1047-1051.

Cockbain, E. (1954). "The adsorption of sodium dodecyl sulphate at the oil-water interface and application of the Gibbs equation." Transactions of the Faraday Society **50**: 874-881.

De Gennes, P.-G. (1985). "Wetting: statics and dynamics." Reviews of modern physics **57**(3): 827.

De Gennes, P. and C. Taupin (1982). "Microemulsions and the flexibility of oil/water interfaces." The Journal of Physical Chemistry **86**(13): 2294-2304.

Dominguez, H., et al. (1994). "Enzymatic pretreatment to enhance oil extraction from fruits and oilseeds: a review." Food chemistry **49**(3): 271-286.

Extrand, C. and S. I. Moon (2009). "Using the Flotation of a Single Sphere to Measure and Model Capillary Forces." Langmuir **25**(11): 6239-6244.

Farzadkia, M., et al. (2014). "The effects of Fenton process on the removal of petroleum hydrocarbons from oily sludge in Shiraz oil refinery, Iran." Journal of Environmental Health Science and Engineering **12**(1): 31.

Finn, R. (1999). "Capillary surface interfaces." Notices of the AMS **46**(7): 770-781.

Garvey, M. J. and I. D. Robb (1979). "Effect of electrolytes on solution behaviour of water soluble macromolecules." Journal of the Chemical Society, Faraday Transactions 1: Physical Chemistry in Condensed Phases **75**: 993-1000.

Grzechulska, J., et al. (2000). "Photocatalytic decomposition of oil in water." Water research **34**(5): 1638-1644.

Hanmoungjai, P., et al. (2001). "Enzymatic process for extracting oil and protein from rice bran." Journal of the American Oil Chemists' Society **78**(8): 817-821.

Hartland, S. (2004). Surface and interfacial tension: measurement, theory, and applications, CRC Press.

Juhasz, A. L. and R. Naidu (2000). "Bioremediation of high molecular weight polycyclic aromatic hydrocarbons: a review of the microbial degradation of benzo[a] pyrene." International Biodeterioration & Biodegradation **45**(1): 57-88.

Kanaly, R. A. and S. Harayama (2000). "Biodegradation of high-molecular-weight polycyclic aromatic hydrocarbons by bacteria." Journal of Bacteriology **182**(8): 2059-2067.

Kostka, J. E., et al. (2011). "Hydrocarbon-degrading bacteria and the bacterial community response in Gulf of Mexico beach sands impacted by the Deepwater Horizon oil spill." Applied and environmental microbiology **77**(22): 7962-7974.

Langmuir, I. (1933). "Oil lenses on water and the nature of monomolecular expanded films." The Journal of Chemical Physics **1**: 756.

Langmuir, I. (1933). "Oil lenses on water and the nature of monomolecular expanded films." The Journal of chemical physics **1**(11): 756-776.

Lazar, I., et al. (2007). "Microbial enhanced oil recovery (MEOR)." Petroleum Science and Technology **25**(11): 1353-1366.

Leahy, J. G. and R. R. Colwell (1990). "Microbial degradation of hydrocarbons in the environment." Microbiological reviews **54**(3): 305-315.

Lima, E., et al. (2013). "Specific ion effects on the interfacial tension of water/hydrocarbon systems." Brazilian Journal of Chemical Engineering **30**(1): 55-62.

Luangpirom, N., et al. (2001). "Contact angle of surfactant solutions on precipitated surfactant surfaces." Journal of Surfactants and Detergents **4**(4): 367-373.

Lucassen-Reynders, E. (1981). Anionic surfactants: Physical chemistry of surfactant action, M. Dekker.

Mackay, D. and W. Y. Shiu (1975). "The determination of the solubility of hydrocarbons in aqueous sodium chloride solutions." The Canadian Journal of Chemical Engineering **53**(2): 239-242.

Man, Y. C., et al. (1996). "Aqueous enzymatic extraction of coconut oil." Journal of the American Oil Chemists' Society **73**(6): 683-686.

McGlone, O. C., et al. (1986). "Coconut oil extraction by a new enzymatic process." Journal of Food Science **51**(3): 695-697.

Miller, C. A. and P. Neogi (2007). "Interfacial phenomena: equilibrium and dynamic effects." Interfacial phenomena: equilibrium and dynamic effects.

Morita, A., et al. (2002). "Influence of drop volume on surface tension evaluated using the pendant drop method." Colloid and Polymer Science **280**(9): 857-864.

Mullins, O. C. (2008). "Review of the molecular structure and aggregation of asphaltenes and petroleomics." Spe Journal **13**(01): 48-57.

Najafian, L., et al. (2009). "Aqueous extraction of virgin olive oil using industrial enzymes." Food research international **42**(1): 171-175.

Natoli, J. (1980). Sodium dodecyl sulfate: A model surfactant for enhanced oil recovery, Carnegie-Mellon University.

Olmez-Hanci, T. (2012). "Treatment of commercial surfactants with chemical and photochemical advanced oxidation processes." Handbook of Environment and Waste Management: Air and Water Pollution Control **1**: 271.

Patel, B., et al. (2003). "Prediction of the salting-out effect of strong electrolytes on water+ alkane solutions." Industrial & engineering chemistry research **42**(16): 3809-3823.

Peroxide, U. (2009). "Introduction to hydrogen peroxide." URL: http://www.h2o2.com/ **2**.

Phan, C. M. (2014). "Stability of a Floating Water Droplet on an Oil Surface." Langmuir **30**(3): 768-773.

Phan, C. M., et al. (2012). "Can Water Float on Oil?" Langmuir **28**(10): 4609-4613.

Rosen, M. J. and J. T. Kunjappu (2012). Surfactants and Interfacial Phenomena. Hoboken, John Wiley & Sons**:** 1 online resource (618 p.).

Rosenthal, A., et al. (1996). "Aqueous and enzymatic processes for edible oil extraction." Enzyme and Microbial Technology **19**(6): 402-420.

Rowlinson, J. and B. Widom (1982). Molecular theory of capillarity. The international series of monographs on chemistry, Oxford: Oxford University Press.

Rubio, J., et al. (2002). "Overview of flotation as a wastewater treatment technique." Minerals Engineering **15**(3): 139-155.

Rühs, P., et al. (2014). "Studying bacterial hydrophobicity and biofilm formation at liquid–liquid interfaces through interfacial rheology and pendant drop tensiometry." Colloids and Surfaces B: Biointerfaces **117**: 174-184.

Rühs, P. A., et al. (2013). "In-Situ Quantification of the Interfacial Rheological Response of Bacterial Biofilms to Environmental Stimuli." PloS one **8**(11): e78524.

Ruppert, G., et al. (1993). "The photo-Fenton reaction—an effective photochemical wastewater treatment process." Journal of Photochemistry and Photobiology A: Chemistry **73**(1): 75-78.

Ruppert, G., et al. (1994). "UV-O3, UV-H2O2, UV-TiO2 and the photo-Fenton reaction: comparison of advanced oxidation processes for wastewater treatment." Chemosphere **28**(8): 1447-1454.

Schramm, L. L. (2000). Surfactants : fundamentals and applications in the petroleum industry. Cambridge, U.K., Cambridge University Press.

Sharma, A., et al. (2001). "Enzyme-assisted aqueous extraction of rice bran oil." Journal of the American Oil Chemists' Society **78**(9): 949-951.

Sharma, A., et al. (2002). "Enzyme-assisted aqueous extraction of peanut oil." Journal of the American Oil Chemists' Society **79**(3): 215-218.

Snir, J. (1991). "Sink or float—what do the experts think?: The historical development of explanations for floatation." Science Education **75**(5): 595-609.

Stasinakis, A. (2008). "Use of selected advanced oxidation processes (AOPs) for wastewater treatment—a mini review." Global NEST Journal **10**(3): 376-385.

Tong, S., et al. (1999). "ASEAN marine water quality criteria for oil and grease." Marine Environment Division, Water quality management Bureau, Pollution control department. ASEAN-CANADA Cooperative programme on Marine Science.

Vecino Bello, X., et al. (2012). "Study of the synergistic effects of salinity, pH, and temperature on the surface-active properties of biosurfactants produced by lactobacillus pentosus." Journal of agricultural and food chemistry **60**(5): 1258-1265.

Vella, D., et al. (2006). "The load supported by small floating objects." Langmuir **22**(14): 5979-5981.

Venkataraman, R. (2007). Effect of surfactants on the dynamic interfacial characteristics of oil-water interfaces. Department of Process Engineering and Applied Science. Canada, Dalhousie University. **Master of Applied Science:** 259.

Walling, C. (1975). "Fenton's reagent revisited." Accounts of chemical research **8**(4): 125-131.

Wang, Z., et al. (2003). "Characteristics of spilled oils, fuels, and petroleum products: 1. Composition and properties of selected oils." US EPA Report EPA/600-R/03 **72**.

West, C. C. and J. H. Harwell (1992). "Surfactants and subsurface remediation." Environmental Science & Technology **26**(12): 2324-2330.

Wolfe, D. A., et al. (1994). "The fate of the oil spilled from the Exxon Valdez." Environmental Science & Technology **28**(13): 560A-568A.

Xie, W.-H., et al. (1997). "A review of the effect of salts on the solubility of organic compounds in seawater." Marine Environmental Research **44**(4): 429-444.

Zylyftari, G., et al. (2013). "Salt effects on thermodynamic and rheological properties of hydrate forming emulsions." Chemical engineering science **95**: 148-160.

Appendix A Modelling of water droplets

A.1 SDS Droplets Images:

IMG_395111 (V= 1.749 mm^3)

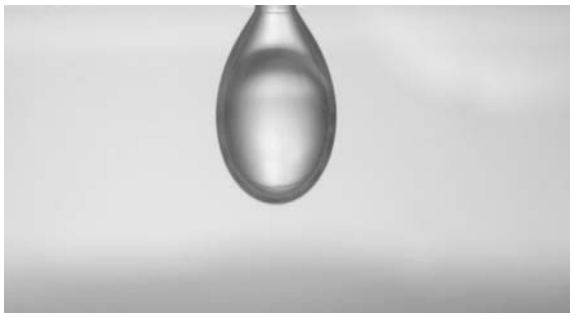

Edge fitting image using MATLAB

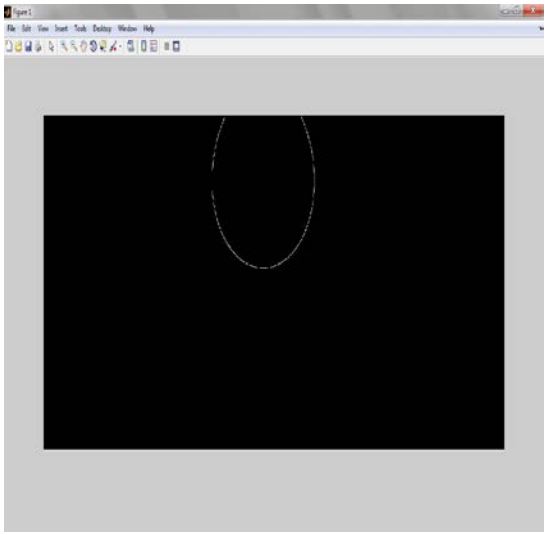

Excel sheet with droplet profile data

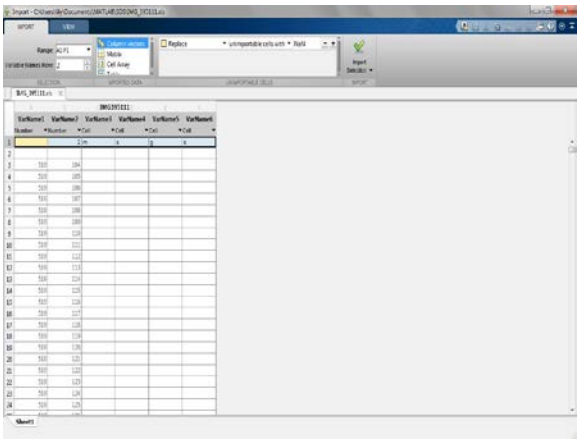

Edge fitting resulting by using a polynomial function

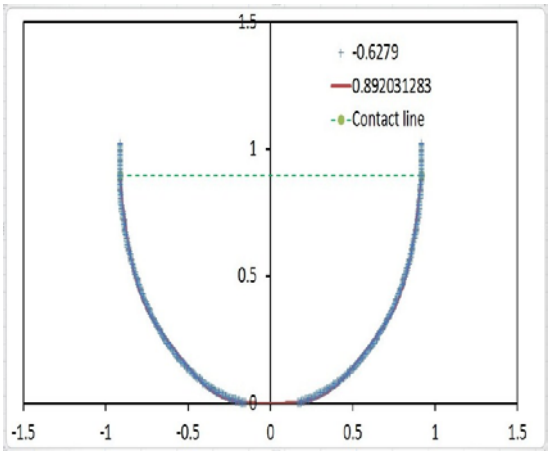

IMG_398111 (V= 1.577 mm^3)

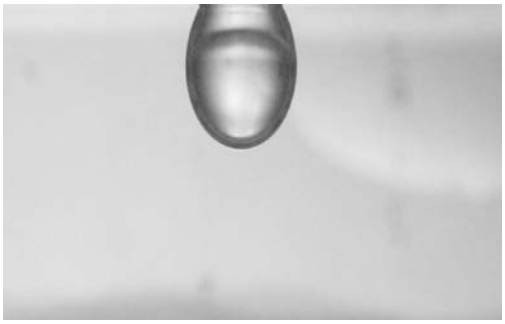

Edge fitting image using MATLAB

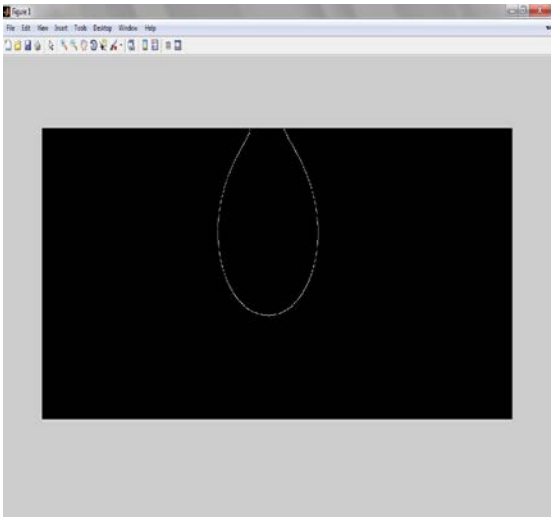

Excel sheet with droplet profile data

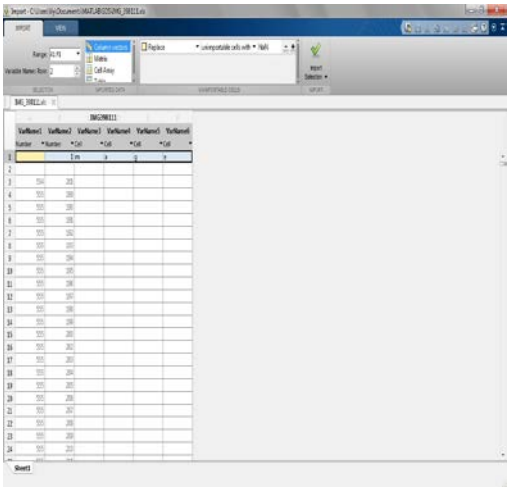

Edge fitting resulting by using a polynomial function

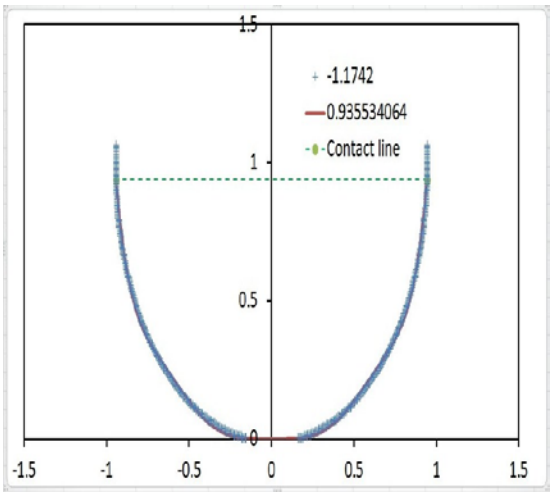

MVI_3969_053501 (V= 2.007 mm^3)

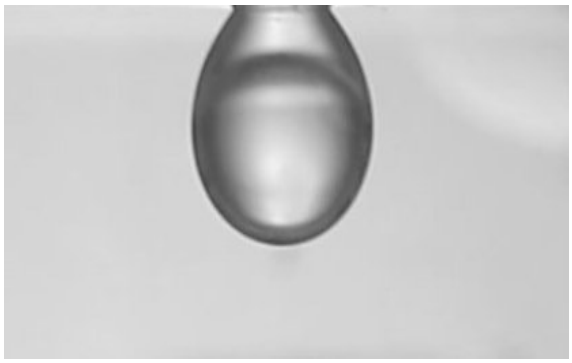

Edge fitting image using MATLAB

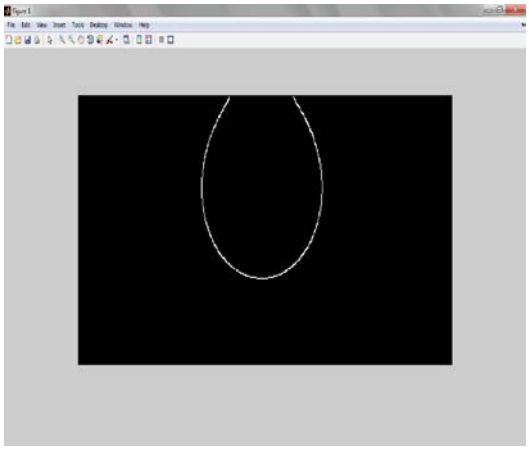

Excel sheet with droplet profile data

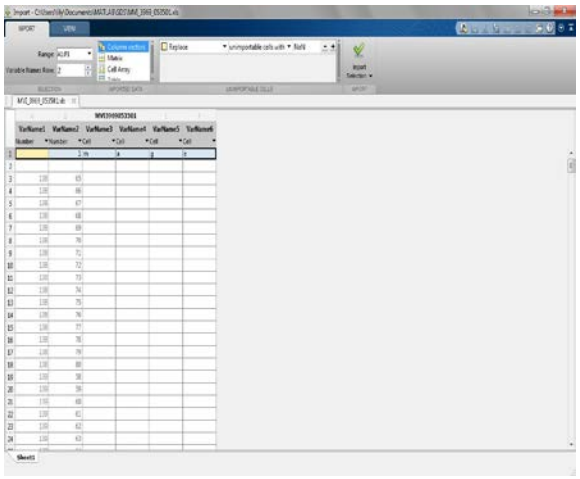

Edge fitting resulting by using a polynomial function

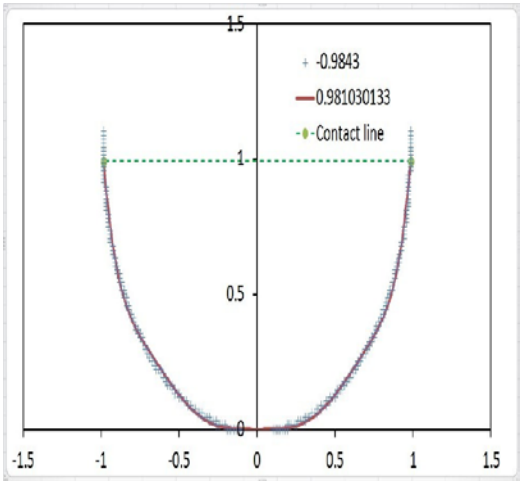

MVI_3961_34001 (V= 1.502 mm^3)

Edge fitting image using MATLAB

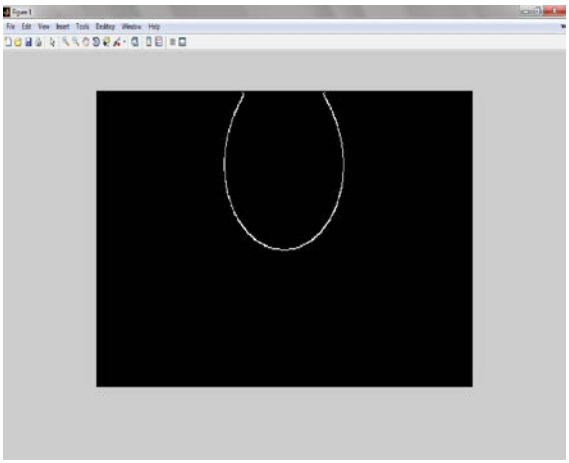

Excel sheet with droplet profile data

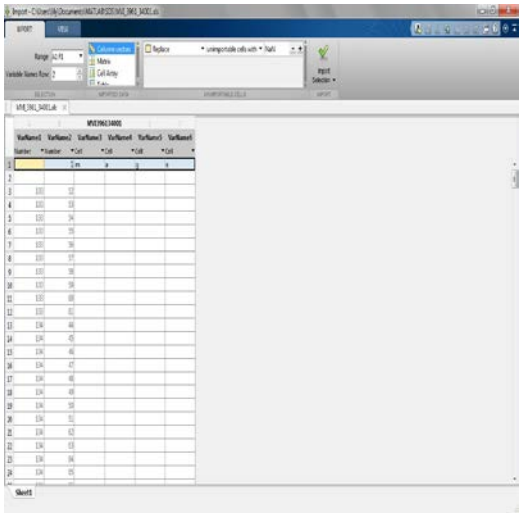

Edge fitting resulting by using a polynomial function

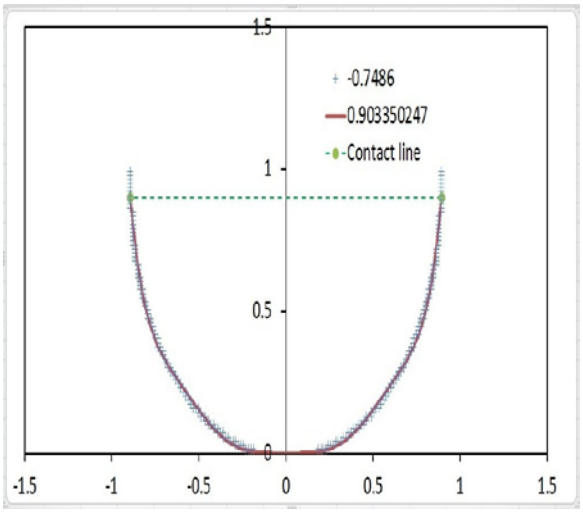

MVI_3939_035001 (V= 1.468 mm^3)

Edge fitting image using MATLAB

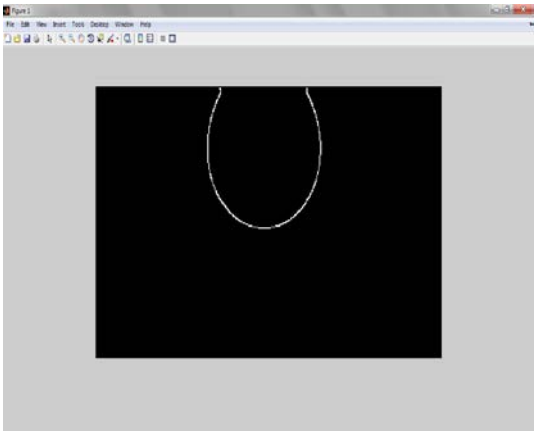

Excel sheet with droplet profile data

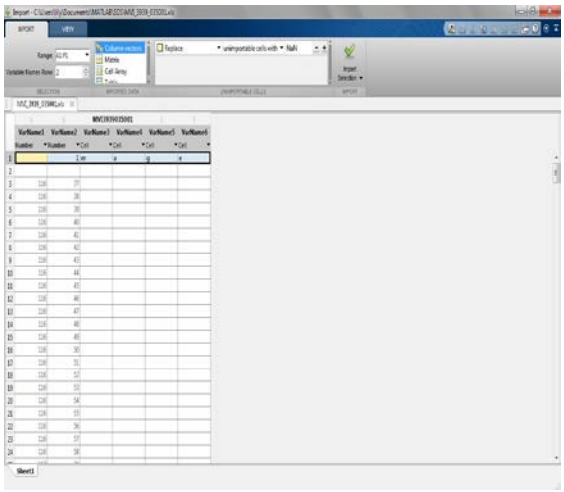

Edge fitting resulting by using a polynomial function

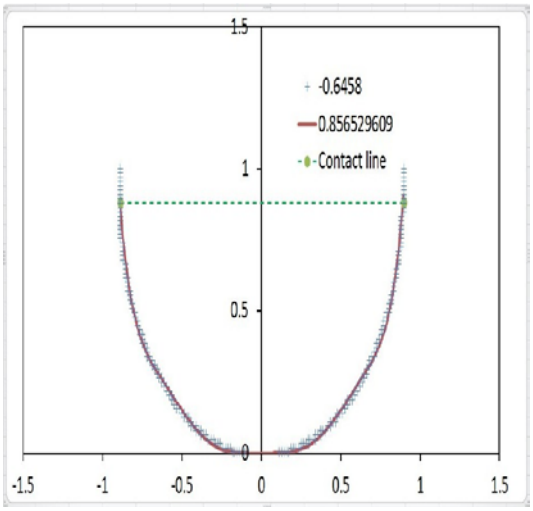

MVI_3930_105001 (V= 2.011 mm^3)

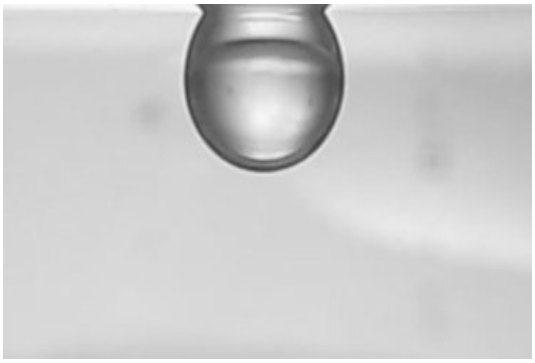

Edge fitting image using MATLAB

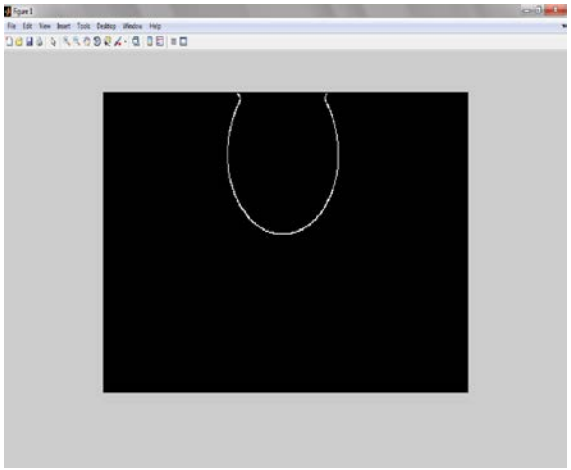

Excel sheet with droplet profile data

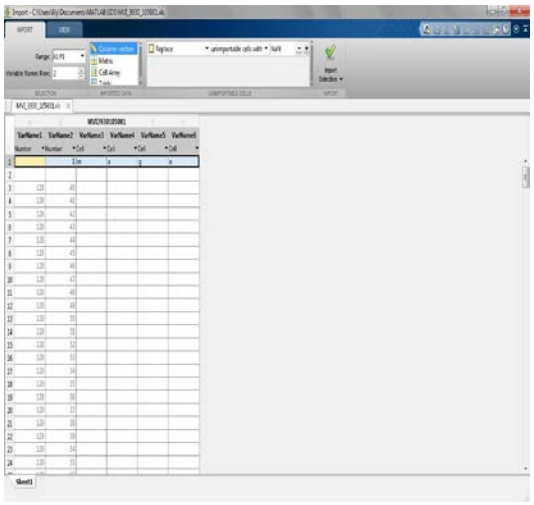

Edge fitting resulting by using a polynomial function

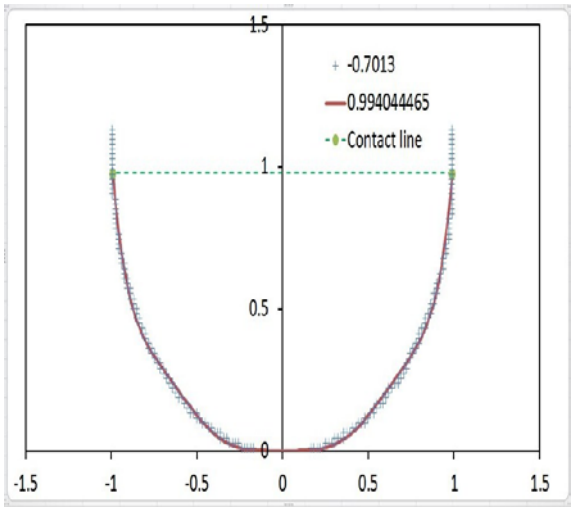

MVI_3930_108001 (V= 2.016 mm^3)

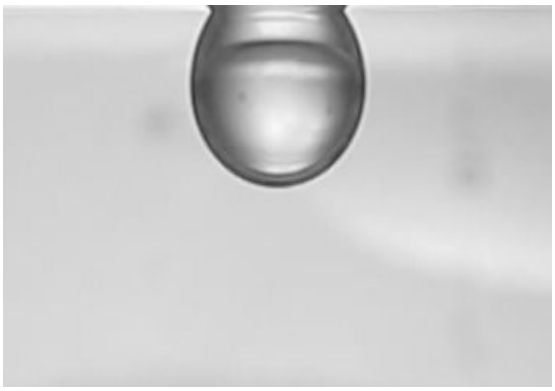

Edge fitting image using MATLAB

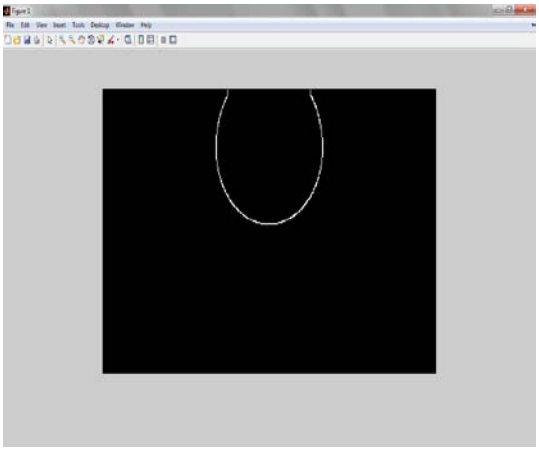

Excel sheet with droplet profile data

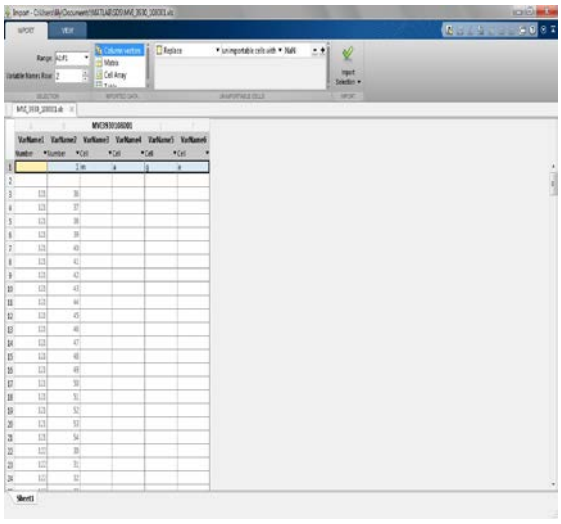

Edge fitting resulting by using a polynomial function

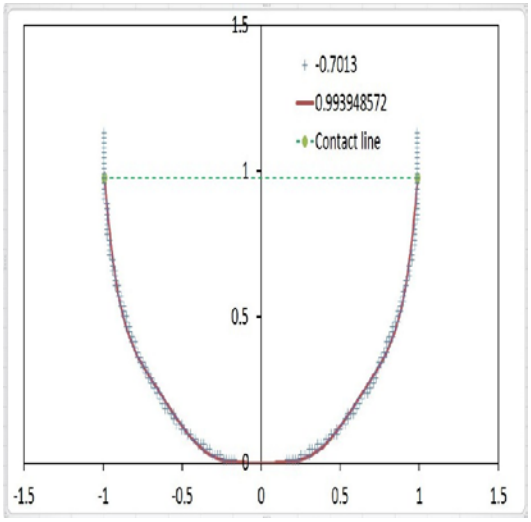

MVI_3923_29501 (V= 1.079 mm^3)

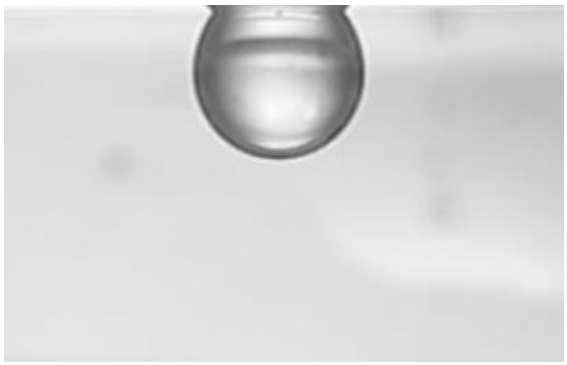

Edge fitting image using MATLAB

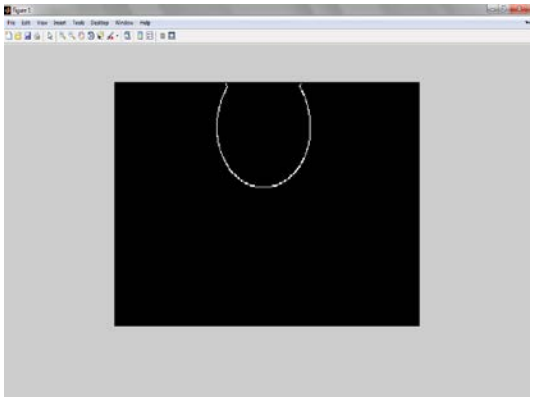

Excel sheet with droplet profile data

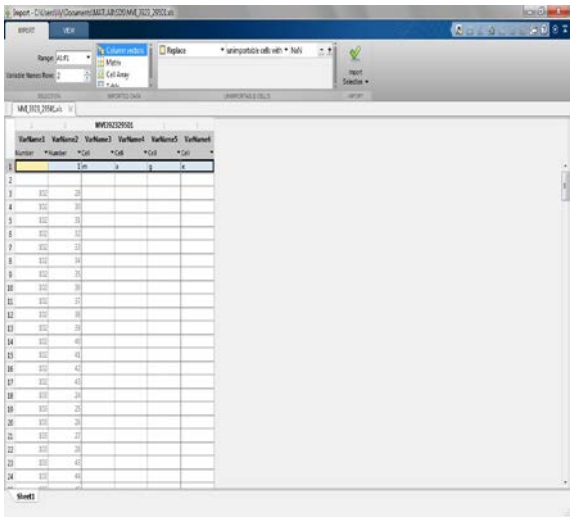

Edge fitting resulting by using a polynomial function

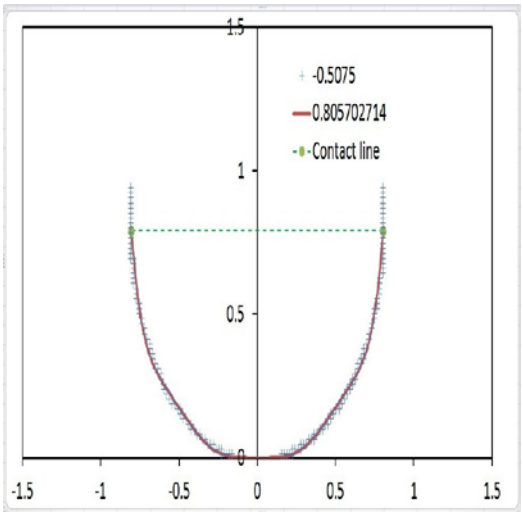

MVI_3923_30001 (V= 1.014 mm^3)

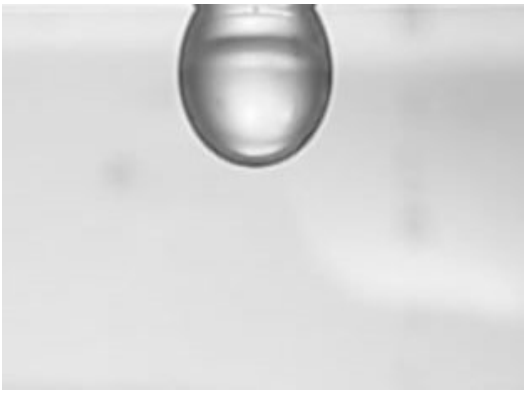

Edge fitting image using MATLAB

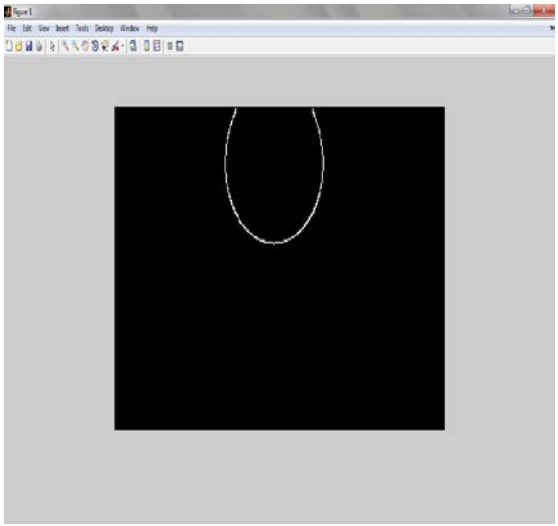

Excel sheet with droplet profile data

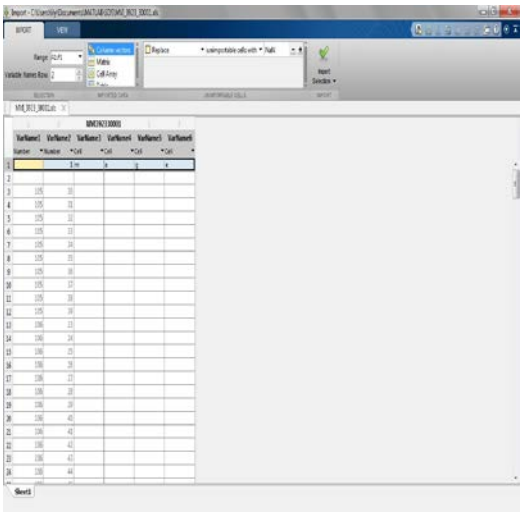

Edge fitting resulting by using a polynomial function

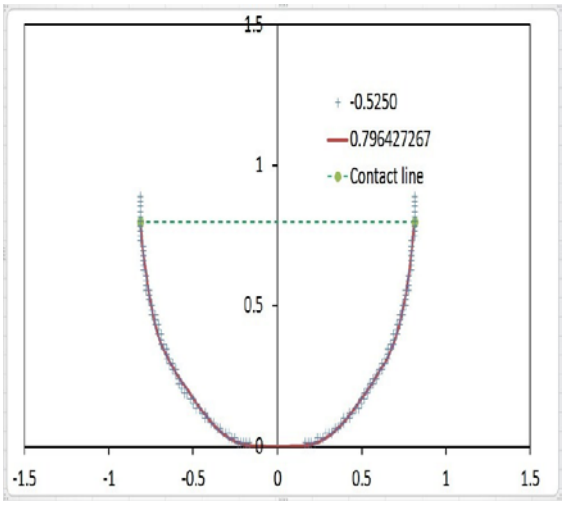

A.2 (SDS and NaCl) Droplets Images:

MVI_9254_22500 (V= 1.301 mm^3)

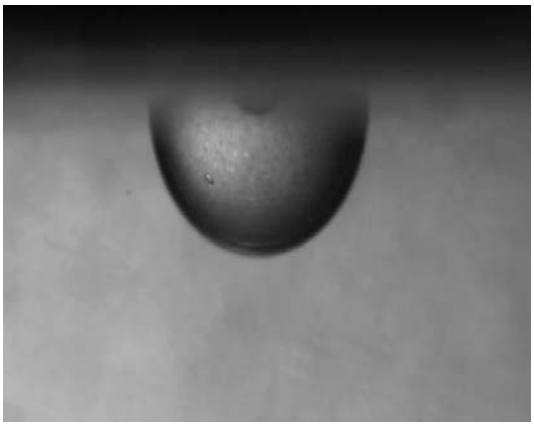

Edge fitting image using MATLAB

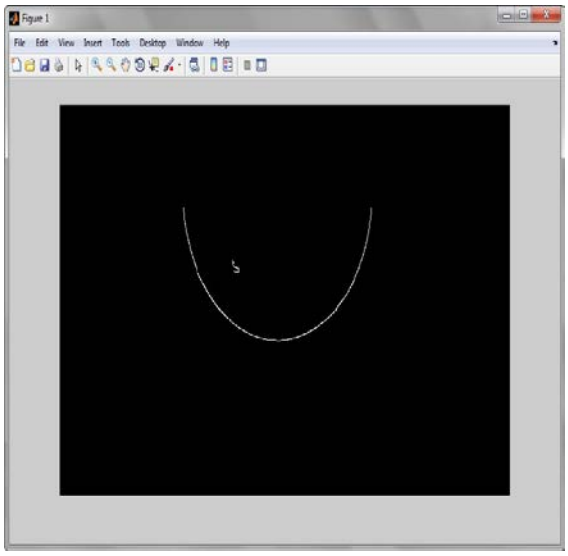

Excel sheet with droplet profile data

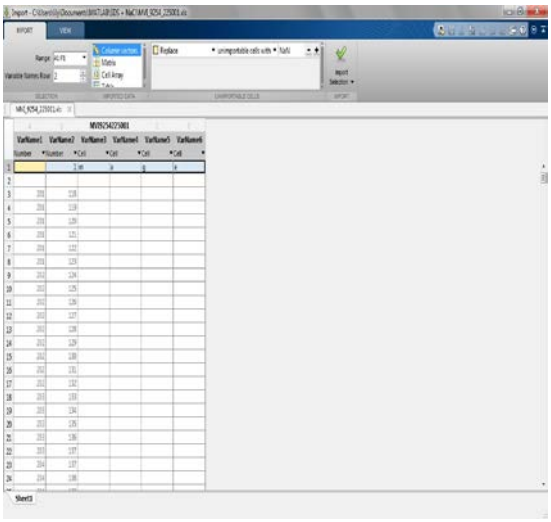

Edge fitting resulting by using a polynomial function

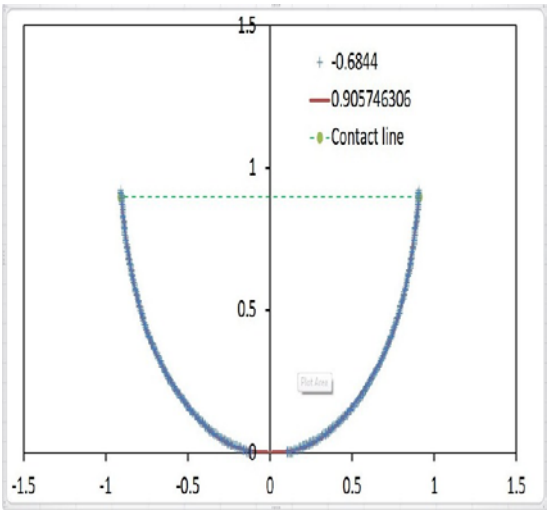

MVI_9287_010001 (V= 3.084 mm^3)

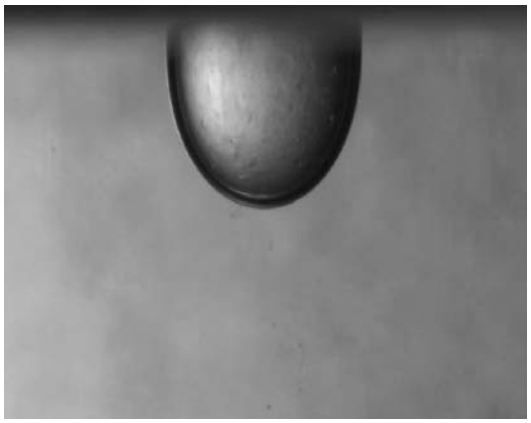

Edge fitting image using MATLAB

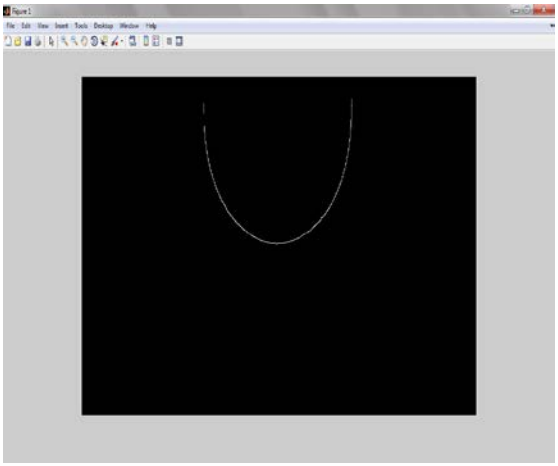

Excel sheet with droplet profile data

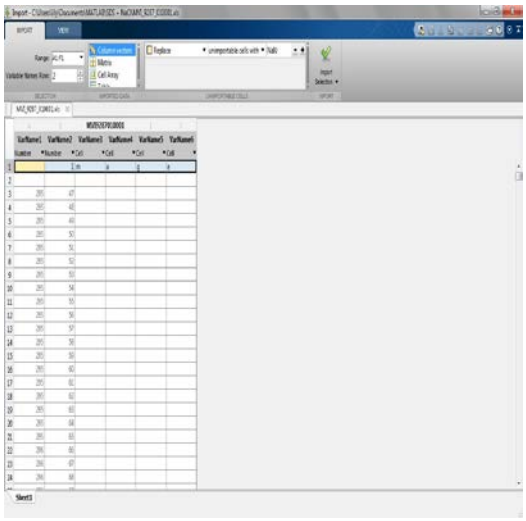

Edge fitting resulting by using a polynomial function

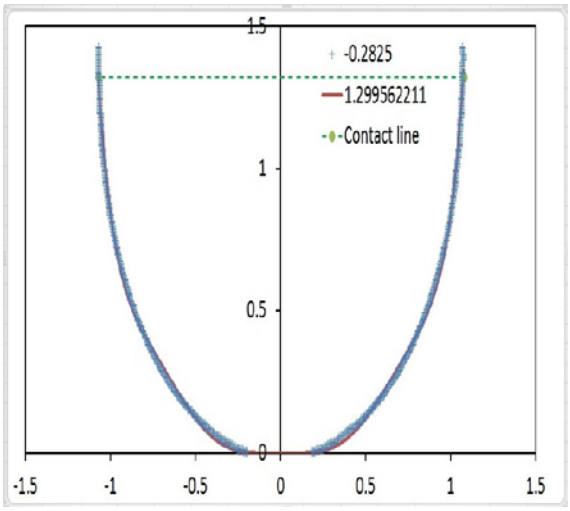

MVI_9287_014001 (V= 2.177 mm^3)

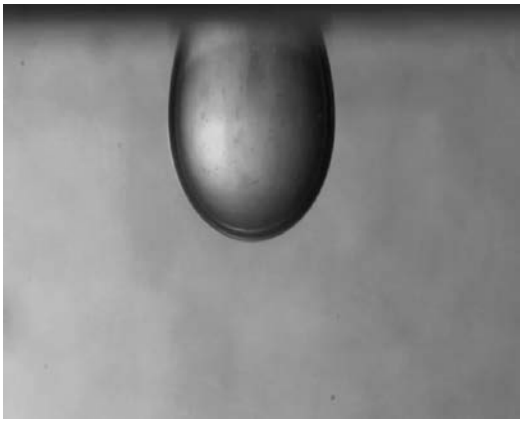

Edge fitting image using MATLAB

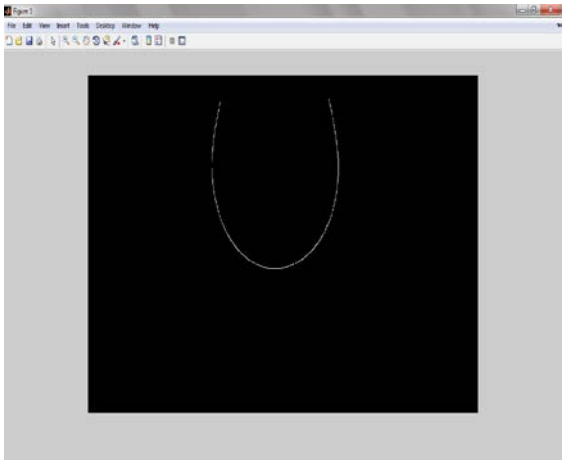

Excel sheet with droplet profile data

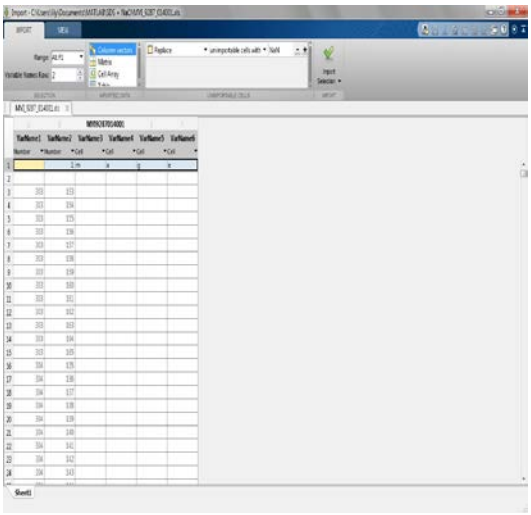

Edge fitting resulting by using a polynomial function

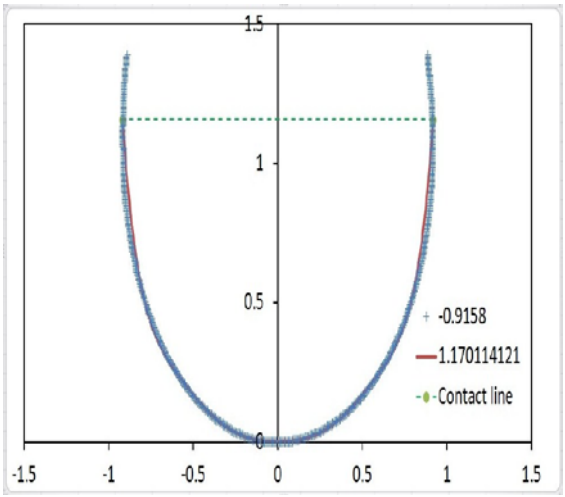

MVI_9287_003501 (V= 7.494 mm^3)

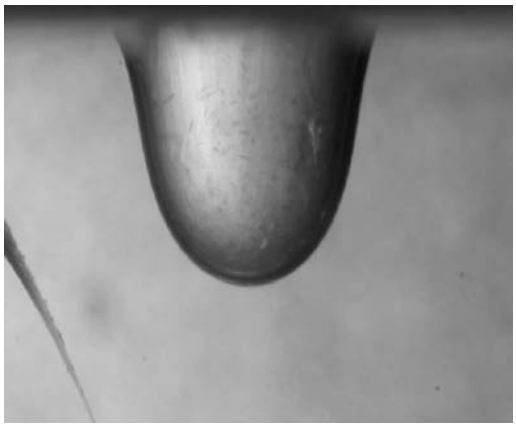

Edge fitting image using MATLAB

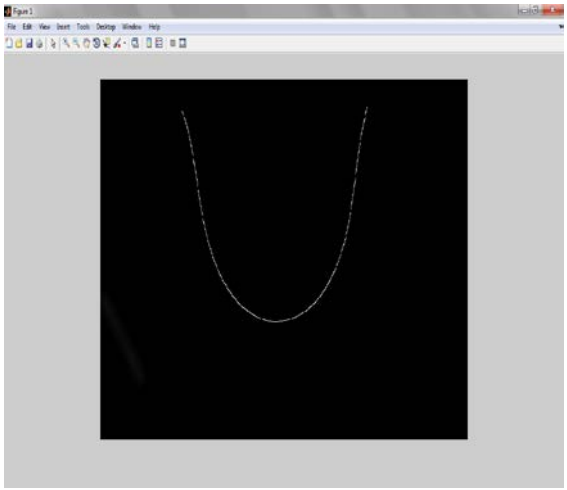

Excel sheet with droplet profile data

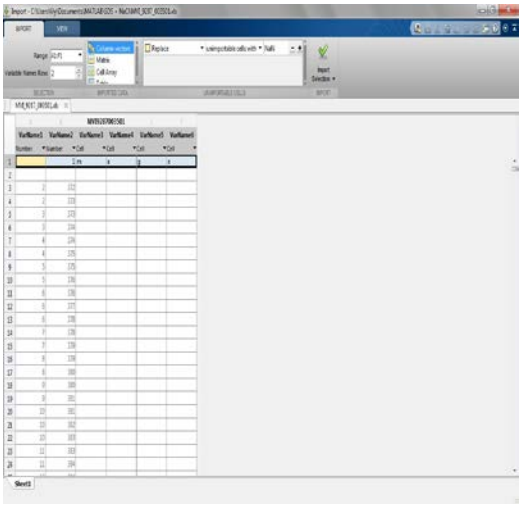

Edge fitting resulting by using a polynomial function

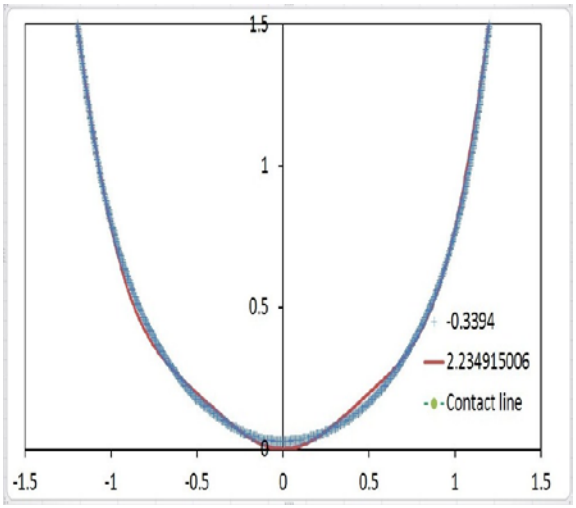

MVI_9004_27000 (V= 6.268 mm^3)

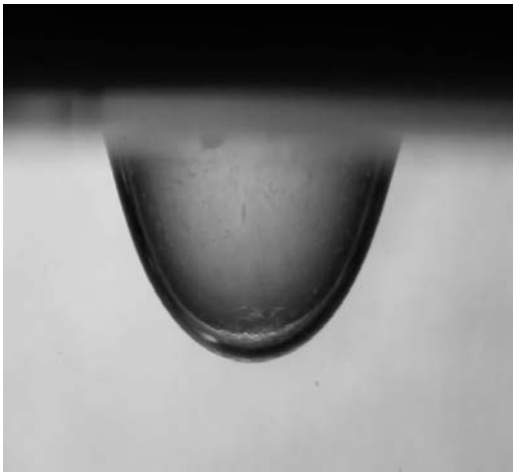

Edge fitting image using MATLAB

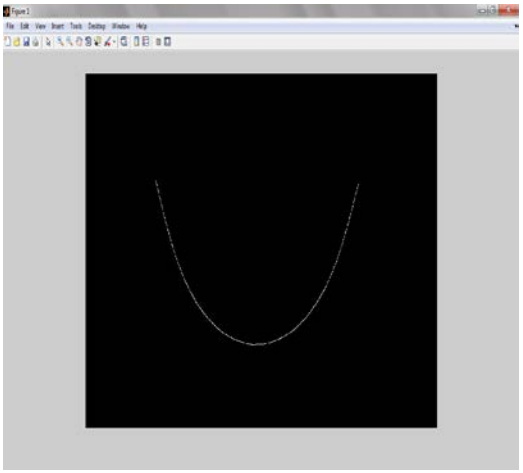

Excel sheet with droplet profile data

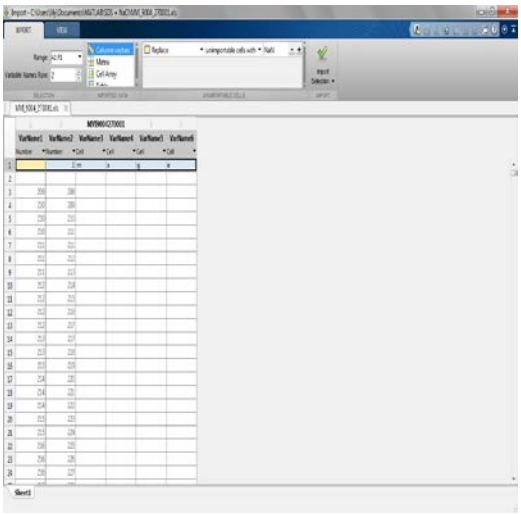

Edge fitting resulting by using a polynomial function

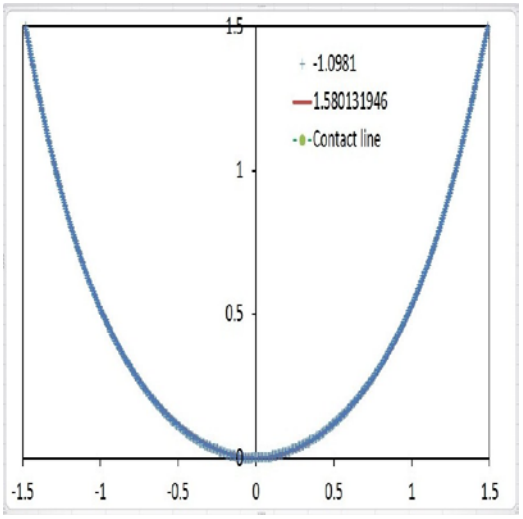

MVI_9004_27500 (V= 6.489 mm^3)

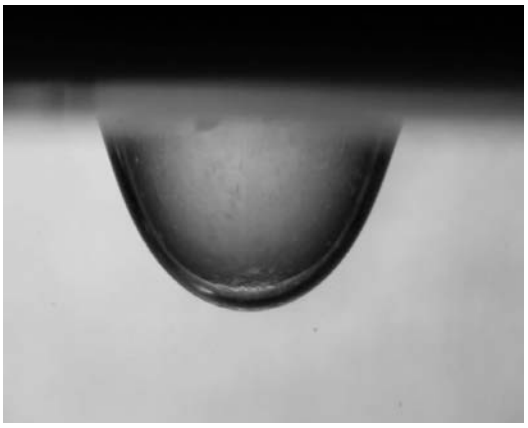

Edge fitting image using MATLAB

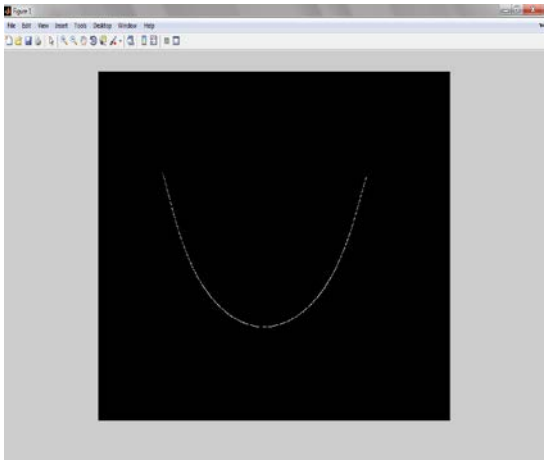

Excel sheet with droplet profile data

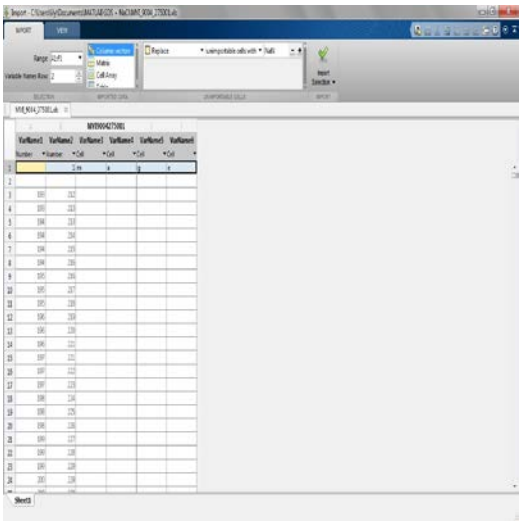

Edge fitting resulting by using a polynomial function

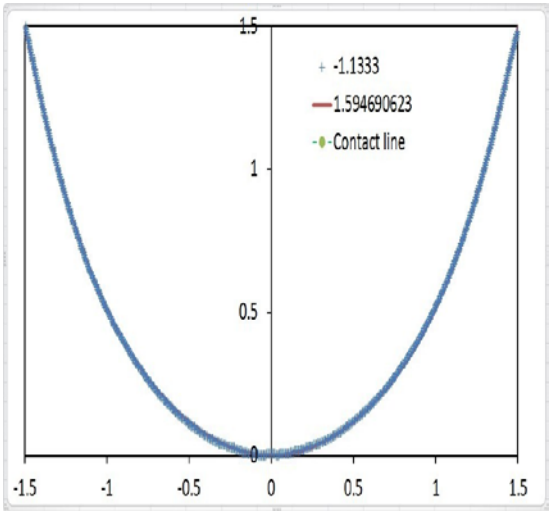

MVI_9267_24800 (V= 5.913 mm^3)

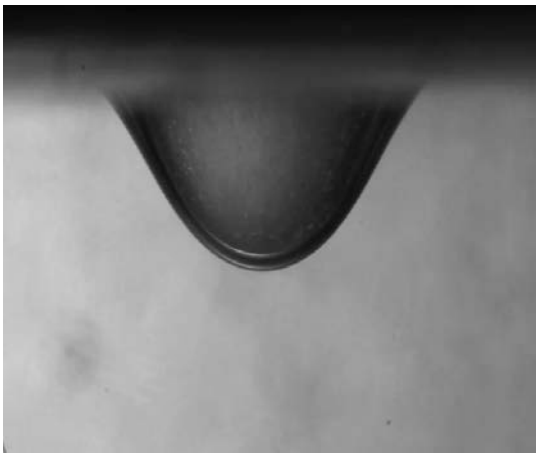

Edge fitting image using MATLAB

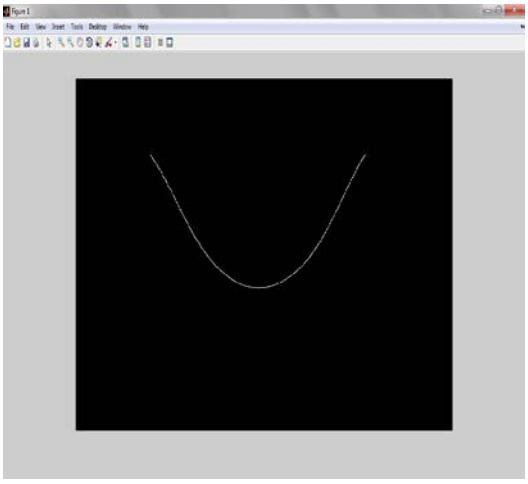

Excel sheet with droplet profile data

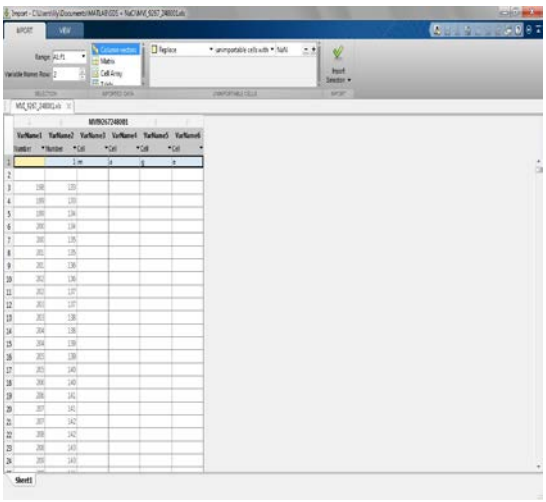

Edge fitting resulting by using a polynomial function

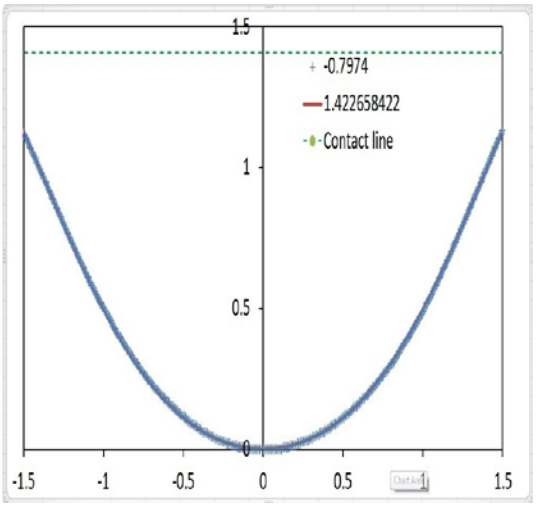

MVI_9284_12500 (V= 8.983 mm^3)

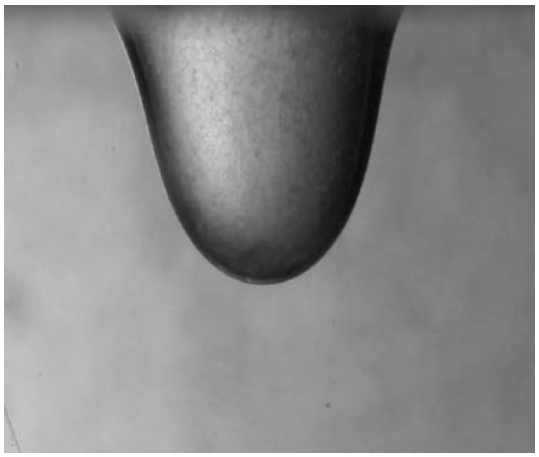

Edge fitting image using MATLAB

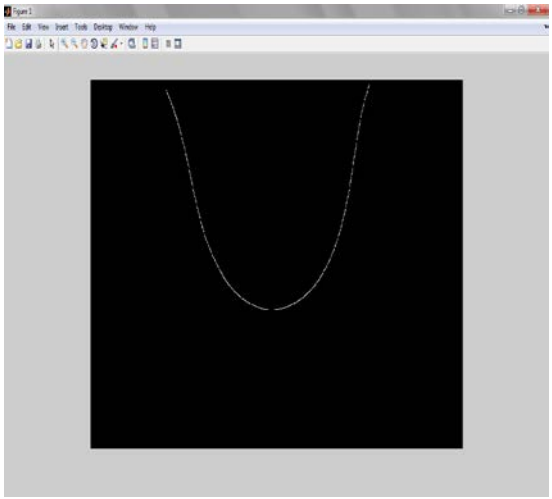

Excel sheet with droplet profile data

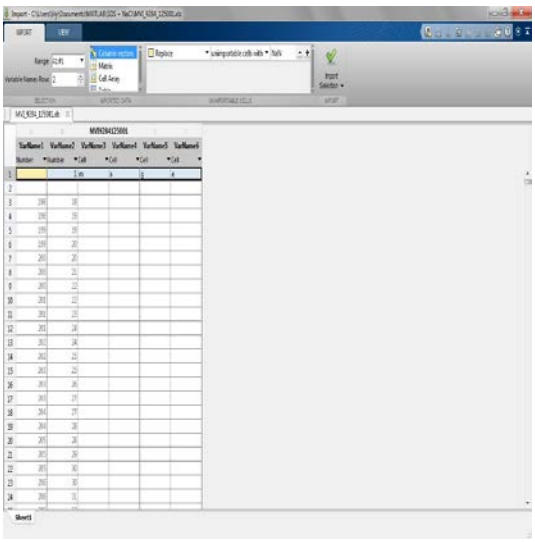

Edge fitting resulting by using a polynomial function

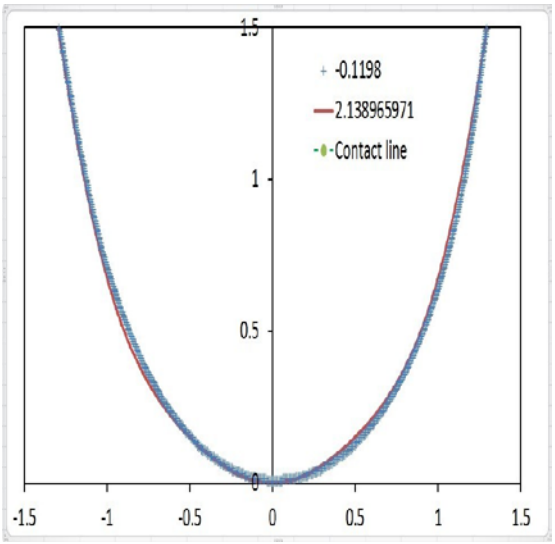

MVI_9284_13000 (V= 8.873 mm^3)

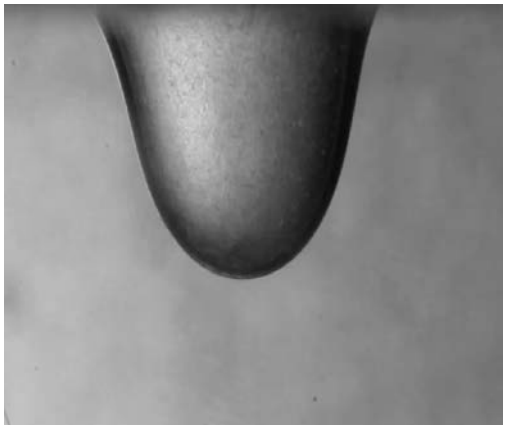

Edge fitting image using MATLAB

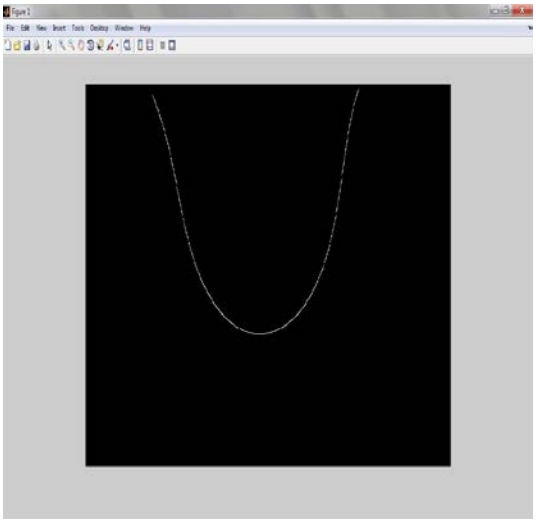

Excel sheet with droplet profile data

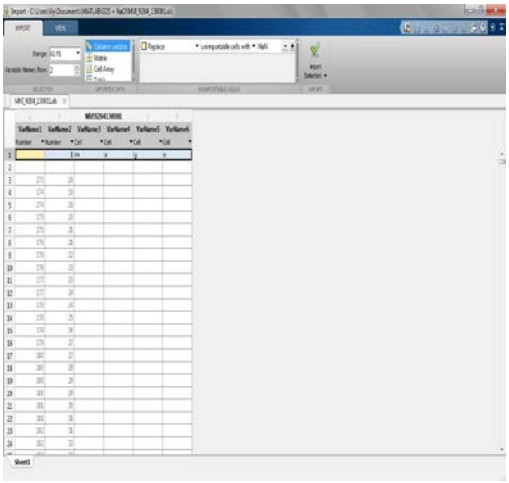

Edge fitting resulting by using a polynomial function

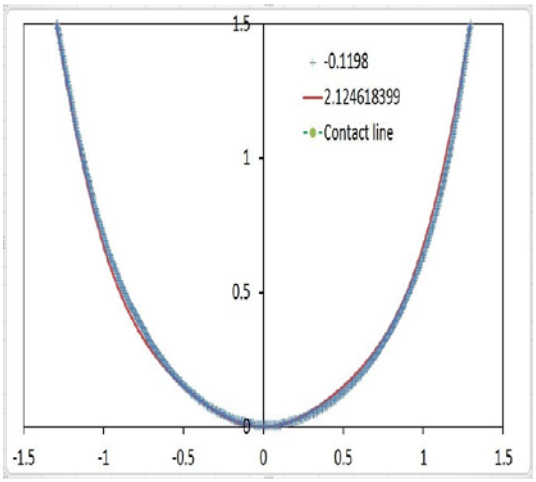

MVI_9286_23000 (V= 4.317 mm^3)

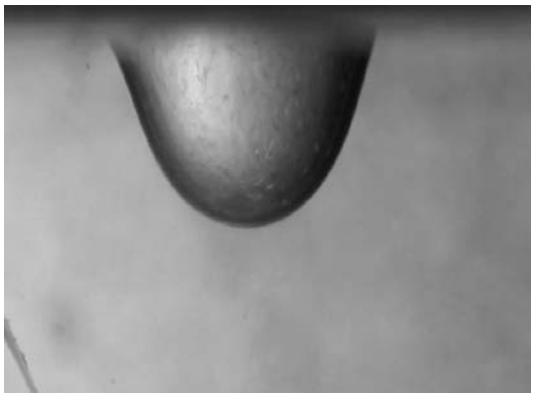

Edge fitting image using MATLAB

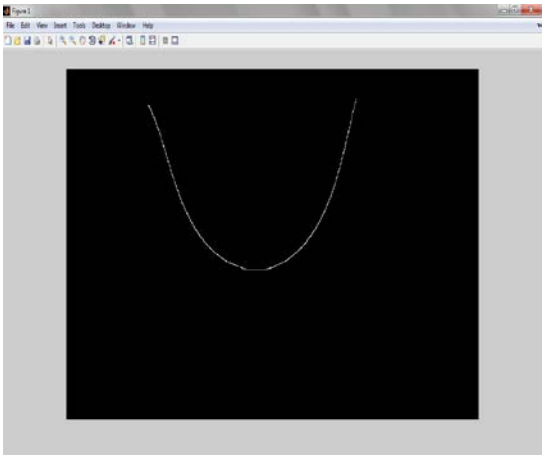

Excel sheet with droplet profile data

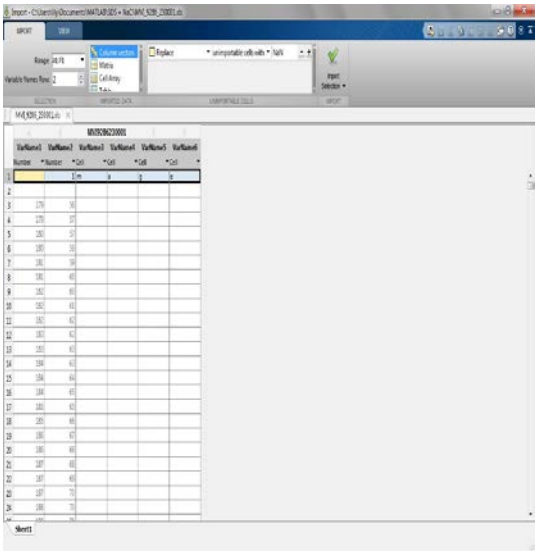

Edge fitting resulting by using a polynomial function

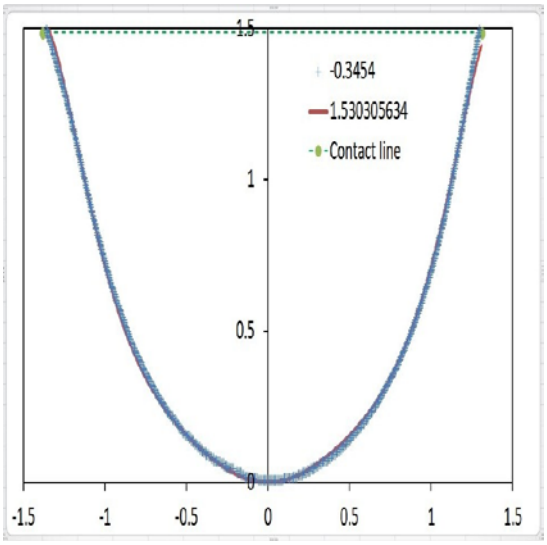

A.3 (SDS and NaCl) at low pH Droplets Images:

MVI_9634_03500 (V = 1.156 mm^3)

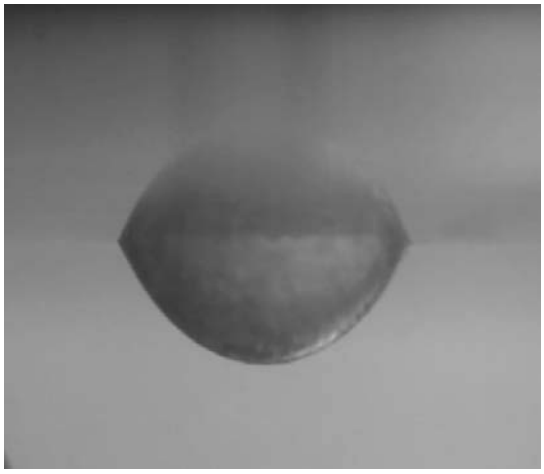

Edge fitting image using MATLAB

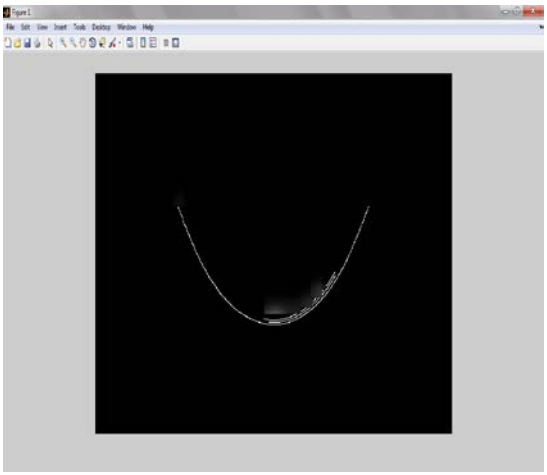

Excel sheet with droplet profile data

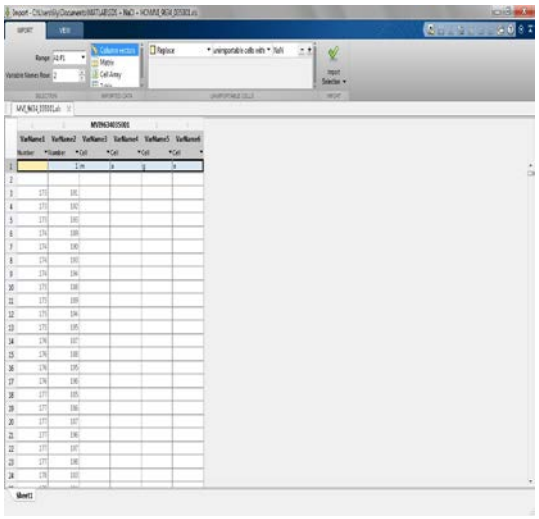

Edge fitting resulting by using a polynomial function

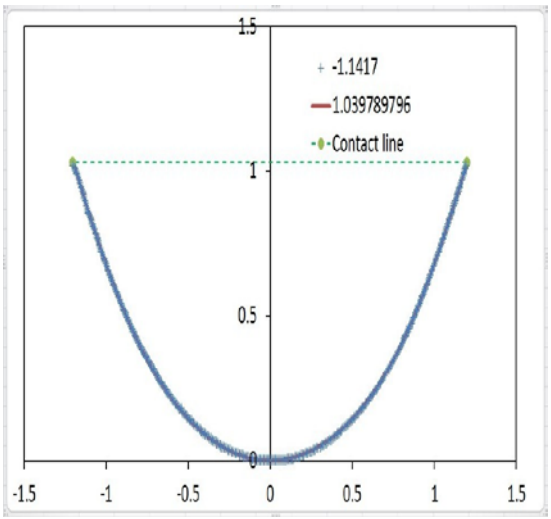

MVI_9634_16000 (V = 1.548 mm^3)

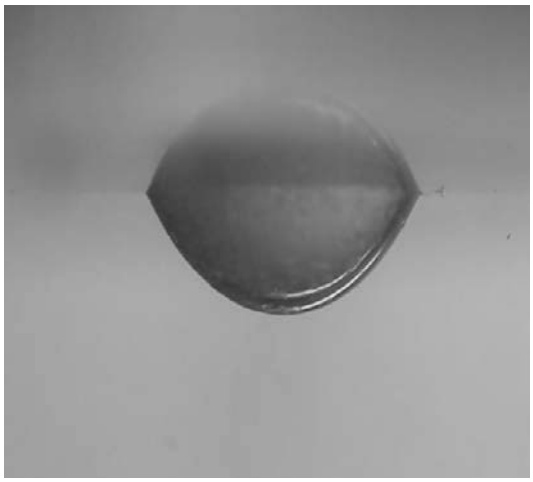

Edge fitting image using MATLAB

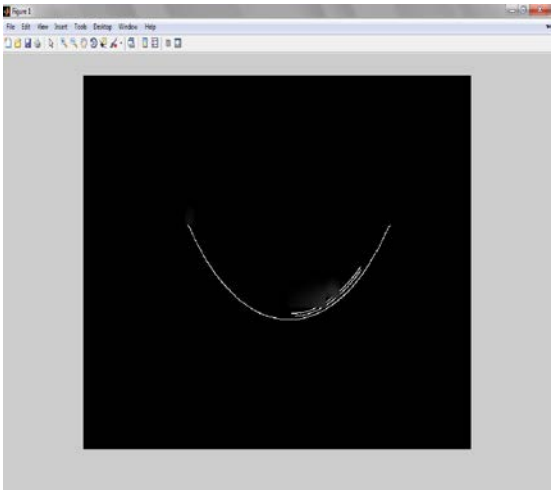

Excel sheet with droplet profile data

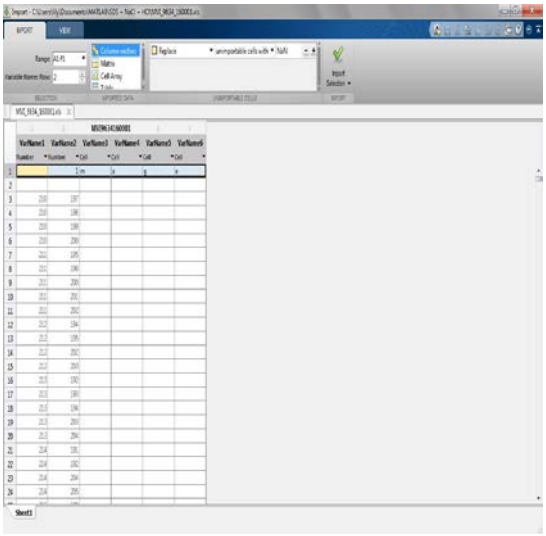

Edge fitting resulting by using a polynomial function

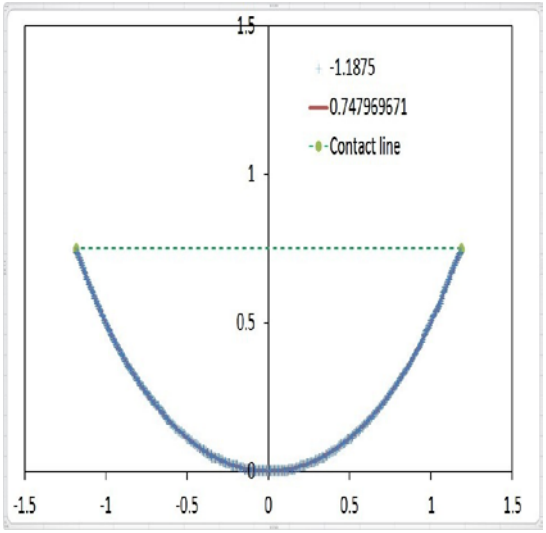

MVI_9634_25500 (V = 2.454 mm^3)

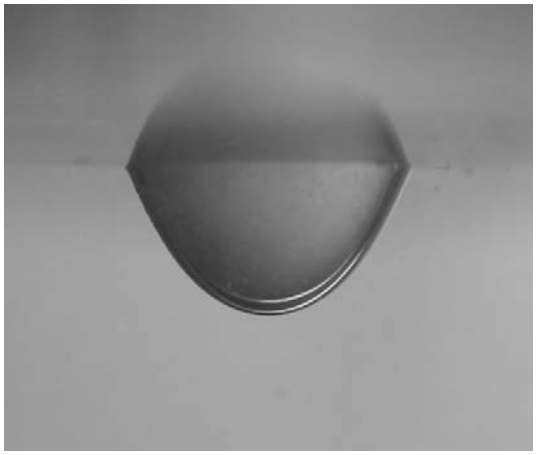

Edge fitting image using MATLAB

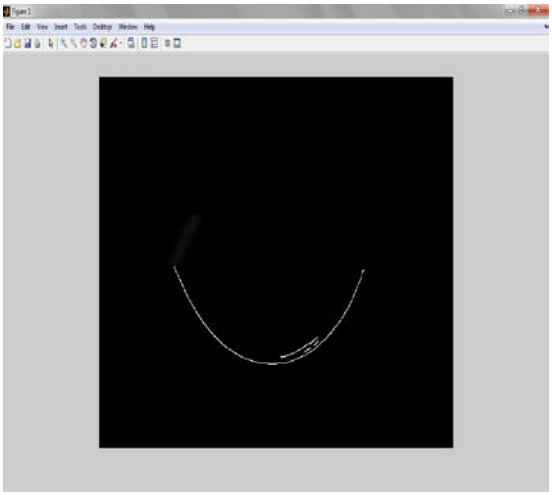

Excel sheet with droplet profile data

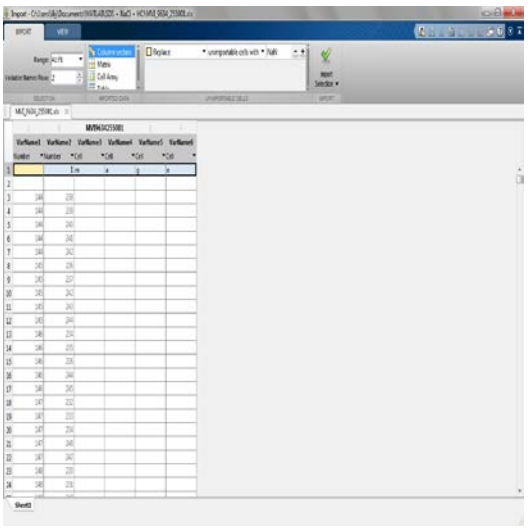

Edge fitting resulting by using a polynomial function

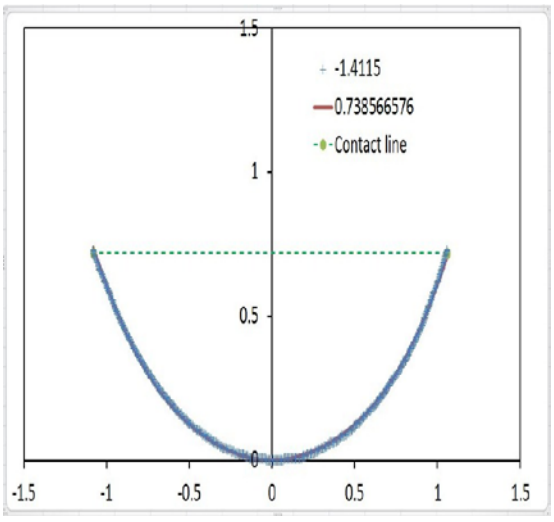

MVI_9636_26000 (V = 3.813 mm^3)

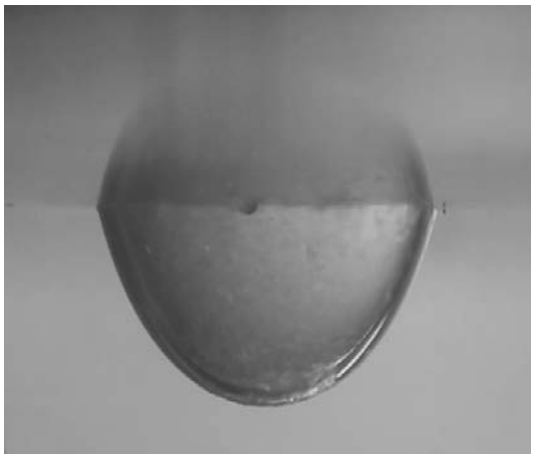

Edge fitting image using MATLAB

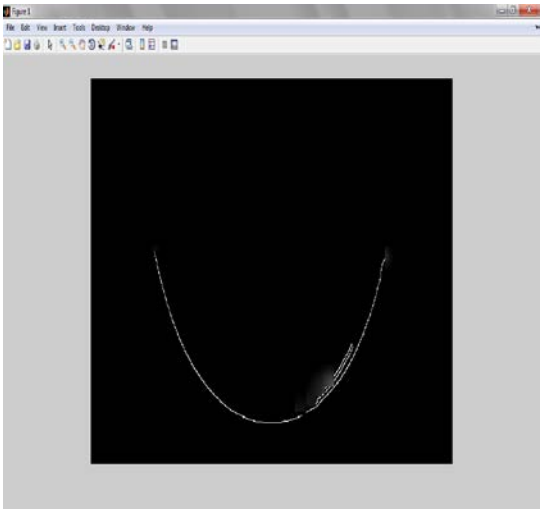

Excel sheet with droplet profile data

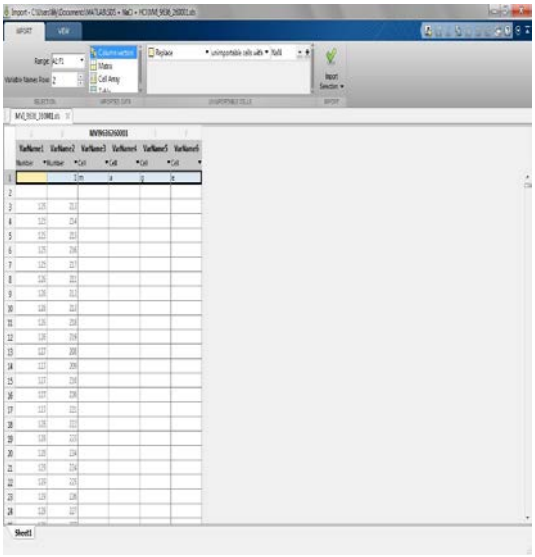

Edge fitting resulting by using a polynomial function

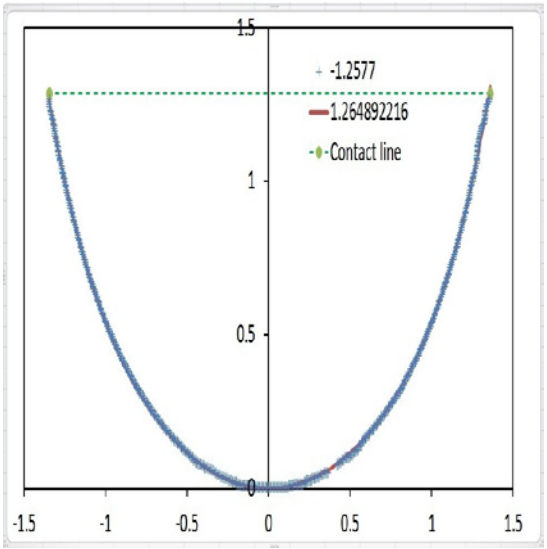

MVI_9636_27000 (V = 3.068 mm^3)

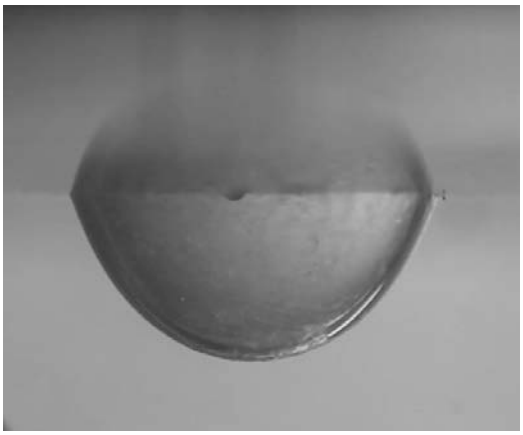

Edge fitting image using MATLAB

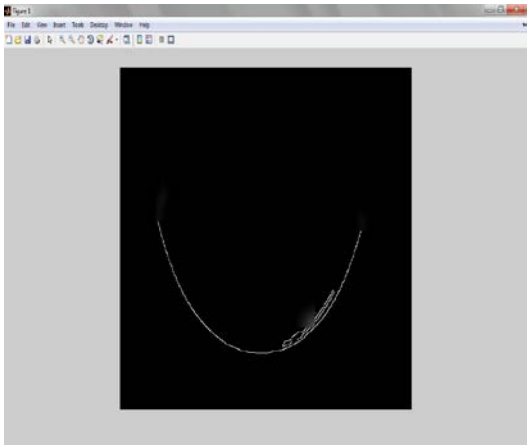

Excel sheet with droplet profile data

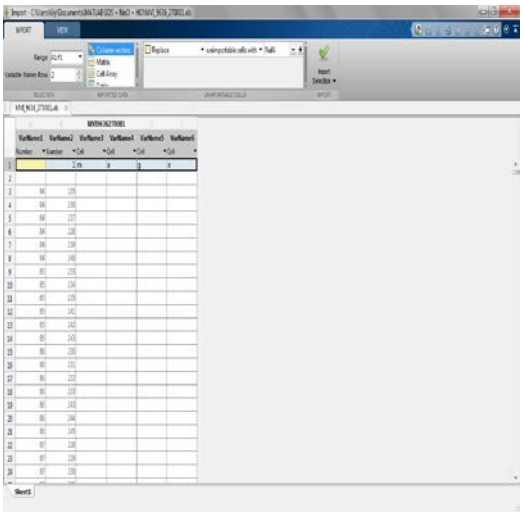

Edge fitting resulting by using a polynomial function

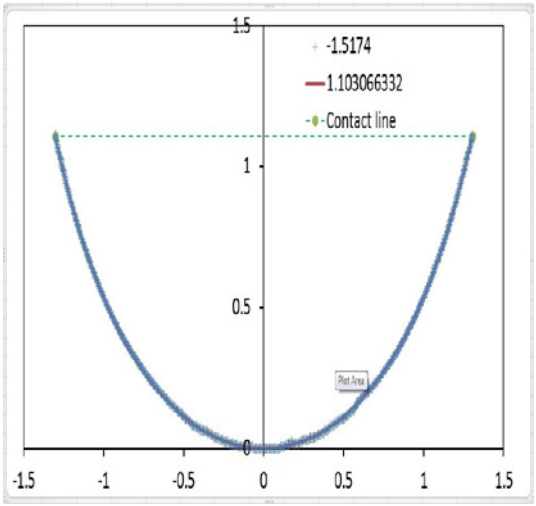

MVI_9639_13000 (V = 5.513 mm^3)

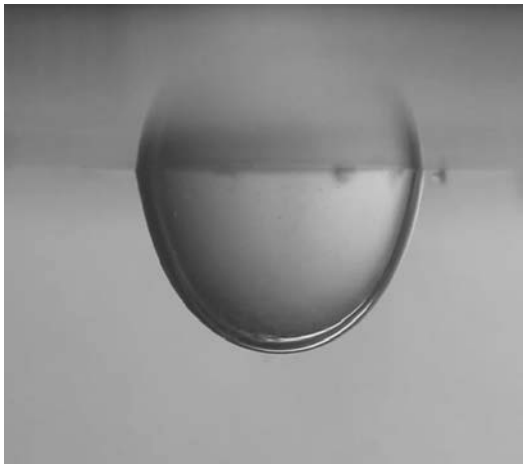

Edge fitting image using MATLAB

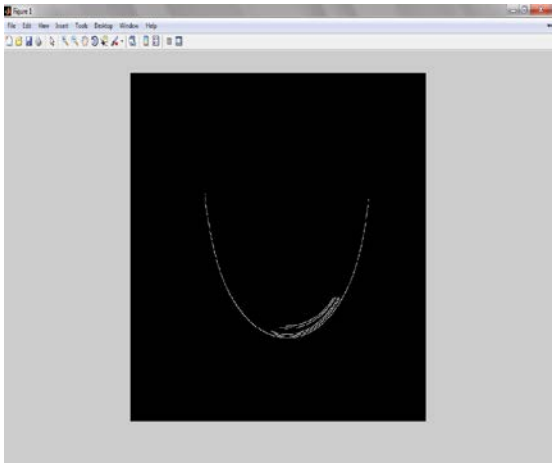

Excel sheet with droplet profile data

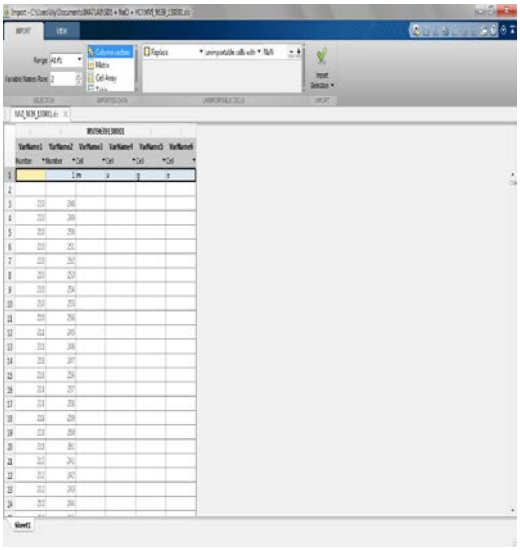

Edge fitting resulting by using a polynomial function

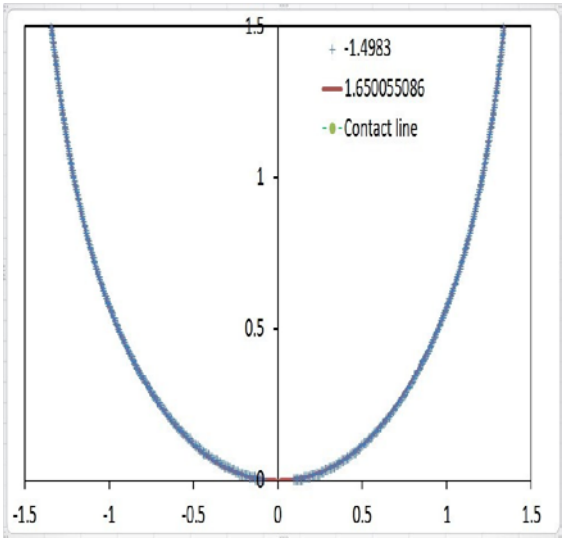

MVI_9639_23000 (V = 4.748 mm^3)

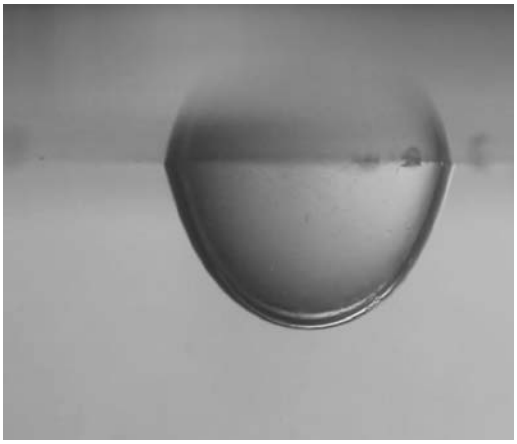

Edge fitting image using MATLAB

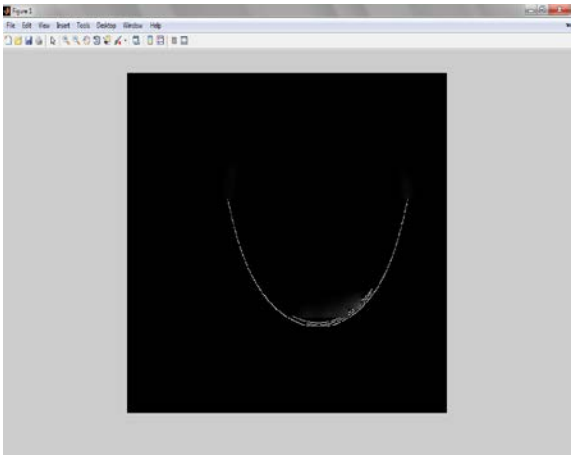

Excel sheet with droplet profile data

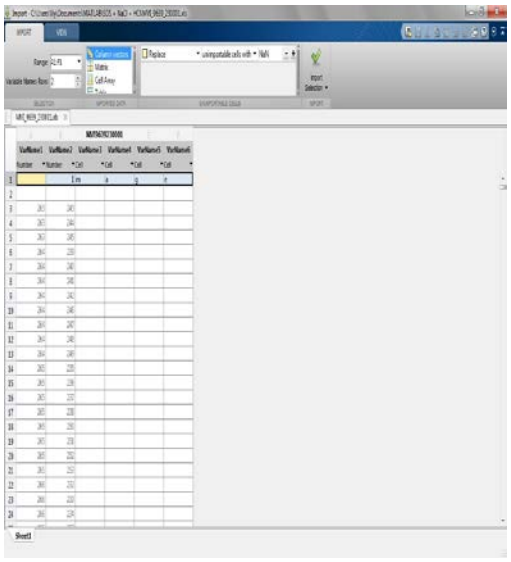

Edge fitting resulting by using a polynomial function

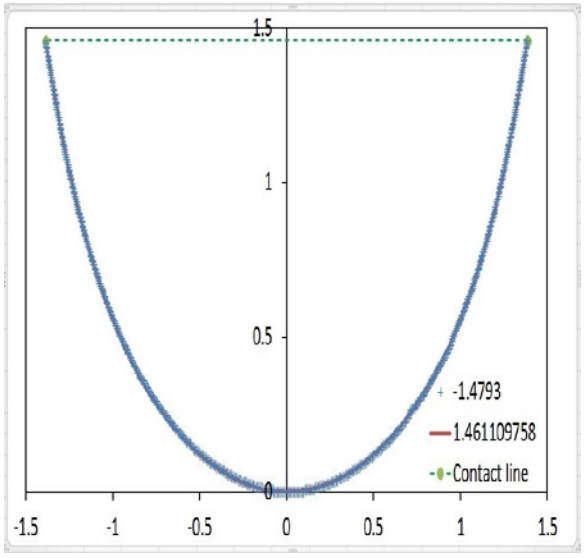

MVI_9641_15500 (V = 5.704 mm^3)

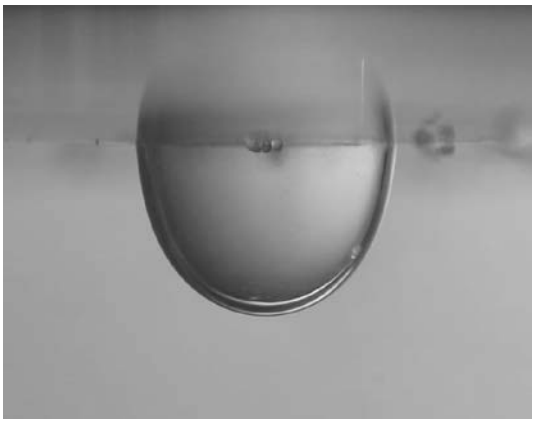

Edge fitting image using MATLAB

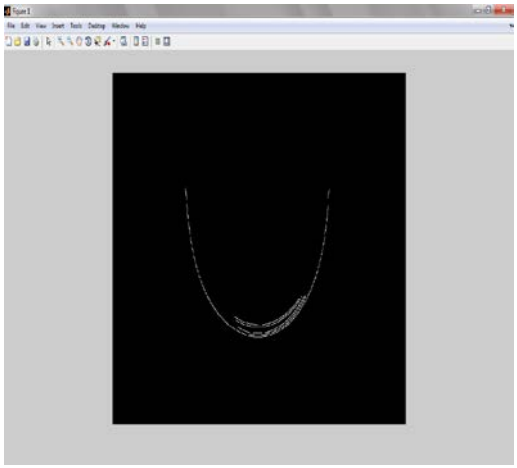

Excel sheet with droplet profile data

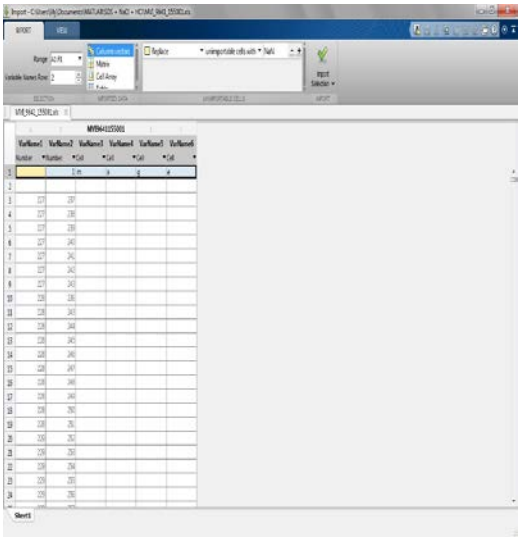

Edge fitting resulting by using a polynomial function

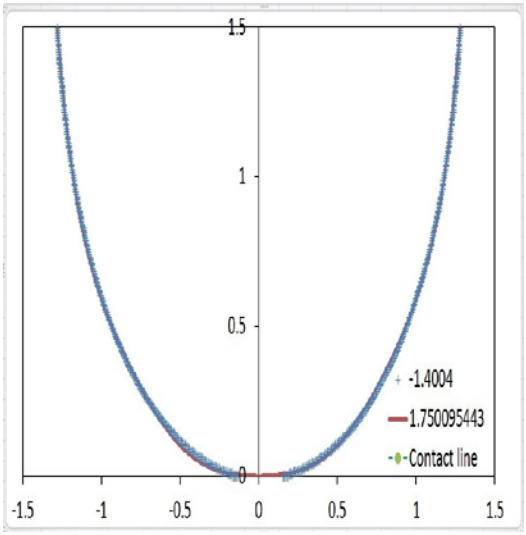

MVI_9641_27078 (V = 5.803 mm^3)

Edge fitting image using MATLAB

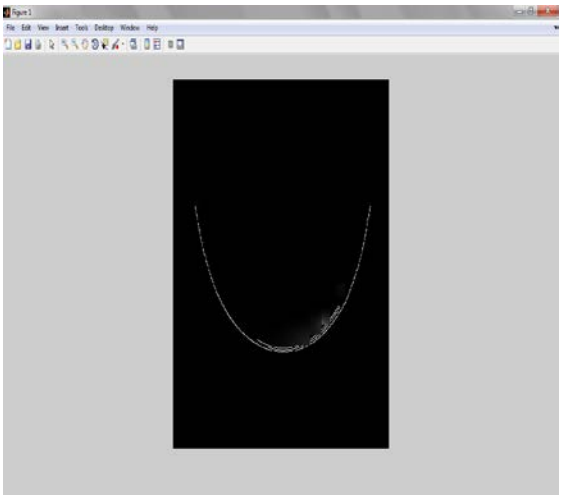

Excel sheet with droplet profile data

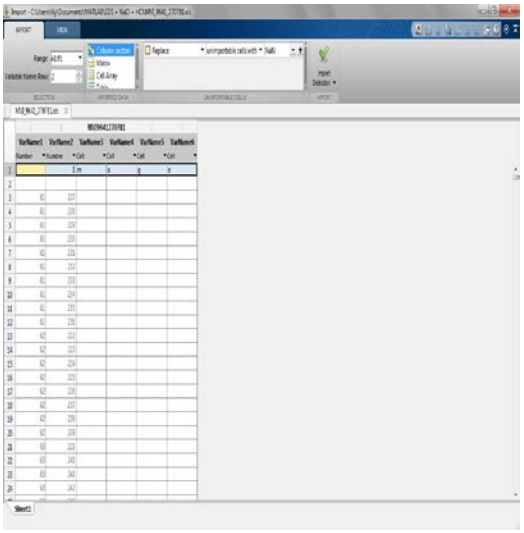

Edge fitting resulting by using a polynomial function

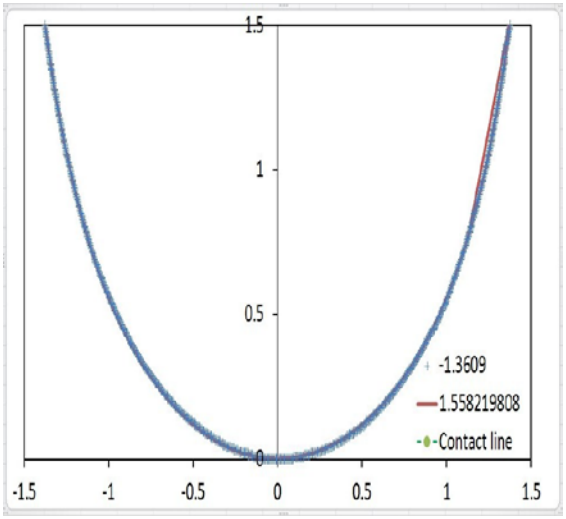

MVI_9642_26000 (V = 6.184 mm^3)

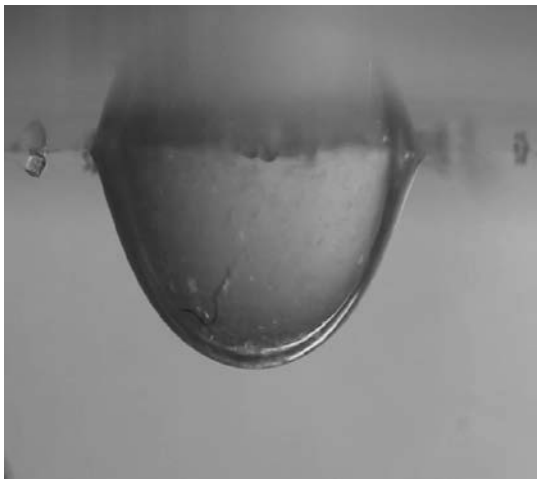

Edge fitting image using MATLAB

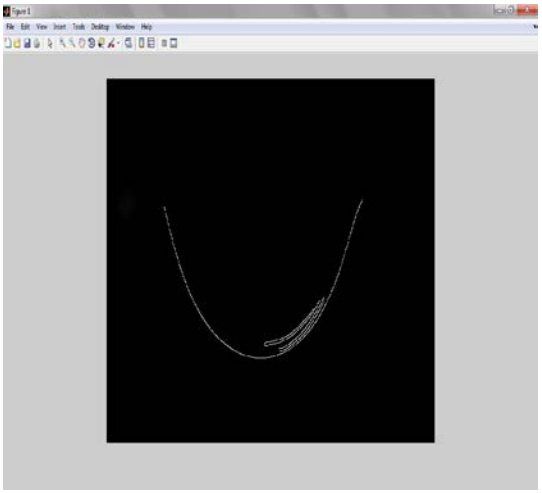

Excel sheet with droplet profile data

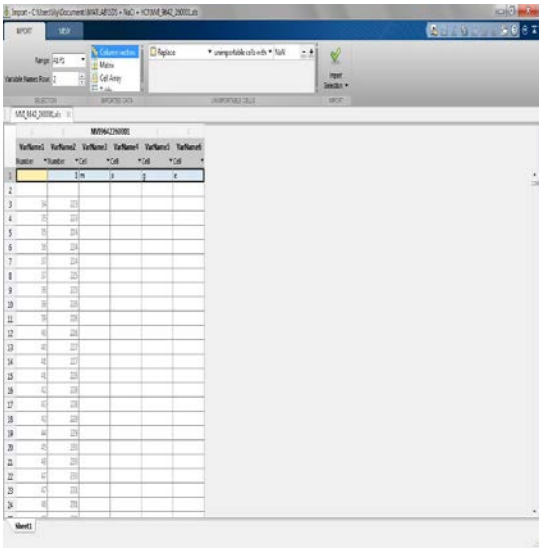

Edge fitting resulting by using a polynomial function

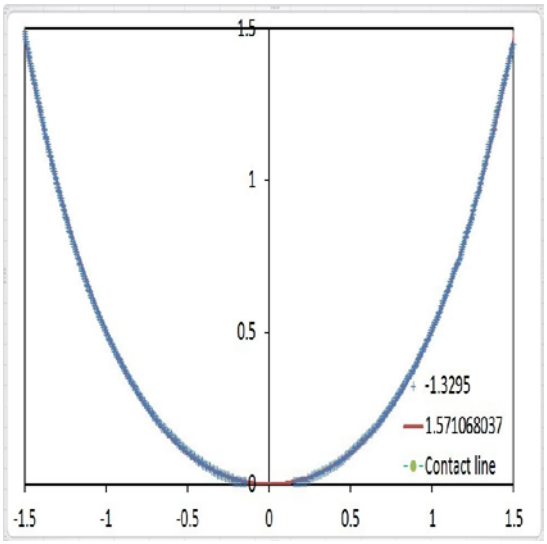

MVI_9642_27834 (V = 6.241 mm^3)

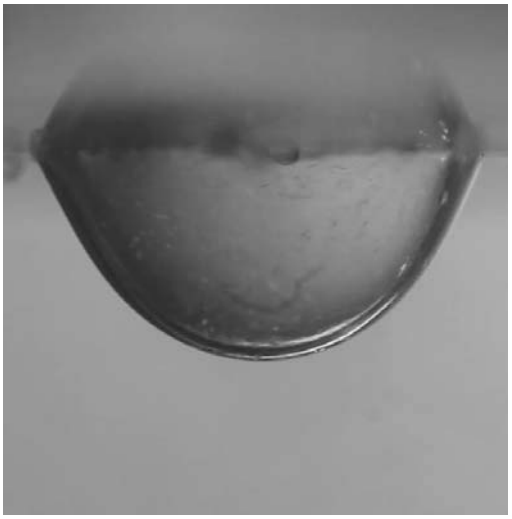

Edge fitting image using MATLAB

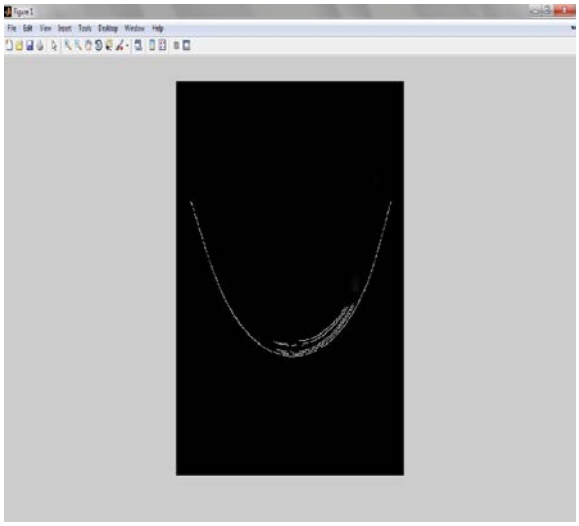

Excel sheet with droplet profile data

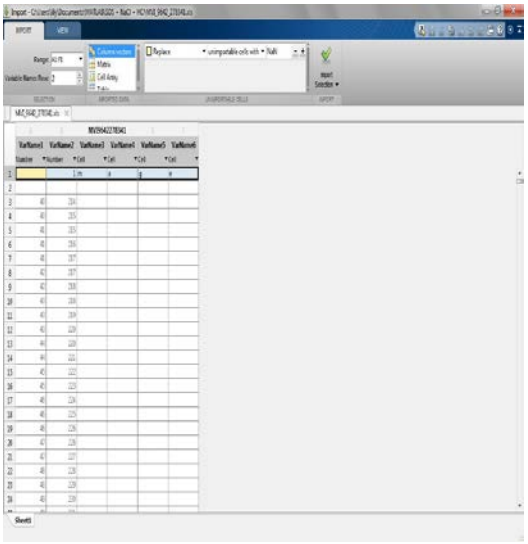

Edge fitting resulting by using a polynomial function

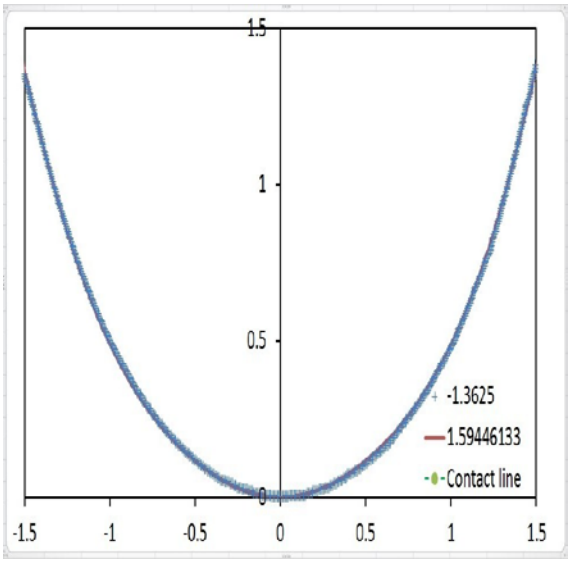

Appendix B MATLAB - Edge detection code

```
% find edge and export to Excel, th is the threshold between 0 and 1
%imm= rgb2gray(im);
numlength = 1;  % Length of numbers in filename including padded zeros
basefilename = 'MVI_9004_27000';
fmt = ['%0' num2str(numlength) 'u'];    % Zero padded integer of specified
length
for i = 1:98
k=i %or 902+i*20;
filename = [basefilename num2str(k,fmt)];
disp(filename)
im=imread( filename, 'jpg' );
threshold=0.75;
Matrix = edge(im, 'canny', threshold);
imshow(Matrix);
[row,col] = find(Matrix);
xlswrite (filename, 'image',1, 'B1');
xlswrite (filename, k,1, 'B1');
xlswrite (filename, col,1, 'A3');
xlswrite (filename, row,1, 'B3');
end
```